# Multi-Agent Coordination: Theory and Applications

by

Jianghai Hu

B.E. (Xi'an Jiaotong University, China) 1994
M.S. (University of California at Berkeley) 1999
M.A. (University of California at Berkeley) 2002

A dissertation submitted in partial satisfaction of the
requirements for the degree of
Doctor of Philosophy

in

Electrical Engineering

in the

GRADUATE DIVISION
of the
UNIVERSITY of CALIFORNIA at BERKELEY

Committee in charge:

Professor Shankar Sastry, Chair
Professor Laurent El Ghaoui
Professor Alan Weinstein

Spring 2003

The dissertation of Jianghai Hu is approved:

Chair Date

Date

Date

University of California at Berkeley

Spring 2003

**Multi-Agent Coordination: Theory and Applications**



by

Jianghai Hu

## Abstract


Multi-Agent Coordination: Theory and Applications

by

Jianghai Hu

Doctor of Philosophy in Electrical Engineering

University of California at Berkeley

Professor Shankar Sastry, Chair

We study the problem of optimal multi-agent coordination and related applications. The dissertation consists of three parts. In the first part, the problem of optimal coordinated motions for multiple agents moving on a plane is studied. In the second part, we study the optimal resolution maneuvers for multiple aircraft flying in three dimensional airspace. In the last part, the problem of optimal collision avoidance and formation switching on Riemannian manifold is studied. In all three parts, the motions of the participating agents need to satisfy some separation constraints, while the underlying space that the agents move on is two dimensional Euclidean space, three dimensional Euclidean space, and general Riemannian manifolds, respectively. We try to find the optimal coordinated motions that minimize a certain energy cost function. Various necessary conditions for the optimal solutions are obtained and numerical alogithms are proposed to compute them.

Dedicated to my parents.

# Contents

# List of Figures

## Acknowledgements

This dissertation would not have been possible without the help of many people. First of all, I would like to express my sincere gratitude to my Ph.D. advisor, Professor Shankar Sastry. He motivated me to work on the air traffic management project from which the topic of this dissertation originated, and has provided constant inspiration and guidance for me. I would also like to thank Professor Alan Weinstein, my MA thesis advisor in the Mathematics Department. My numerous consultations with him on problems related to or unrelated to the dissertation were always rewarded with sharp advice and warm reception, making it a great experience working with him. I also learnt a great deal from Professor Laurent El Ghaoui's course on Convex Analysis, and, more importantly, from his enthusiasm towards his research subject and his students.

Maria Prandini, now an Assistant Professor at Politecnico di Milano, Italy, has been collaborating with me closely ever since I started working on this subject, and her contributions throughout the dissertation are too numerous to be listed out individually. Professor Allen Knutson from the Mathematics Department read through Chapter 4 of the dissertation and provided many valuable suggestions for revisions. Many other individuals have also contributed to this dissertation, either directly or indirectly, including, but not limited to, John Lygeros, Claire Tomlin, Datta Godbole, George Pappas, Yi Ma, Joseph Yan, John Koo, Cenk Cavusoglu, Jun Zhang, Arnab Nilim, Omid Shakernia, Rene Vidal. I am grateful to all of them. I am also grateful to many of my other friends at Berkeley, who make my life in Berkeley memorable.

# Chapter 1

# Background

In this dissertation we study the optimal coordinated motion planning problem for multiple agents moving in various spaces. We shall review in this chapter the background materials of some of the applications that motivate this research.

The most important motivating application is air traffic management. Air travel has experienced a dramatical increase in the last few decades, and this trend is projected to continue or accelerate in the near future despite the recent setback to air industry. On the other hand, in spite of technological advances, the air traffic control system currently in use has remained largely the same semi-automatic process as when it was installed in the early 1970's. This system is ill-equipped for the growth in air traffic, as is evidenced by the frequent ground holdings and airborne delays due to congestion in the skies. Therefore, it has become an urgent task to automate the current air traffic control system.

The main concern of any automated Air Traffic Management (ATM) systems is guaranteeing *safety*. This is achieved by avoiding the occurrence of *conflicts*, i.e., of those situations where two aircraft come closer to each other than a minimum allowed horizontal separation $r$ *and* a minimum allowed vertical separation $h$ at the same time. Currently $r$ is set equal to 5 nautical miles (nmi) in en-route airspace, and 3 nmi inside the Terminal Radar Approach Control facilities (TRACONs), whereas $h$ is 2000 feet (ft) above the altitude of $29,000$ ft (FL290), and 1000 ft below FL290. Conflict avoidance is typically decomposed into two phases:

– *conflict detection*, where potential conflicts that may arise in the future are detected by predicting the aircraft future motions based on the available information on their current positions, headings, and flight plans;

– *conflict resolution*, where the flight plans of the aircraft involved in the detected conflicts are re-planned to prevent the conflicts from actually occurring.

Some of the work on conflict detection, particularly those based on probabilistic methods, can be found in [16, 29, 57, 59, 73], to name a few. In this dissertation, we shall focus on the conflict resolution problem.

The existing approaches to aircraft conflict resolution can be classified according to various criteria. The interested reader is referred to the up-to-date survey [39] on the different conflict resolution approaches proposed in the literature. In the following we shall review briefly some of the most relevant ones.

Based on the level of coordination or, alternatively, on the level of mutual trust among participating aircraft, conflict resolution methods can be classified as *noncooperative* and *cooperative* [58].

In the noncooperative case, the aircraft involved in the encounter do not exchange information on their intentions and do not trust one another at all, hence the worst case approach is adopted. In the solution proposed in [70, 71], the two-aircraft conflict resolution problem is formulated as each aircraft playing a zero-sum noncooperative game against disturbances that model the uncertainty in the other aircraft intentions, with the value function being the aircraft separation. The differential game methodology is also used in [69] for determining the safe region for aircraft approaching closely spaced parallel runways.

At the other extreme with respect to the noncooperative case, there is the cooperative conflict resolution scenario, where the current positions and intentions of the aircraft are assumed to be perfectly known to a supervising central controller. Each aircraft completely trusts the central controller (and hence all the other aircraft), and is ready to follow its advice. The cooperative conflict resolution problem is typically formulated as an optimization problem, where the central controller designs the flight plans of all the aircraft so as to avoid conflicts and at the same time minimize a certain cost function. Contributions in the literature belonging to this class include [47, 18, 25, 48, 74], to mention only a few.

In between the extremes of noncooperative and cooperative conflict resolution there are the *probabilistic* conflict resolution approaches. In these approaches, the aircraft positions are assumed to be distributed according to certain probabilistic laws, thus modeling not only the effect of disturbances on aircraft motions but also the fact that each aircraft has only partial confidence in the information on the intentions of other aircraft. References in this category include, for example, [16, 38] for the two aircraft case, and [23, 60] for the multiple aircraft case.

Based on whether vertical maneuvers are employed or not, conflict resolution methods can be classified as *three-dimensional* (3D) or *two-dimensional* (2D), with the latter being a particular case of the former. Typically conflicts are resolved by resorting to three different kinds of aircraft actions (or any combination of them): turn, climb/descend, and accelerate/decelerate, which affect the aircraft heading, altitude, and speed, respectively. Resolution strategies adopting one or more of these actions are analyzed and compared in terms of cost and efficacy in [37]. It is found that climb/descend is the most efficient action for resolving short-term conflicts, since the horizontal separation requirement is much more stringent than the vertical one. In fact, vertical maneuvers are used to resolve imminent conflicts in the Traffic Alert and Collision Avoidance System (TCAS [61]) currently operating on board of all commercial aircraft carrying more than thirty passengers. However, compared with horizontal maneuvers, excessive changes of altitude are likely to cause more discomfort to passengers, and are not as compatible with the current vertically layered structure of the airspace. These facts together with the relative simplicity of dealing with the two dimensional case have caused most of the approaches proposed in the literature to focus on 2D conflict resolution, assuming level flight and horizontal resolution maneuvers.

It is important to consider conflict resolution problem for multiple aircraft, not just for two aircraft. Conflict situations involving more than two aircraft may actually occur in areas with high traffic density, and resolving them is intrinsically more difficult than dealing with the two aircraft case. For example, it may happen that by solving a two-aircraft conflict without taking into consideration the surrounding aircraft, a new conflict with a third aircraft is generated (domino effect). Only a few of the existing treatments on conflict resolution deal with the multiple aircraft case. Some of them [23, 35, 60] use the potential and vortex field method to determine coordinated maneuvers. However, the maneuvers thus generated are not guaranteed to be safe. Another approach consists in formulating multiple aircraft conflict resolution as a constrained optimization problem with a suitable cost function to be optimized under the conflict-free constraint. The contributions [5, 18, 25, 28, 47, 48, 56] belonging to this category differ in the choice of model and cost function, and also in the computational method adopted to solve the resultant optimization problem, e.g., linear programming [56] , genetic algorithms [47], semidefinite programming combined with a branch-and-bound search [18], and sequential quadratic programming (SQP) using linear approximation of the feasible region [48]. Solutions using computational geometric approaches are presented in [9, 10, 32].

The problems studied in Chapter 2 and Chapter 3 are the *optimal cooperative conflict resolution involving multiple aircraft* in 2D and 3D airspace, respectively. In fact, in Chapter 2, we formulate the conflict resolution problem for multiple aircraft flying at the same altitude as a special instance of a more general problem, the optimal coordinated motion planning for multiple agents moving on a plane, to include other relevant applications such as path planning of mobile robots, collision avoidance of naval or ground based vehicles [49], etc. For example, for multiple cooperating mobile robots moving in a common workspace, the requirement that there is no collision among them can be reformulated as that their joint maneuver be conflict-free, with $r$ being twice the robot radius. The problem of multiple robot motion planning with static or dynamic obstacles has been well studied in the literature (see e.g. [4, 15, 19, 40, 66], and the survey [31]). However, a large portion of them focus on the feasibility and the algorithmic complexity aspects of the problem. Some of them indeed deal with multiple robots case using certain optimality criteria.

To name a few, [5] studies the problem of time-optimal cooperative motions of multiple Dubin vehicles moving at constant speed with bounded curvature, while in [41], each robot minimizes its own independent cost function by using techniques from multi-objective optimization and game theory. [11] addresses the problem of optimal motion planning for multiple nonholonomic manipulators transporting a grasped object.

In Chapter 4, we study an even more general problem, the optimal collision avoidance (OCA) and optimal formation switching (OFS) problems on Riemannian manifolds. The goal is still to find the motions than can guide a group of agents from a starting configuration to a desired destination configuration in an optimal way, subject to certain separation constraints. However, instead of two dimensional or three dimensional Euclidean spaces, the space that the group of agents move on is a Riemannian manifold. The difference between the OCA and the OFS problems is that for the latter the participating agents may assume only a subset of all the possible formation patterns.

In addition to being a generalization of aircraft conflict resolution, the OCA and the OFS problems also find applications in a host of other fields. Examples include a team of mobile robots cooperating to carry a common object [11], a multi-link reconfigurable robot performing configuration switchings, a group of surveillance cameras monitoring a museum at night, a cluster of communication satellites covering earth surface, etc. Another example is multi-user wireless communication, where each user has to be assigned a (possibly time-varying) subspace in the signal space, and sufficient separation among these subspaces should be maintained for satisfactory signal-to-noise ratio. In this case the appropriate Riemannian manifold is a

Grassmann manifold [75]. In this dissertation we only consider problem with holonomic constraints, as opposed to the numerous papers dealing with nonholonomic constraints (see e.g. [5, 8, 34, 36, 68, 72]). Other relevant work includes, for example, [17, 42], where the problems of stable and optimal coordinate control of vehicle formations are studied.

This dissertation is organized as follows. First in Chapter 2 we study the optimal conflict-free motion planning problem for multiple agents moving on a plane. After a formal classification of conflict-free maneuvers into homotopy types by using the notion of pure braids group, we propose various necessary conditions for the optimal solutions. In particular, the optimal conflict-free maneuvers for the two-agent case are derived. For the general case of more than two agents, we propose a stochastic algorithm to choose homotopy types, and a convex optimization algorithm to solve for solutions in each homotopy type, which combined form a randomized optimization algorithm. In Chapter 3, the problem of multi-aircraft conflict resolution in three dimensional airspace is considered. By generalizing the results in Chapter 2, we derive a convex optimization algorithm that can obtain multi-legged approximated solutions for multi-aircraft encounters. Practical constraints such as maximal turning angle and aircraft speed are also considered. In Chapter 4, we study the the optimal collision avoidance and optimal formation switching problems on Riemannian manifolds, and derived various necessary conditions for the optimal solutions under some symmetry assumption. These conditions generalize those obtained in the previous two chapters. Finally in Chapter 5 we summarize the dissertation and point out some future directions.

# Chapter 2

# Optimal Conflict-Free Maneuvers on a Plane

## 2.1 Introduction

In this chapter, the problem of designing optimal coordinated maneuvers for multiple agents moving on a plane is studied. The joint maneuver has to be chosen so as to guide each agent from its starting position to its target position, while avoiding *conflicts*, that is, situations where the Euclidean distance between any two agents is smaller than some fixed threshold $r > 0$. Among all the conflict-free joint maneuvers, we aim at determining the one with the least overall cost. Here the cost of a single agent's maneuver is its energy, and the overall cost is a weighted sum of the maneuver energies of all individual agents, with the weights representing the priorities of the agents. A precise formulation of the problem is given in Section 2.3.

This problem is of great interest since it is actually encountered in many different practical areas, such as aircraft conflict resolution, robot motion planning, navigation of ground based or naval vehicles, etc. The existing methods are surveyed briefly in Chapter 1. The distinguishing feature of our approach to coordinated motion planning consists in the interpretation of maneuvers as braids. Besides giving a complete homotopic classification of conflict-free maneuvers, it also provides us insights on the derivation of optimality conditions. Although the space-time representation of motions is not new in the literature (see e.g. [15, 64]), to our knowledge, however, it has never been used to such an extent in the optimality analysis of coordinated motions.

This chapter is organized as follows. In Section 2.2, we introduce a formal classification of conflict-free maneuvers into homotopy types by using the notion of pure braids group. The problem under study is then defined in Section 2.3. Inspired by the braid representation of conflict-free maneuvers, we define various transformations of joint maneuvers that preserve the minimum separation condition. Such transformations are used in the variational analysis in Section 2.4 to derive local and global necessary conditions on optimal conflict-free maneuvers. In particular, the optimal conflict-free maneuvers for the two-agent case are derived in Section 2.4.2. In Section 2.5 we analyze an interesting example of three-agent encounter. Two mechanical interpretations of the problem are given in Section 2.6.

As the number of agents increases, it is difficult in practice to derive analytically the optimal conflict-free maneuvers. By focusing on those maneuvers specified by a set of waypoints, we are able to use convex optimization techniques to obtain multi-legged approximated solutions to the constrained optimization problem within each homotopy type (Section 2.7). A stochastic algorithm is proposed in Section 2.7.4

to address the problem of selecting the homotopy type, thus leading to a randomized convex optimization algorithm.

## 2.2 Classification of conflict-free maneuvers

In this section we introduce a qualitative classification of conflict-free maneuvers involving multiple agents moving on the plane. Roughly speaking, two conflict-free maneuvers are classified as of the same "type" if there exists a continuous conflict-free deformation of one to the other. Thus switching between conflict-free maneuvers of different types cannot be done smoothly without causing a conflict. This implies, in practice, that it is preferable for the agents in the encounter to avoid "changes of mind" by determining through negotiation or arbitration a particular type of conflict-free maneuvers at an early stage and sticking to it throughout the whole encounter.

Consider $k$ agents (numbered from 1 to $k$) moving in $\mathbb{R}^2$, where each agent, say agent $i$, starts at position $a_i \in \mathbb{R}^2$ at time $t_0$, and ends in position $b_i \in \mathbb{R}^2$ at time $t_1$. Let $T \triangleq [t_0, t_1]$ be the time interval of the encounter. Denote by $\mathbf{P}_i \triangleq \{\alpha_i \in C(T, \mathbb{R}^2) : \alpha_i(t_0) = a_i,\ \alpha_i(t_1) = b_i\}$ the set of maneuvers for agent $i$ consisting of all the continuous maps from $T$ to $\mathbb{R}^2$ that take the values $a_i$ and $b_i$ at times $t_0$ and $t_1$, respectively. Define $\mathbf{P}(\mathbf{a}, \mathbf{b}) \triangleq \prod_{i=1}^{k} \mathbf{P}_i$, where $\mathbf{a} \triangleq \langle a_i \rangle_{i=1}^{k} = (a_1, \ldots, a_k)$ and $\mathbf{b} \triangleq \langle b_i \rangle_{i=1}^{k} = (b_1, \ldots, b_k)$ are ordered $k$-tuples representing the joint starting and destination positions of the $k$ agents, respectively. Each element $\alpha = \langle \alpha_i \rangle_{i=1}^{k} = (\alpha_1, \ldots, \alpha_k) \in \mathbf{P}(\mathbf{a}, \mathbf{b})$ is called a *joint maneuver* ($k$-maneuver or simply maneuver when there is no ambiguity) for the $k$-agent system. The *minimum separation over encounter (MSE)* for a joint maneuver $\alpha$ is defined to be the minimum Euclidean distance between any pair of agents during the whole time interval $T$, i.e.,

$$\Delta(\alpha) \triangleq \min_{1\leq i<j\leq k} \inf_{t\in T} \|\alpha_i(t) - \alpha_j(t)\|.$$

The set of *conflict-free maneuvers* is then defined as

$$\mathbf{P}(r, \mathbf{a}, \mathbf{b}) \triangleq \{\alpha \in \mathbf{P}(\mathbf{a}, \mathbf{b}) : \Delta(\alpha) > r\}$$

for some $r \geq 0$. In practice, for example, $r$ could be the radius of the protection zone surrounding an aircraft or twice the radius of a circular robot. We assume that the minimum distance between any pair in $\langle a_i \rangle_{i=1}^k$ and any pair in $\langle b_i \rangle_{i=1}^k$ is strictly greater than $r$. Hence $\mathbf{P}(r, \mathbf{a}, \mathbf{b})$ is nonempty.

We distinguish different maneuvers in $\mathbf{P}(r, \mathbf{a}, \mathbf{b})$ according to the following equivalence relation.

**Definition 1 ($r$-homotopy)** *Two maneuvers in* $\mathbf{P}(r, \mathbf{a}, \mathbf{b})$ *are $r$-homotopic if there exists a continuous deformation of one to the other in* $\mathbf{P}(r, \mathbf{a}, \mathbf{b})$, *or equivalently, if there exists a continuous deformation of one to the other in* $\mathbf{P}(\mathbf{a}, \mathbf{b})$ *such that the joint maneuvers obtained throughout the deformation are conflict-free.*

The objective of this section is to characterize the structure of the equivalence classes of $\mathbf{P}(r, \mathbf{a}, \mathbf{b})$ induced by the $r$-homotopy relation. With this purpose in mind, we now recall the concept of braids ([6, 54]).

**Definition 2 (Braids)** *A braid joining* $\mathbf{a} = \langle a_i \rangle_{i=1}^k$ *to* $\mathbf{b} = \langle b_i \rangle_{i=1}^k$ *is a $k$-tuple* $\langle \gamma_i \rangle_{i=1}^k$ *of continuous curves in* $\mathbb{R}^2 \times T \subset \mathbb{R}^3$ *satisfying the following conditions:*

- *Each point* $(a_i, t_0)$, $i = 1, \ldots, k$, *is joined by exactly one curve in* $\langle \gamma_i \rangle_{i=1}^k$ *to one of the points* $(b_j, t_1)$, $1 \leq j \leq k$;

- *The plane $t = \tau$ intersects each curve at exactly one point for all $\tau \in T$;*

- *$\gamma_i \cap \gamma_j = \emptyset$ whenever $i \neq j$.*

In the following, we shall occasionally use the term *$k$-braid* to indicate the number of curves in the braid. The set of all braids joining $\mathbf{a}$ to $\mathbf{b}$ is denoted by $\mathbf{B}(\mathbf{a}, \mathbf{b})$. If $i$ and $j$ are required to be identical in the first condition of Definition 2, the corresponding braid is called a *pure braid*. The set of all pure braids joining $\mathbf{a}$ to $\mathbf{b}$ is denoted by $\mathbf{PB}(\mathbf{a}, \mathbf{b})$. An example of a pure 3-braid is shown in the right-hand-side of Figure 2.1.

There is a simple equivalence relation defined on $\mathbf{B}(\mathbf{a}, \mathbf{b})$ and hence on $\mathbf{PB}(\mathbf{a}, \mathbf{b})$ as well ([54]).

**Definition 3 (String isotopy)** *Two braids in $\mathbf{B}(\mathbf{a}, \mathbf{b})$ are said to be string isotopic if the $k$ curves of one of them can be continuously deformed to those of the other in such a way that the $k$ curves in $\mathbb{R}^2 \times T$ obtained throughout the deformation satisfy all the conditions in Definition 2.*

The reason for introducing the notion of braids is that there exists a natural one-to-one correspondence between joint maneuvers in $\mathbf{P}(0, \mathbf{a}, \mathbf{b})$ and pure braids in $\mathbf{PB}(\mathbf{a}, \mathbf{b})$. To see this, for each $\alpha = \langle \alpha_i \rangle_{i=1}^k \in \mathbf{P}(0, \mathbf{a}, \mathbf{b})$, let $\hat{\alpha}_i$ be the curve in $\mathbb{R}^2 \times T$ joining $(a_i, t_0)$ to $(b_i, t_1)$ defined as the image of the map $t \mapsto (\alpha_i(t), t)$, $t \in T$. Then, it is clear from the definition of $\mathbf{P}(0, \mathbf{a}, \mathbf{b})$ that the $k$-tuple $\langle \hat{\alpha}_i \rangle_{i=1}^k$ of curves is indeed a pure braid in $\mathbf{PB}(\mathbf{a}, \mathbf{b})$, which we shall denote by $\hat{\alpha}$ (see Figure 2.1 for a 3-maneuver in $\mathbf{P}(0, \mathbf{a}, \mathbf{b})$ and its braid representation). The map $\alpha \mapsto \hat{\alpha}$ can be verified to be a bijection between $\mathbf{P}(0, \mathbf{a}, \mathbf{b})$ and $\mathbf{PB}(\mathbf{a}, \mathbf{b})$. Furthermore, the following result is an immediate consequence of the above definitions.

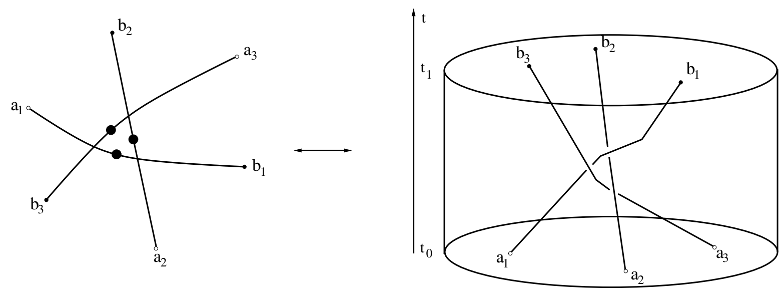


Figure 2.1: A 3-maneuver in $\mathbf{P}(0, \mathbf{a}, \mathbf{b})$ and its braid representation.

**Proposition 1 (Equivalence of 0-homotopy and string isotopy)** *$\alpha$ and $\beta$ in $\mathbf{P}(0, \mathbf{a}, \mathbf{b})$ are 0-homotopic if and only if $\hat{\alpha}$ and $\hat{\beta}$ are string isotopic in $\mathbf{PB}(\mathbf{a}, \mathbf{b})$.*

As a result of Proposition 1, there is a one-to-one correspondence between the 0-homotopy classes of $\mathbf{P}(0, \mathbf{a}, \mathbf{b})$ and the (string) isotopy classes of $\mathbf{PB}(\mathbf{a}, \mathbf{b})$.

We next show that the isotopy classes of braids with identical starting and ending points, say, $\mathbf{B}(\mathbf{a}, \mathbf{a})$, form a group under a suitable product operation. For each $\hat{\alpha} \in \mathbf{B}(\mathbf{a}, \mathbf{b})$ and $\hat{\beta} \in \mathbf{B}(\mathbf{b}, \mathbf{c})$, define the product $\hat{\gamma} \triangleq \hat{\alpha} \cdot \hat{\beta}$ as the braid $\hat{\gamma} \in \mathbf{B}(\mathbf{a}, \mathbf{c})$ obtained by first concatenating the $k$ curves of $\hat{\alpha}$ with those of $\hat{\beta}$, and then renormalizing the $t$ axis linearly such that the resultant $k$ curves connect $\langle (a_i, t_0) \rangle_{i=1}^k$ to $\langle (c_i, t_1) \rangle_{i=1}^k$ via $\langle (b_i, \frac{t_0 + t_1}{2}) \rangle_{i=1}^k$. Note that the ending points of $\hat{\alpha}$ and the starting points of $\hat{\beta}$ have to coincide for the product to be well defined. It can be easily checked that this product operation preserves string isotopy, i.e., if $\hat{\alpha}'$ is string isotopic to $\hat{\alpha}$ in $\mathbf{B}(\mathbf{a}, \mathbf{b})$ and $\hat{\beta}'$ is string isotopic to $\hat{\beta}$ in $\mathbf{B}(\mathbf{b}, \mathbf{c})$, then $\hat{\alpha}' \cdot \hat{\beta}'$ is string isotopic to $\hat{\alpha} \cdot \hat{\beta}$ in $\mathbf{B}(\mathbf{a}, \mathbf{c})$. Therefore, it induces a product operation on the isotopy classes of braids. This induced product operation makes the isotopy classes of $\mathbf{B}(\mathbf{a}, \mathbf{a})$ into a group, with the inverse operation being the reflection of the $k$ curves across the plane $t = \frac{t_0+t_1}{2}$. We denote this group by $\mathbf{B}_k$. Similarly the isotopy classes of pure braids $\mathbf{PB}(\mathbf{a}, \mathbf{a})$ form under the same induced product operation a group, which we denote by $\mathbf{PB}_k$. $\mathbf{PB}_k$ is a normal subgroup of $\mathbf{B}_k$. Readers are referred to [22] or [54] for a detailed derivation of the above claims.

Now if we fix a braid $\hat{\beta}$ in $\mathbf{PB}(\mathbf{b}, \mathbf{a})$, then $\hat{\alpha} \mapsto \hat{\alpha} \cdot \hat{\beta}$ defines a map from $\mathbf{PB}(\mathbf{a}, \mathbf{b})$ to $\mathbf{PB}(\mathbf{a}, \mathbf{a})$. Since this map preserves string isotopy, it induces a map from the isotopy classes of $\mathbf{PB}(\mathbf{a}, \mathbf{b})$ to the isotopy classes of $\mathbf{PB}(\mathbf{a}, \mathbf{a})$, i.e., $\mathbf{PB}_k$. The induced map is easily verified to be a bijection. This fact combined with the result in Proposition 1 implies that there exists a bijection between the 0-homotopy classes of $\mathbf{P}(0, \mathbf{a}, \mathbf{b})$ and the elements of $\mathbf{PB}_k$.

The above conclusions remain valid for the case of an arbitrary $r > 0$. Hence,

**Theorem 1 (Classification of conflict-free $k$-maneuvers)** *There exists a one-to-one correspondence between the $r$-homotopy classes of conflict-free maneuvers in $\mathbf{P}(r, \mathbf{a}, \mathbf{b})$ and the elements of the group of pure $k$-braids $\mathbf{PB}_k$.*

In Remark 1 of Section 2.3, we will give an alternative interpretation of the above result. For a discussion on the use of braid groups to classify motions on a graph, see [1].

The group $\mathbf{PB}_k$ is described by a set of generators together with a set of relations defined on them ([54, 55]). Therefore, Theorem 1 completely characterizes the structure of the homotopy types of conflict-free maneuvers for $k$-agent encounters. On the other hand, the characterization is unsatisfactory in practical terms since the description of $\mathbf{PB}_k$ is very complicated. However, when $k$ is small, the result in Theorem 1 may have simple interpretations. Consider for example the two-agent

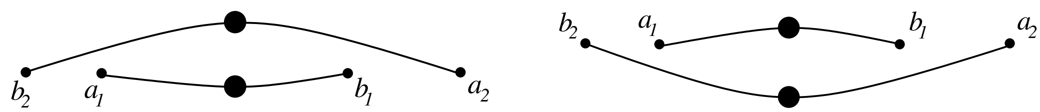


Figure 2.2: A two-agent encounter. Left: Maneuver 1 - Right: Maneuver 2.

encounter shown in Figure 2.2. Theorem 1 says that each maneuver in $\mathbf{P}(0, \mathbf{a}, \mathbf{b})$ is 0-homotopic to maneuver 1, or maneuver 2, or one of the following two maneuvers:

- Maneuver 1 followed by the motions where agent 2 stays at $b_2$, and agent 1 starts from $b_1$, circles around agent 2 counterclockwise $n$ times for some integer $n \geq 1$ and returns to $b_1$.

- Maneuver 2 followed by the motions where agent 2 stays at $b_2$, agent 1 starts from $b_1$, circles around agent 2 clockwise $n$ times for some integer $n \geq 1$ and returns to $b_1$.

The angle one agent turns with respect to the other during $T$ plays a decisive role in determining the homotopy type of the conflict-free 2-maneuvers. Maneuver 1 and maneuver 2 are representatives of the only two types for which the absolute values of this angle do not exceed $360°$. We shall call such types *fundamental*. Then there are exactly two fundamental types for any 2-agent encounter.

It is tempting to extend this definition to the $k$-agent case, and conclude that there are exactly $2^{\frac{k(k-1)}{2}}$ fundamental types of conflict-free maneuvers, since there are two fundamental types for each of the $\frac{k(k-1)}{2}$ agent pairs. Unfortunately this is

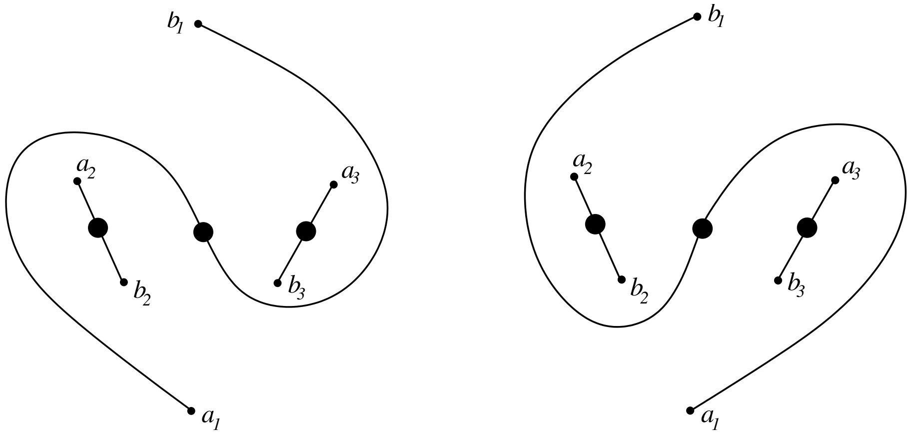


Figure 2.3: Two 3-maneuvers with the same turning angles but of different types.

not the case. Shown in Figure 2.3 are the plots of two conflict-free maneuvers for a 3-agent encounter that have the same turning angle within the range $(-360°, 360°)$ between any pair of agents, but in fact belong to different types.

## 2.3 Optimal conflict-free maneuvers

In this section, the problem of finding optimal conflict-free maneuvers for multi-agent encounters is formulated. To ensure that the problem is well defined and admits a solution, we modify some of the notations introduced in the previous section. In particular, the set of maneuvers for agent $i$, $\mathbf{P}_i$, is redefined to be the set of all continuous *and piecewise* $C^2$ maps[1] from $T$ to $\mathbb{R}^2$ that take the values $a_i$ and $b_i$ at times $t_0$ and $t_1$, respectively. The set of joint maneuvers $\mathbf{P}(\mathbf{a}, \mathbf{b})$ and the MSE $\Delta(\alpha)$, $\alpha \in \mathbf{P}(\mathbf{a}, \mathbf{b})$, are defined as in Section 2.2, whereas $\mathbf{P}(r, \mathbf{a}, \mathbf{b})$ is redefined to

[1]Piecewise $C^2$ means that there is a finite subdivision of $T$ such that the map is continuously differentiable till the second order on each (open) subinterval. In the sequel when we use $\dot{\alpha}_i(t), \ddot{\alpha}_i(t)$, we shall mean at those $t$ where they are well defined, i.e., except at a finite set of time instants $t$.

be the set of all joint maneuvers with a MSE greater than *or equal to* $r$. Note that the results in Section 2.2 on the qualitative classification of conflict-free maneuvers still hold for the newly defined $\mathbf{P}(r, \mathbf{a}, \mathbf{b})$ by the compactness of $T$.

Consider a maneuver of a single agent, say $\alpha_i \in \mathbf{P}_i$, $i \in \{1, \ldots, k\}$. The *energy* of $\alpha_i$ is defined as

$$J(\alpha_i) = \frac{1}{2} \int_{t_0}^{t_1} ||\dot{\alpha}_i(t)||^2 \, dt. \tag{2.1}$$

Let $l_{\alpha_i}$ be the arc length of the curve $\alpha_i$, i.e., $l_{\alpha_i} = \int_{t_0}^{t_1} ||\dot{\alpha}_i(t)|| \, dt$. Then the application of Cauchy-Schwarz inequality to equation (2.1) yields ([50]):

$$J(\alpha_i) \geq \frac{1}{2} \frac{l_{\alpha_i}^2}{(t_1 - t_0)}, \tag{2.2}$$

where the equality holds if and only if $\|\dot{\alpha}_i(t)\|$ is constant. This implies that if agent $i$ is forced to move along some fixed curve and if we ignore the presence of other agents temporarily, then of all the different parameterizations, the one with a constant speed has the minimal energy, and the minimal energy is proportional to the square of the curve length. Therefore, in the presence of *static* obstacles, the maneuver of agent $i$ with the least energy is the shortest curve between its starting and ending positions parameterized proportionally to the arc length. In particular, if there are no obstacles, the energy-minimizing maneuver of agent $i$ is the constant speed motion along the line segment from $a_i$ to $b_i$. It follows from this discussion that the energy-minimizing maneuvers tend to be straighter and smoother, which has practical implications, for example, in terms of passenger comfort, brake erosion, fuel consumption, etc.

The *(weighted) energy* of a joint maneuver $\alpha = \langle \alpha_i \rangle_{i=1}^k \in \mathbf{P}(\mathbf{a}, \mathbf{b})$ is defined as

$$J(\alpha) \triangleq \sum_{i=1}^{k} \lambda_i J(\alpha_i), \tag{2.3}$$

where $\lambda_1, \ldots, \lambda_k$ are $k$ positive numbers adding up to 1 (i.e., $\sum_{i=1}^{k} \lambda_i = 1$) representing the priorities of the agents.

Our goal is to find the conflict-free maneuver with the least energy, i.e.,

$$\text{minimize } J(\alpha) \text{ subject to } \alpha \in \mathbf{P}(r, \mathbf{a}, \mathbf{b}). \tag{2.4}$$

If $\alpha$ is required to belong to a certain type in $\mathbf{P}(r, \mathbf{a}, \mathbf{b})$, then we get a restricted version of problem (2.4). All the necessary conditions obtained in the next section remain valid for the restricted problem, with the only exception of Proposition 4.

**Remark 1 (Geodesics in a manifold with boundary)** *Problem (2.4) can also be formulated in an alternative way. By viewing $\alpha \in \mathbf{P}(\mathbf{a}, \mathbf{b})$ as a curve in $\mathbb{R}^{2k}$, and $\mathbf{a}, \mathbf{b}$ as two points in $\mathbb{R}^{2k}$, a conflict-free maneuver in $\mathbf{P}(r, \mathbf{a}, \mathbf{b})$ corresponds to a curve in $\mathbb{R}^{2k}$ joining $\mathbf{a}$ to $\mathbf{b}$ and avoiding the obstacle $W$ defined by*

$$W = \{\langle p_i \rangle_{i=1}^{k} \in \mathbb{R}^{2k} : p_i \in \mathbb{R}^2, 1 \leq i \leq k, \text{ and } \|p_i - p_j\| < r \text{ for some } i \neq j\}.$$

*If the coefficients $\lambda_i$, $i = 1, \ldots, k$, are identical, then the energy of a joint maneuver is proportional to the energy of the corresponding curve in $\mathbb{R}^{2k}$. Therefore, problem (2.4) is equivalent to finding the curve in $\mathbb{R}^{2k} \setminus W$ joining $\mathbf{a}$ to $\mathbf{b}$ with the least energy, which is necessarily a minimizing geodesic of $\mathbb{R}^{2k} \setminus W$ connecting $\mathbf{a}$ to $\mathbf{b}$. Note that $\mathbb{R}^{2k} \setminus W$ is a manifold with nonsmooth boundary whose fundamental group is isomorphic to $\mathbf{PB}_k$ by Theorem 1. The general case of arbitrary $\langle \lambda_i \rangle_{i=1}^{k}$ can be reduced to this special case by scaling the $p_i$ axes of $\mathbb{R}^{2k}$ by a factor of $\sqrt{\lambda_i}$, $i = 1, \ldots, k$. The interested readers are referred to [30] for further details.*

## 2.4 Analytical results

This section is devoted to the analytical derivation of optimal solutions to problem (2.4), a variational problem with complicated and nonsmooth constraints. Inspired by the braid representation introduced in Section 2.2, we propose various transformations of joint maneuvers that preserve the MSE, and use these transformations in the variational analysis to obtain necessary conditions for optimal conflict-free maneuvers.

### 2.4.1 $\lambda$-alignment of optimal conflict-free maneuvers

As explained in Section 2.2, each conflict-free maneuver $\alpha \in \mathbf{P}(r, \mathbf{a}, \mathbf{b})$ has a natural braid representation $\hat{\alpha} \in \mathbf{PB}(\mathbf{a}, \mathbf{b})$, whose $k$ strings are determined by the images of the maps $t \mapsto (\alpha_i(t), t)$, $t \in T$, $i = 1, \ldots, k$. Furthermore, $\hat{\alpha}$ satisfies the *$r$-separation property* in that the intersection of $\hat{\alpha}$ with the plane $t = \tau$ for any $\tau \in T$ consists of $k$ points whose pairwise minimum distance is at least $r$. All the operations on conflict-free maneuvers we shall introduce in the following preserve this separation property in the braid representation, hence they are indeed transformations of conflict-free maneuvers.

We first introduce the tilt operation. For each $w \in \mathbb{R}^2$, denote by $\mathbf{b} + w$ the $k$-tuple $\langle b_i + w \rangle_{i=1}^{k}$.

**Definition 4 (Tilt operator $\mathcal{T}_w$)** *The tilt operator $\mathcal{T}_w : \mathbf{P}(r, \mathbf{a}, \mathbf{b}) \to \mathbf{P}(r, \mathbf{a}, \mathbf{b} + w)$ is a map such that for any $\alpha \in \mathbf{P}(r, \mathbf{a}, \mathbf{b})$, $\beta = \mathcal{T}_w(\alpha)$ is defined by*

$$\beta_i(t) = \alpha_i(t) + \frac{t - t_0}{t_1 - t_0} w, \quad t \in T, \quad i = 1, \ldots, k.$$

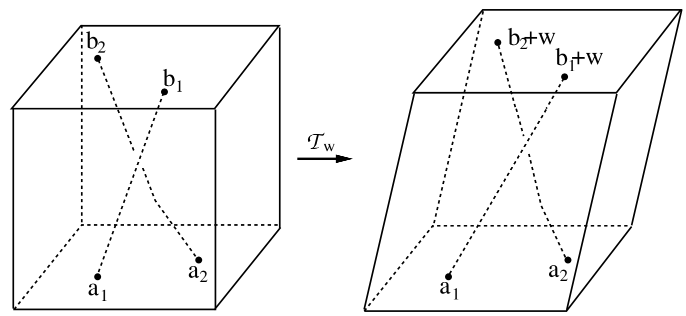


Figure 2.4: Tilt operation $\mathcal{T}_w$ on a 2-maneuver.

It is easily seen that $\mathcal{T}_w$ is *MSE-preserving* in the sense that $\alpha$ and $\mathcal{T}_w(\alpha)$ have the same MSE. Hence $\mathcal{T}_w$ maps $\mathbf{P}(r, \mathbf{a}, \mathbf{b})$ into $\mathbf{P}(r, \mathbf{a}, \mathbf{b} + w)$. In fact, $\mathcal{T}_w$ is a bijection from $\mathbf{P}(r, \mathbf{a}, \mathbf{b})$ to $\mathbf{P}(r, \mathbf{a}, \mathbf{b} + w)$ since $\mathcal{T}_w \circ \mathcal{T}_{-w} = \mathcal{T}_{-w} \circ \mathcal{T}_w = id$. In the braid representation, $\hat{\beta}$ is obtained by tilting $\hat{\alpha}$ linearly, hence the name for the operator $\mathcal{T}_w$. More precisely, in order to get $\hat{\beta}$ from $\hat{\alpha}$, the plane $t = t_0$ is kept invariant (shifted by 0), the plane $t = t_1$ is shifted by $w$, and each intermediate plane $t = \tau$, $\tau \in (t_0, t_1)$, is shifted by an amount determined by the linear interpolation of 0 and $w$ according to the position of $\tau$ in $T$. Figure 2.4 illustrates the effect of the $\mathcal{T}_w$ operator on the braid representation of a 2-maneuver.

The importance of introducing $\mathcal{T}_w$ lies in the following result.

**Proposition 2** *Suppose that $\alpha^*$ is a conflict-free maneuver in $\mathbf{P}(r, \mathbf{a}, \mathbf{b})$ with the least energy. Fix $w \in \mathbb{R}^2$. Then $\beta^* = \mathcal{T}_w(\alpha^*)$ is a conflict-free maneuver in $\mathbf{P}(r, \mathbf{a}, \mathbf{b}+ w)$ with the least energy.*

**Proof:** For any $\beta \in \mathbf{P}(r, \mathbf{a}, \mathbf{b} + w)$, let $\alpha = \mathcal{T}_{-w}(\beta)$. Then $\alpha \in \mathbf{P}(r, \mathbf{a}, \mathbf{b})$ and $J(\beta)$

can be expressed as

$$\begin{aligned} J(\beta) &= \frac{1}{2}\int_{t_0}^{t_1}\sum_{i=1}^{k}\lambda_i\|\dot{\beta}_i(t)\|^2\,dt = \frac{1}{2}\int_{t_0}^{t_1}\sum_{i=1}^{k}\lambda_i\Big\|\dot{\alpha}_i(t)+\frac{w}{t_1-t_0}\Big\|^2\,dt \\ &= \frac{1}{2}\int_{t_0}^{t_1}\sum_{i=1}^{k}\lambda_i\|\dot{\alpha}_i(t)\|^2\,dt + \int_{t_0}^{t_1}\frac{w^T}{t_1-t_0}\sum_{i=1}^{k}\lambda_i\dot{\alpha}_i(t)\,dt + \frac{\|w\|^2}{2(t_1-t_0)} \\ &= J(\alpha) + \frac{w^T[\sum_{i=1}^{k}\lambda_i(b_i-a_i)+w/2]}{t_1-t_0}. \end{aligned} \tag{2.5}$$

Note that the second term in the last equation of (2.5) is a constant independent of $\beta$. Denote it by $C$. It follows by equation (2.5) and the optimality of $\alpha^*$ that $J(\beta) \geq J(\alpha^*) + C$, $\forall\beta \in \mathbf{P}(r, \mathbf{a}, \mathbf{b} + w)$, with the equality if $\alpha = \alpha^*$, i.e., $\beta = \beta^*$. ∎

Consider arbitrary starting and destination positions $\mathbf{a}$ and $\mathbf{b}$, and set $\mathbf{b}' \triangleq \mathbf{b} + w$ where $w = \sum_{i=1}^{k}\lambda_i(a_i - b_i)$. Then $\mathbf{a}$ and $\mathbf{b}'$ are $\lambda$-*aligned* in the sense that they have the same $\lambda$-centroid, i.e.,

$$\sum_{i=1}^{k}\lambda_i a_i = \sum_{i=1}^{k}\lambda_i b'_i. \tag{2.6}$$

By Proposition 2, solutions to problem (2.4) for general $\mathbf{a}$ and $\mathbf{b}$ can be obtained from solutions to problem (2.4) for $\lambda$-aligned $\mathbf{a}$ and $\mathbf{b}'$ by applying the tilt operator $\mathcal{T}_{-w}$ with $w = \sum_{i=1}^{k}\lambda_i(a_i - b_i)$. This is the reason why we can focus on the special case of $\lambda$-aligned $\mathbf{a}$ and $\mathbf{b}$.

The next transformation we shall introduce is the *drift operation*. Let $\gamma : T \to \mathbb{R}^2$ be a continuous and piecewise $C^2$ map such that $\gamma(t_0) = \gamma(t_1) = 0$.

**Definition 5 (Drift operator $\mathcal{D}_\gamma$)** *The drift operator $\mathcal{D}_\gamma : \mathbf{P}(r, \mathbf{a}, \mathbf{b}) \to \mathbf{P}(r, \mathbf{a}, \mathbf{b})$ is a map such that for any $\alpha \in \mathbf{P}(r, \mathbf{a}, \mathbf{b})$, $\beta = \mathcal{D}_\gamma(\alpha)$ is defined by*

$$\beta_i(t) = \alpha_i(t) + \gamma(t), \quad t \in T, \quad i = 1, \ldots, k.$$

In the braid representation, $\hat{\beta}$ is obtained from $\hat{\alpha}$ by drifting each plane $t = \tau$, $\tau \in T$, by an offset $\gamma(\tau) \in \mathbb{R}^2$. It can be verified that $\mathcal{D}_\gamma$ is MSE-preserving and a bijection of $\mathbf{P}(r, \mathbf{a}, \mathbf{b})$ onto itself since $\mathcal{D}_\gamma \circ \mathcal{D}_{-\gamma} = \mathcal{D}_{-\gamma} \circ \mathcal{D}_\gamma = id$. By using the drift operator, we can prove the following result.

**Proposition 3** *Suppose that* $\mathbf{a}$ *and* $\mathbf{b}$ *are* $\lambda$*-aligned and* $\alpha^* \in \mathbf{P}(r, \mathbf{a}, \mathbf{b})$ *is an optimal solution to problem (2.4). Then*

$$\sum_{i=1}^{k} \lambda_i \alpha_i^*(t) = \sum_{i=1}^{k} \lambda_i a_i = \sum_{i=1}^{k} \lambda_i b_i, \quad \forall t \in T.$$

**Proof:** For each $s \in \mathbb{R}$ define $\beta_s \triangleq \mathcal{D}_{s\gamma}(\alpha^*)$. Note that $\beta_s \in \mathbf{P}(r, \mathbf{a}, \mathbf{b})$ and $\beta_0 = \alpha^*$. Moreover,

$$\begin{aligned} J(\beta_s) &= \frac{1}{2} \int_{t_0}^{t_1} \sum_{i=1}^{k} \lambda_i \|\dot{\alpha}_i^*(t) + s\dot{\gamma}(t)\|^2 \, dt \\ &= J(\alpha^*) + \frac{s^2}{2} \int_{t_0}^{t_1} \|\dot{\gamma}(t)\|^2 \, dt + s \int_{t_0}^{t_1} \dot{\gamma}(t)^T \sum_{i=1}^{k} \lambda_i \dot{\alpha}_i^*(t) \, dt \,. \end{aligned}$$

The difference $J(\beta_s) - J(\alpha^*)$ is a quadratic function of $s$, which, by the optimality of $\alpha^*$, must be nonnegative for all $s$. Hence we have $\int_{t_0}^{t_1} \dot{\gamma}(t)^T \sum_{i=1}^{k} \lambda_i \dot{\alpha}_i^*(t) \, dt = 0$, which must hold for any choice of $\gamma$ such that $\gamma(t_0) = \gamma(t_1) = 0$. Since $\mathbf{a}$ and $\mathbf{b}$ are $\lambda$-aligned, we can choose $\gamma(t) = \sum_{i=1}^{k} \lambda_i \alpha_i^*(t) - \sum_{i=1}^{k} \lambda_i a_i$. Given that $\alpha^*$ is piecewise $C^2$, this leads to $\sum_{i=1}^{k} \lambda_i \dot{\alpha}_i^*(t) = 0$ for almost all $t \in T$, and hence, by integration, to the desired conclusion. ■

We can now use Proposition 2 to get the formulation of Proposition 3 for arbitrary $\mathbf{a}$ and $\mathbf{b}$.

**Corollary 1** *Suppose that $\alpha^* \in \mathbf{P}(r, \mathbf{a}, \mathbf{b})$ is an optimal solution to problem (2.4). Then*

$$\sum_{i=1}^{k} \lambda_i \alpha_i^*(t) = \sum_{i=1}^{k} \lambda_i a_i + \frac{t - t_0}{t_1 - t_0} (\sum_{i=1}^{k} \lambda_i b_i - \sum_{i=1}^{k} \lambda_i a_i), \quad \forall t \in T.$$

In other words, the $\lambda$-centroid of $\langle \alpha_i^*(t) \rangle_{i=1}^k$ moves from the $\lambda$-centroid of $\mathbf{a}$ at time $t_0$ to the $\lambda$-centroid of $\mathbf{b}$ at time $t_1$ with constant velocity.

**Remark 2** *A geometric interpretation of Corollary 1 can be given as follows. Suppose for simplicity that the $\lambda_i$'s are identical. Let $W$ be the obstacle in $\mathbb{R}^{2k}$ defined as in Remark 1. An important observation is that $W$ is cylindrical in the direction of the 2-dimensional subspace $N$ spanned by vectors $(1, 0, 1, 0, \ldots, 1, 0)^T$ and $(0, 1, 0, 1, \ldots, 0, 1)^T$ in $\mathbb{R}^{2k}$, in the sense that for any $x \in \mathbb{R}^{2k}$, $x \in W$ if and only if $x + N \subset W$. Let $V$ be the orthogonal complement of $N$ in $\mathbb{R}^{2k}$. Then $\mathbf{a}$ and $\mathbf{b}$ are $\lambda$-aligned if and only if $\mathbf{a}$ and $\mathbf{b}$ are on the same $V$-slice in $\mathbb{R}^{2k}$, i.e., if and only if $\mathbf{a} - \mathbf{b} \in V$. The conclusions of Proposition 2 and Corollary 1 say that for $\mathbf{a}$ and $\mathbf{b}$ that are not necessarily $\lambda$-aligned, the shortest geodesic in $\mathbb{R}^{2k} \setminus W$ from $\mathbf{a}$ to $\mathbf{b}$ can be decomposed into two parts: its projection onto $N$, which is a constant speed motion along the straight line from $\pi_N(\mathbf{a})$ to $\pi_N(\mathbf{b})$, where $\pi_N : \mathbb{R}^{2k} \to N$ denotes the orthogonal projection map onto $N$; and its projection onto $V$, which is the shortest geodesic in $V \cap W^c$ connecting $\pi_V(\mathbf{a})$ and $\pi_V(\mathbf{b})$, where $\pi_V : \mathbb{R}^{2k} \to V$ denotes the orthogonal projection map onto $V$. Since $V$ is of dimension $2k - 2$, this effectively reduces the dimension of the problem by $2$.*

### 2.4.2 Optimal conflict-free maneuvers for two agents

We now show that the solution to problem (2.4) in the case when there are only two agents follows directly from Corollary 1.

Assume that $\mathbf{a} = (a_1, a_2)$ and $\mathbf{b} = (b_1, b_2)$ are $\lambda$-aligned, and denote by $c$ their common $\lambda$-centroid. If $\alpha^* = (\alpha_1^*, \alpha_2^*) \in \mathbf{P}(r, \mathbf{a}, \mathbf{b})$ is an optimal solution to problem (2.4), then, by Proposition 3, the $\lambda$-centroid of $\alpha_1^*(t)$ and $\alpha_2^*(t)$ is equal to $c$ for any $t \in T$, or equivalently,

$$\alpha_1^*(t) - c = -\frac{\lambda_2}{\lambda_1}(\alpha_2^*(t) - c), \quad \forall t \in T. \tag{2.7}$$

From equation (2.7), it then follows that the energies of $\alpha_1^*$ and $\alpha_2^*$ are related by $\lambda_1^2 J(\alpha_1^*) = \lambda_2^2 J(\alpha_2^*)$, and that the separation constraint $\|\alpha_1^*(t) - \alpha_2^*(t)\| \geq r$ is equivalent to $\|\alpha_1^*(t) - c\| \geq \lambda_2 r$. Therefore, problem (2.4) can be reduced to

$$\text{minimize } J(\alpha_1) \text{ subject to } \alpha_1 \in \mathbf{P}_1 \text{ and } \alpha_1 : T \to B^c(c, \lambda_2 R), \tag{2.8}$$

where $B^c(c, \lambda_2 R)$ denotes the complement in $\mathbb{R}^2$ of the open disk of radius $\lambda_2 r$ centered at $c$. Thus the problem becomes finding the minimum energy maneuver for a single agent in the presence of the static obstacle $B(c, \lambda_2 R)$.

By assumption, both $a_1$ and $b_1$ belong to $B^c(c, \lambda_2 R)$ since otherwise the problem is infeasible. From the discussion at the beginning in Section 2.3, we know that the optimal solution to problem (2.8) is a constant speed motion along the shortest curve joining $a_1$ to $b_1$ while avoiding the obstacle $B(c, \lambda_2 R)$. Let $\partial B$ be the boundary of the disk $B(c, \lambda_2 R)$. The geometric construction of the shortest curve within a given fundamental type is shown in Figure 2.5. The curve is composed of three pieces: first from $a_1$ to $p_1 \in \partial B$ along a straight line tangent to $\partial B$, then from $p_1$ to $q_1$ along $\partial B$, and finally from $q_1$ to $b_1$ along another straight line tangent to

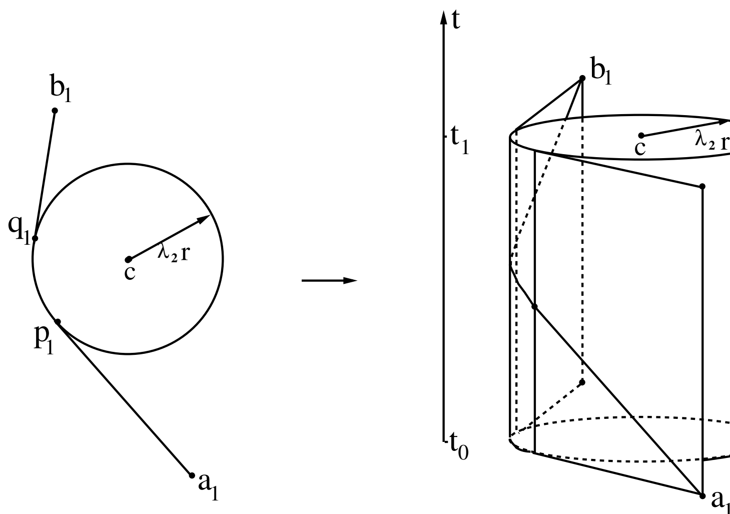


Figure 2.5: An optimal 2-maneuver and its braid representation.

$\partial B$. Here choosing a fundamental type is equivalent to choosing a side of the cylinder in the braid representation. The globally optimal solution $\alpha_1^*$ is the one of the two locally optimal solutions with shorter arc length (or either one of them if they have the same length). $\alpha_2^*$ is then obtained from $\alpha_1^*$ by equation (2.7). This is for the $\lambda$-aligned case. Denote by $\gamma_i^*(\mathbf{a}, \mathbf{b})$, $i = 1, 2$, the obtained optimal maneuvers. For the general case when $\mathbf{a}$ and $\mathbf{b}$ are not necessarily $\lambda$-aligned, we have by Proposition 2

**Theorem 2 (Optimal conflict-free 2-maneuver)** *If $k = 2$, then the optimal solution $\alpha^* \in \mathbf{P}(r, \mathbf{a}, \mathbf{b})$ to problem (2.4) is given by:*

$$\begin{cases} \alpha_1^*(t) = \gamma_1^*(\mathbf{a}, \mathbf{b} + w)(t) - \frac{t - t_0}{t_1 - t_0} w \\ \alpha_2^*(t) = \gamma_2^*(\mathbf{a}, \mathbf{b} + w)(t) - \frac{t - t_0}{t_1 - t_0} w \end{cases}, \quad \forall t \in T, \tag{2.9}$$

*where $w = \lambda_1 a_1 - \lambda_1 b_1 + \lambda_2 a_2 - \lambda_2 b_2$.*

Consider the case when the priority of agent 1 is much higher than that

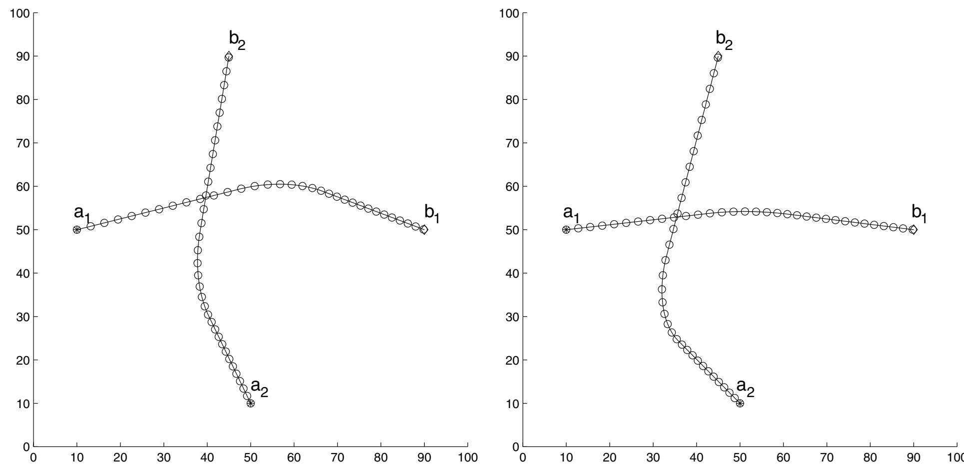


Figure 2.6: Optimal 2-maneuvers ($r = 30$). Left: $\lambda_1 = \lambda_2 = 0.5$, Right: $\lambda_1 = 0.8$, $\lambda_2 = 0.2$.

of agent 2, which can be modeled by $\lambda_2 \simeq 0$. In the $\lambda$-aligned case, this implies $a_1 \simeq b_1 \simeq c$, and that the radius of the disk $B(c, \lambda_2 R)$ is about 0. Therefore, $\gamma_1^*$ is nearly a zero motion. For general **a** and **b**, it follows from Theorem 2 that the optimal maneuver for agent 1 is almost a constant speed motion along the line segment from $a_1$ to $b_1$. Hence, as expected, agent 2 is the one assuming most of the responsibility of avoiding conflicts.

Shown in Figure 2.6 are the plots of optimal conflict-free maneuvers for a typical 2-agent encounter with two different sets of priorities. The circles represent the positions of the two agents at evenly distributed time instants. The plots show that, in the case when **a** and **b** are not $\lambda$-aligned, the speeds of the agents in the optimal maneuvers are not constant. As the priority of agent 1 increases, however, its optimal maneuver gets closer to the constant speed motion along the straight line connecting $a_1$ to $b_1$.

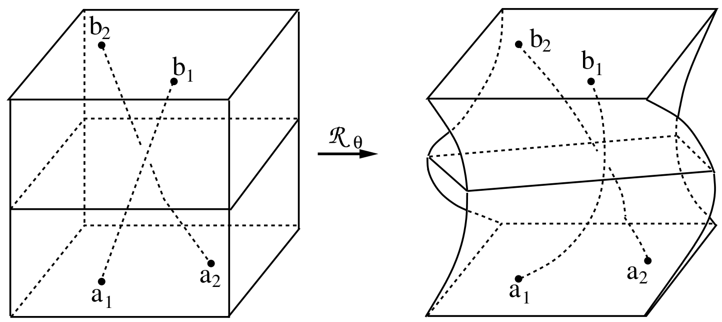


Figure 2.7: Twist operation $\mathcal{R}_\theta$ on a 2-maneuver.

### 2.4.3 Twist optimality

Another MSE-preserving operator can be introduced as follows. Suppose that $\theta : T \to \mathbb{R}$ is a continuous and piecewise $C^2$ map satisfying $\theta(t_0) = 0$, $\theta(t_1) = 2n\pi$ for some $n \in \mathbb{Z}$.

**Definition 6 (Twist operator $\mathcal{R}_\theta$)** *The twist operator $\mathcal{R}_\theta$ is defined as the map from $\mathbf{P}(r, \mathbf{a}, \mathbf{b})$ to $\mathbf{P}(r, \mathbf{a}, \mathbf{b})$ such that for any $\alpha \in \mathbf{P}(r, \mathbf{a}, \mathbf{b})$, $\beta = \mathcal{R}_\theta(\alpha)$ is given by*

$$\beta_i(t) = T[\theta(t)]\alpha_i(t), \quad t \in T, \quad i = 1, \ldots, k,$$

*where $T[\theta(t)]$ is the matrix corresponding to a rotation of $\theta(t)$ counterclockwise:*

$$T[\theta(t)] = \begin{pmatrix} \cos[\theta(t)] & -\sin[\theta(t)] \\ \sin[\theta(t)] & \cos[\theta(t)] \end{pmatrix}.$$

The constraints on $\theta(t_0)$ and $\theta(t_1)$ ensure that $\mathcal{R}_\theta(\alpha)$ and $\alpha$ have the same starting and ending positions. It is easy to see that $\mathcal{R}_\theta$ is MSE-preserving and hence has its image in $\mathbf{P}(r, \mathbf{a}, \mathbf{b})$. Figure 2.7 shows the effect of $\mathcal{R}_\theta$ ($n = 0$) on the braid representation of a 2-maneuver.

By considering the perturbed maneuvers generated by $\mathcal{R}_\theta$, we have

**Proposition 4** *Suppose that $\alpha^* \in \mathbf{P}(r, \mathbf{a}, \mathbf{b})$ is an optimal solution to problem (2.4). Then for any $q \in \mathbb{R}^2$,*

$$\frac{1}{2}\sum_{i=1}^{k} \lambda_i(\alpha_i^*(t) - q)^t T(\pi/2)\dot{\alpha}_i^*(t) = C, \quad \forall t \in T, \tag{2.10}$$

*where $C$ is a constant in $[-\frac{\pi}{z}, \frac{\pi}{z}]$, with $z \triangleq 2\int_{t_0}^{t_1}\left[\sum_{i=1}^{k}\lambda_i\|\alpha_i^*(t) - q\|^2\right]^{-1} dt$.*

**Proof:** Consider first the case when $q = 0$. For each $\alpha \in \mathbf{P}(r, \mathbf{a}, \mathbf{b})$, let $\beta = \mathcal{R}_\theta(\alpha)$. Then for $i = 1, \ldots, k$,

$$\dot{\beta}_i(t) = T[\theta(t)]\dot{\alpha}_i(t) + \left(\frac{d}{dt}T[\theta(t)]\right)\alpha_i(t) = T[\theta(t)]\dot{\alpha}_i(t) + \dot{\theta}(t)T[\theta(t) + \pi/2]\alpha_i(t).$$

Since $T[\theta(t)]$ and $T[\theta(t)+\pi/2]$ are orthonormal and $T^t[\theta(t)+\pi/2] = T[-\theta(t)-\pi/2]$, we have

$$\|\dot{\beta}_i(t)\|^2 = \|\dot{\alpha}_i(t)\|^2 + \|\alpha_i(t)\|^2|\dot{\theta}(t)|^2 + 2\dot{\theta}(t)\alpha_i^t(t)T(-\pi/2)\dot{\alpha}_i(t), \quad i = 1, \ldots, k\,.$$

Integrating and summing over $i$, we can write the cost difference $\Delta J(\theta)$ as

$$\Delta J(\theta) = J(\beta) - J(\alpha) = \int_{t_0}^{t_1} [f_1(t)|\dot{\theta}(t)|^2 + 2f_2(t)\dot{\theta}(t)]\, dt\,, \tag{2.11}$$

where $f_1$ and $f_2$ are functions defined by

$$f_1(t) \triangleq \frac{1}{2}\sum_{i=1}^{k}\lambda_i\|\alpha_i(t)\|^2, \quad f_2(t) \triangleq \frac{1}{2}\sum_{i=1}^{k}\lambda_i\alpha_i^t(t)T(-\pi/2)\dot{\alpha}_i(t), \quad \forall t \in T\,. \tag{2.12}$$

Note that we use the notation $\Delta J(\theta)$ to indicate its dependence on $\theta$. We next compute the optimal twist $\theta^*$ such that $\Delta J(\theta)$ is minimized. $\theta$ is subject to the constraint that $\theta(t_0) = 0$, $\theta(t_1) = 2n\pi$ for some *fixed* $n \in \mathbb{Z}$. For $\dot{\theta}$, this translates into $\int_{t_0}^{t_1}\dot{\theta}(t)\, dt = 2n\pi$. We can then write the Lagrangian function for this variational problem as

$$\begin{aligned}\mathcal{L}(\dot\theta,\mu) &\triangleq \Delta J(\theta) + \mu\left[\int_{t_0}^{t_1}\dot\theta(t)\,dt - 2n\pi\right]\\ &= \int_{t_0}^{t_1}\left\{f_1(t)\left[\dot\theta(t)+\frac{f_2(t)+\frac{\mu}{2}}{f_1(t)}\right]^2 - \frac{[f_2(t)+\frac{\mu}{2}]^2}{f_1(t)}\right\}dt - 2\mu n\pi\,,\end{aligned}$$

where $\mu$ is the Lagrangian multiplier. Thus $\dot\theta^*(t) = -[f_2(t)+\mu^*/2]/f_1(t)$ where, since $\int_{t_0}^{t_1}\dot\theta(t)\,dt = 2n\pi$, $\mu^*$ is given by:

$$\mu^* = -2\left[\int_{t_0}^{t_1}\frac{f_2(t)}{f_1(t)}\,dt + 2n\pi\right]\Big/\int_{t_0}^{t_1}\frac{1}{f_1(t)}\,dt.$$

Then, we have the following expression for $\dot\theta^*(t)$:

$$\dot\theta^*(t) = -\frac{f_2(t)}{f_1(t)} + \left[\int_{t_0}^{t_1}\frac{f_2(t)}{f_1(t)}\,dt + 2n\pi\right]\Big/\left[f_1(t)\int_{t_0}^{t_1}\frac{1}{f_1(t)}\,dt\right].$$

Substituting this into equation (2.11), we get the minimal $\Delta J(\theta)$:

$$\Delta J(\theta^*) = \left[\int_{t_0}^{t_1}\frac{f_2(t)}{f_1(t)}\,dt + 2n\pi\right]^2\Big/\int_{t_0}^{t_1}\frac{1}{f_1(t)}\,dt - \int_{t_0}^{t_1}\frac{f_2^2(t)}{f_1(t)}\,dt\,.$$

If $\alpha = \alpha^*$ is an optimal maneuver, then $\Delta J(\theta^*) \geq 0$. Hence,

$$\left[\int_{t_0}^{t_1}\frac{f_2(t)}{f_1(t)}\,dt + 2n\pi\right]^2 \geq \int_{t_0}^{t_1}\frac{1}{f_1(t)}\,dt\cdot\int_{t_0}^{t_1}\frac{f_2^2(t)}{f_1(t)}\,dt\,. \tag{2.13}$$

In the case when $n = 0$, the equality holds in equation (2.13) since the lower bound $\Delta J(\theta^*) \geq 0$ can be strictly achieved by choosing $\theta^*(t) \equiv 0$. Therefore,

$$\left[\int_{t_0}^{t_1}\frac{f_2(t)}{f_1(t)}\,dt\right]^2 = \int_{t_0}^{t_1}\frac{1}{f_1(t)}\,dt\cdot\int_{t_0}^{t_1}\frac{f_2^2(t)}{f_1(t)}\,dt\,.$$

Applying the Cauchy-Schwarz inequality to functions $1/\sqrt{f_1(t)}$ and $f_2(t)/\sqrt{f_1(t)}$, we have that the above equality holds if and only if $f_2(t)/\sqrt{f_1(t)} = C/\sqrt{f_1(t)}$ for some constant $C$, i.e., if and only if $f_2(t) \equiv C$. In this case, equation (2.13) degenerates into:

$$(Cz + 2n\pi)^2 \geq C^2z^2, \quad \forall n \in \mathbb{Z}\,,$$

with $z = \int_{t_0}^{t_1} 1/f_1(t)\,dt$, or equivalently, $n\pi Cz + n^2\pi^2 \geq 0$ for all $n \in \mathbb{Z}$. This is possible if and only if $-\pi \leq Cz \leq \pi$, thus completing the proof for the case $q = 0$.

The general case when $q \neq 0$ can be reduced to the above case by first noticing that the optimality of $\alpha^*$ in $\mathbf{P}(r, \mathbf{a}, \mathbf{b})$ implies the optimality of $\alpha^* - q = \langle \alpha_i^* - q \rangle_{i=1}^k$ in $\mathbf{P}(r, \mathbf{a} - q, \mathbf{b} - q)$, and then applying the results proved for the case $q = 0$ to the optimal maneuver $\alpha^* - q$. ■

If $n \neq 0$, then the operator $\mathcal{R}_\theta$ changes the homotopy type of conflict-free maneuvers in $\mathbf{P}(r, \mathbf{a}, \mathbf{b})$, thus enabling us to compare the performance of conflict-free maneuvers of different types. In this sense, the result in Proposition 4 is global. We illustrate this statement by the following example.

**Example 1** *Assume that* $k = 2$ *and* $\lambda_1 = \lambda_2 = \frac{1}{2}$. *Let* $t_0 = 0$ *and* $t_1 = \tau$ *for some* $\tau \in (0, 2\pi)$. *Set* $a_1 = \frac{r}{2}(1, 0)^t$, $b_1 = \frac{r}{2}(\cos\tau, \sin\tau)^t$, $a_2 = -a_1$ *and* $b_2 = -b_1$. *Consider the conflict-free maneuvers* $\alpha$ *and* $\beta$ *in* $\mathbf{P}(r, \mathbf{a}, \mathbf{b})$ *defined by* $\alpha_1(t) = \frac{r}{2}(\cos t,\, \sin t)^t$, $\alpha_2(t) = -\alpha_1(t)$, *and* $\beta_1(t) = \frac{r}{2}(\cos(\frac{\tau - 2\pi}{\tau} t),\ \sin(\frac{\tau - 2\pi}{\tau} t))^t$, $\beta_2(t) = -\beta_1(t)$, *for all* $t \in [0, \tau]$. *The two agents under maneuver* $\alpha$ *(*$\beta$*) rotate around the origin at constant angular velocity counterclockwise (clockwise) during* $[0, \tau]$. *Note that* $\beta$ *can be obtained from* $\alpha$ *by applying the twist operator* $\mathcal{R}_\theta$ *with* $\theta(t) = -2\pi t/\tau$ *satisfying* $\theta(\tau) = -2\pi$, *and that* $\alpha$ *and* $\beta$ *belong to different types. Since* $\mathbf{a}$ *and* $\mathbf{b}$ *are* $\lambda$*-aligned, the results in Section 2.4.2 imply that* $\alpha$ *and* $\beta$ *are the optimal solutions to problem (2.4) restricted to the two fundamental types. The global optimal solution is the one of them with smaller arc length, which can be easily seen to be* $\alpha$ *if* $\tau \in (0, \pi)$ *and* $\beta$ *if* $\tau \in (\pi, 2\pi)$. *This conclusion can also be reached directly by an application of Proposition 4. In fact, if we choose* $q = 0$ *and compute* $C$ *and* $z$ *defined in Proposition 4 with* $\alpha$ *in the place of* $\alpha^*$, *we get* $C = r^2/8$ *and* $z = 8\tau/r^2$, *and the inequality $|C| \leq \pi/z$ becomes $\tau \leq \pi$, which implies that $\alpha$ is not globally optimal for $\tau \in (\pi, 2\pi)$. If we compute $C$ and $z$ with $\beta$ in the place of $\alpha^*$, we get $C = r^2(\tau - 2\pi)/8\tau$ and $z = 8\tau/r^2$, and the inequality $|C| \leq \pi/z$ becomes $\tau \geq \pi$. Hence $\beta$ is not globally optimal for $\tau \in (0, \pi)$.*

Note that by choosing different $q \in \mathbb{R}^2$, Proposition 4 provides a family of inequalities of the form $-\frac{\pi}{z} \leq C \leq \frac{\pi}{z}$ that an optimal solution $\alpha^*$ to problem (2.4) must satisfy, where $C$ and $z$ are functions of $q$ and $\alpha^*$. In the case when $\mathbf{a}$ and $\mathbf{b}$ are $\lambda$-aligned, by Proposition 3, we have $\sum_{i=1}^k \lambda_i q^t T(-\pi/2)\dot{\alpha}_i^*(t) \equiv 0$. Hence the inequality becomes

$$\left|\frac{1}{2}\sum_{i=1}^k \lambda_i \alpha_i^*(t)^t T(-\pi/2)\dot{\alpha}_i^*(t)\right| \leq \frac{\pi}{2}\left\{\int_{t_0}^{t_1}\left[\sum_{i=1}^k \lambda_i \|\alpha_i^*(t) - q\|^2\right]^{-1} dt\right\}^{-1}.$$

The most restrictive bound is obtained by setting $q$ equal to the common $\lambda$-centroid of $\mathbf{a}$ and $\mathbf{b}$, which minimizes the right-hand-side of the above equation. Moreover, one can derive further optimality conditions by applying Proposition 4 to $\mathcal{T}_w(\alpha^*)$ for any $w \in \mathbb{R}^2$, since by Proposition 2 $\mathcal{T}_w(\alpha^*)$ is optimal in $\mathbf{P}(r, \mathbf{a}, \mathbf{b} + w)$.

### 2.4.4 Analysis by partial operators

Further optimality conditions can be derived by considering those transformations that change the maneuvers of only a subset of the $k$ agents (partial operators).

Let $\alpha$ be an arbitrary conflict-free maneuver in $\mathbf{P}(r, \mathbf{a}, \mathbf{b})$. At each time $t \in T$, we can construct an undirected graph $\mathcal{G}_\alpha(t)$ as follows: $\mathcal{G}_\alpha(t)$ has $k$ vertices, numbered from 1 to $k$, corresponding to the $k$ agents, and an edge connects vertices $i$ and $j$ if and only if $\|\alpha_i(t) - \alpha_j(t)\| = r$. If there does exist an edge between vertex

$i$ and vertex $j$ in $\mathcal{G}_\alpha(t)$, we say that agent $i$ and agent $j$ *contact* at time $t$. $\mathcal{G}_\alpha(t)$ is called the *formation pattern* of $\alpha$ at time $t$. For a general definition of formation pattern, see Chapter 4.

We start from a very special case. Assume that $\alpha$ is a conflict-free maneuver in $\mathbf{P}(r, \mathbf{a}, \mathbf{b})$ such that during the whole encounter the distance of agent 1 from any of the other agents is strictly greater than $r$ except possibly from agent 2, i.e., $\|\alpha_1(t) - \alpha_i(t)\| > r$, $\forall t \in T$, $i = 3, \ldots, k$. We shall introduce operators that leave $\alpha_i$ unchanged for $i = 2, \ldots, k$ and perturb $\alpha_1$ slightly, so that the perturbed $\alpha_1$ has the same minimum distance from $\alpha_2$ in the time interval $T$. If such a perturbation is small enough, then the perturbed $\alpha_1$ does not cause a conflict between agent 1 and any of the agents with index $i \geq 3$, given that their original minimum distance in the time interval $T$ was strictly greater than $r$.

Let $h : T \to T$ be a reparameterization of $T$, i.e., a bijection such that both $h$ and $h^{-1}$ are continuous and piecewise $C^2$, and $h(t_0) = t_0$ and $h(t_1) = t_1$.

**Definition 7 (Partial slide operator $\mathcal{L}_h^{12}$)** $\mathcal{L}_h^{12} : \mathbf{P}(r, \mathbf{a}, \mathbf{b}) \to \mathbf{P}(\mathbf{a}, \mathbf{b})$ *is a map such that for any* $\alpha \in \mathbf{P}(r, \mathbf{a}, \mathbf{b})$, $\beta = \mathcal{L}_h^{12}(\alpha)$ *is defined by:*

$$\begin{cases} \beta_1(t) = \alpha_1[h(t)] - \alpha_2[h(t)] + \alpha_2(t), \quad t \in T, \\ \beta_i(t) = \alpha_i(t), \quad t \in T, \quad i = 2, \ldots, k. \end{cases} \tag{2.14}$$

Note that $\inf_{t \in T} \|\beta_1(t) - \beta_2(t)\| = \inf_{t \in T} \|\alpha_1(t) - \alpha_2(t)\|$. Also for $h$ sufficiently close to the identity map, the minimum distance in the time interval $T$ between $\beta_1$ and $\beta_i$ is greater than $r$ for $i \geq 3$ by our assumption on $\alpha$, implying that $\beta \in \mathbf{P}(r, \mathbf{a}, \mathbf{b})$.

Figure 2.8 shows how $\beta$ is constructed geometrically. First, the operator $\mathcal{D}_{\bar{\alpha}_2 - \alpha_2}$ is performed on $(\alpha_1, \alpha_2)$ to "straighten" the string corresponding to $\alpha_2$, where

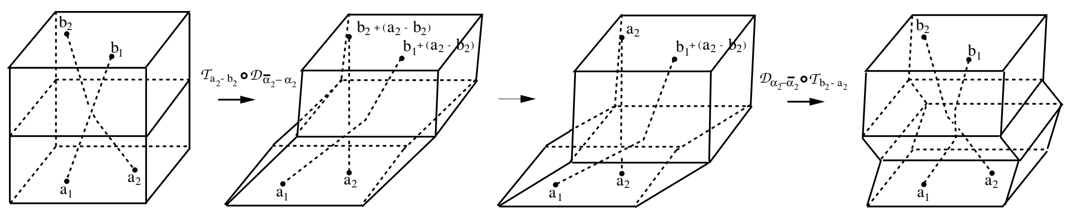

Figure 2.8: Slide operation $\mathcal{L}_h^{12}$ on braids.

$\bar{\alpha}_2$ denotes the constant velocity motion along the straight line between $a_2$ and $b_2$. Next, the operator $\mathcal{T}_{a_2-b_2}$ is applied to the resulting 2-maneuver to get a 2-maneuver $\gamma = (\gamma_1, \gamma_2)$ with $\gamma_1 = \alpha_1 - \alpha_2 + a_2$ and $\gamma_2 \equiv a_2$. Then, $\gamma$ is reparameterized by $h$ to obtain $\eta = (\eta_1, \eta_2)$ with $\eta_1 = (\alpha_1 \circ h) - (\alpha_2 \circ h) + a_2$ and $\eta_2 \equiv a_2$. Finally, the reverse procedures of the second and first steps are applied subsequently to obtain $(\beta_1, \beta_2)$ from $\eta$. Roughly speaking, $\hat{\beta}$ is obtained by "sliding" $\hat{\alpha}_1$ along $\hat{\alpha}_2$, hence the name "slide operator" for $\mathcal{L}_h^{12}$. Note that the superscript and the subscript in $\mathcal{L}_h^{12}$ indicate respectively the two strings the operator works on and the reparameterization used.

By using the partial slide operator to generate the perturbation in the variational analysis, we get (see [22] for the detailed proof):

**Proposition 5** *Suppose that $\alpha^* \in \mathbf{P}(r, \mathbf{a}, \mathbf{b})$ is an optimal solution to problem (2.4), and that there exists a subinterval $(t_0', t_1') \subset T$ such that $\|\alpha_1^*(t) - \alpha_i^*(t)\| > r$, $i = 3, \ldots, k$, for all $t \in (t_0', t_1')$. Then $\alpha^*$ satisfies*

$$\ddot{\alpha}_1^*(t)^t [\dot{\alpha}_1^*(t) - \dot{\alpha}_2^*(t)] \equiv 0, \qquad \forall t \in (t_0', t_1'). \tag{2.15}$$

Instead of sliding $\alpha_1$ along $\alpha_2$, we can rotate it. Let $\theta : T \to \mathbb{R}$ be a continuous and piecewise $C^2$ map with $\theta(t_0) = \theta(t_1) = 0$.

**Definition 8 (Partial rotation operator $\mathcal{R}_\theta^{12}$)** *The partial rotation operator $\mathcal{R}_\theta^{12}$ is a map from $\mathbf{P}(r, \mathbf{a}, \mathbf{b})$ to $\mathbf{P}(\mathbf{a}, \mathbf{b})$ such that for any $\alpha \in \mathbf{P}(r, \mathbf{a}, \mathbf{b})$, $\beta = \mathcal{R}_\theta^{12}(\alpha)$ is defined by:*

$$\begin{cases} \beta_1(t) = T[\theta(t)][\alpha_1(t) - \alpha_2(t)] + \alpha_2(t), \quad t \in T, \\ \beta_i(t) = \alpha_i(t), \quad t \in T, \quad i = 2, \ldots, k. \end{cases}$$

In the braid representation, $\hat{\beta}$ is obtained by rotating the string $\hat{\alpha}_1$ around the string $\hat{\alpha}_2$. If $\theta$ is close enough to the zero map, $\beta = \mathcal{R}_\theta^{12}(\alpha) \in \mathbf{P}(r, \mathbf{a}, \mathbf{b})$. Similarly to the proof of Proposition 5, by using the partial rotation operator, we get ([22]):

**Proposition 6** *Under the hypotheses of Proposition 5, $\alpha^*$ satisfies*

$$\ddot{\alpha}_1^*(t)^t T(-\pi/2)[\alpha_1^*(t) - \alpha_2^*(t)] \equiv 0, \quad \forall t \in (t_0', t_1'). \tag{2.16}$$

It can be verified that the optimal solution for the two agents case obtained in Theorem 2 indeed satisfies both conditions (2.15) and (2.16). Moreover, if one of the two agents has a predetermined maneuver throughout $T$, equations (2.15) and (2.16) will govern the motion of the other agent. Note also that if in addition $\|\alpha_1^* - \alpha_2^*\| = r$ on $(t_0', t_1')$, then these two equations are equivalent, since in this case $\|\alpha_1^* - \alpha_2^*\|^2 \equiv r^2$ implies that $(\dot{\alpha}_1^* - \dot{\alpha}_2^*)^t(\alpha_1^* - \alpha_2^*) \equiv 0$, i.e., $\dot{\alpha}_1^* - \dot{\alpha}_2^*$ and $T(\pi/2)(\alpha_1^* - \alpha_2^*)$ have the same direction. The intuitive understanding is that, in the braid representation, the slide and rotation operations of a string on the surface of a cylinder lead to the same orthogonal perturbation.

The above idea can be carried out even further. Suppose that the formation pattern of an optimal maneuver $\alpha^* \in \mathbf{P}(r, \mathbf{a}, \mathbf{b})$ remains constant on some subinterval $(t_0', t_1') \subset T$. We can perturb $\alpha^*$ by sliding (rotating) slightly the maneuvers of a subset of the $k$ agents with respect to that of agent $i$ in the time subinterval $(t_0', t_1')$.

To ensure that the perturbed joint maneuver belongs to $\mathbf{P}(r, \mathbf{a}, \mathbf{b})$, any agent in this subset should have a minimum distance strictly greater than $r$ from any of the agents not belonging to the subset, except possibly from agent $i$, in the time interval $(t_0', t_1')$. Since $\alpha^*$ is optimal, its energy cannot be decreased by such a perturbation. By using the same arguments leading to Proposition 5 and Proposition 6, we then have ([22])

**Proposition 7** *Suppose that* $\alpha^* \in \mathbf{P}(r, \mathbf{a}, \mathbf{b})$ *is an optimal solution to problem (2.4), and that its formation pattern remains constant on some subinterval* $(t_0', t_1') \subset T$. *Pick any agent, say, agent* $i$, *and let* $\mathcal{I} \subset \{1, 2, \ldots, k\} \backslash \{i\}$ *be a subset of the remaining agents that corresponds to a maximal connected component of the graph obtained by removing node* $i$ *and all the edges connected with it from the formation pattern during* $(t_0', t_1')$. *Then for all* $t \in (t_0', t_1')$,

$$\begin{aligned} &\sum_{j \in \mathcal{I}} \lambda_j \ddot{\alpha}_j^*(t)^t (\dot{\alpha}_j^*(t) - \dot{\alpha}_i^*(t)) \equiv 0, \\ &\sum_{j \in \mathcal{I}} \lambda_j \ddot{\alpha}_j^*(t)^t T(\pi/2)(\alpha_j^*(t) - \alpha_i^*(t)) \equiv 0. \end{aligned} \tag{2.17}$$

Note that (2.15) and (2.16) are special cases of (2.17) when $i = 2$ and $\mathcal{I} = \{1\}$.

**Remark 3** *All the optimality conditions we have obtained so far admit mechanical interpretations, as will be shown in Section 2.6. However, it should be pointed out that in general they cannot completely characterize the optimal maneuver with an arbitrary formation pattern. A complete set of local optimality conditions can be derived by considering all possible local perturbations of maneuvers that preserve the formation pattern, or, in the light of Remark 1, by writing down the geodesics equation in a suitable Riemannian manifold.*

### 2.4.5 Regularity of optimal conflict-free maneuvers

The regularity of optimal conflict-free maneuvers is a tricky issue. For example, it is already not a trivial problem to prove that, for each optimal $\alpha^*$, there exists a *finite* subdivision of $T$ such that the formation pattern $\mathcal{G}_{\alpha^*}(t)$ remains constant during each subinterval and contiguous subintervals correspond to different formation patterns. It is proved in [2] that, in a Euclidean space under the presence of open obstacles with locally analytic boundary, a geodesic can have, in any segment of finite arc length, only a finite number of *switch points* where it switches from an interior segment to a segment on the boundary of an obstacle or vice versa. Unfortunately, this result does not apply in our case, since the obstacle $W$ as defined in Remark 1 has nonsmooth boundary.

On the other hand, it can be proved that an optimal $\alpha^*$ is always $C^1$, i.e., there is no sharp turns in the optimal conflict-free maneuvers. In fact, this follows from a general result proved in [24], which states that if a manifold $M$ with (nonsmooth) boundary is a subset of $\mathbb{R}^n$ obtained by removing from $\mathbb{R}^n$ a finite union of open convex subsets, each of which has a smooth boundary, then any geodesic of $M$ is of class $C^1$. Note that the convex subsets are not required to be disjoint for this conclusion. In our case, by Remark 1, the obstacle is the union of $\frac{k(k-1)}{2}$ convex cylinders in $\mathbb{R}^{2k}$.

## 2.5 An interesting example

In this section we will show by a simple example how the optimality conditions obtained in Section 2.4 can be used to determine the optimal maneuver with a particular formation pattern. This example will also serve as a counterexample to the conjecture that for each multi-agent encounter, there is a unique optimal conflict-free maneuver within each homotopy type, which is true for $k = 2$ by Theorem 2.

Consider three agents with equal priorities $\lambda_1 = \lambda_2 = \lambda_3 = \frac{1}{3}$ and $r = 1$. Suppose that $\alpha^*$ is an optimal conflict-free maneuver for some starting position $\mathbf{a} = (a_1, a_2, a_3)$ and destination position $\mathbf{b} = (b_1, b_2, b_3)$ that are $\lambda$-aligned with the common $\lambda$-centroid at the origin, and that on some subinterval of $T$ (which we may assume without loss of generality to be $T$ itself), its formation pattern $\mathcal{G}_{\alpha^*}(t)$ is constant with edges between vertices 1 and 3 and between vertices 2 and 3, but no edges between vertices 1 and 2. Then, by Corollary 1 and Proposition 7, $\alpha^* = (\alpha_1^*, \alpha_2^*, \alpha_3^*)$ must satisfy for $t \in T$

$$\begin{cases} \sum_{i=1}^{3} \alpha_i^*(t) = 0, \\ \ddot{\alpha}_1^*(t)^t T(\pi/2)(\alpha_1^*(t) - \alpha_3^*(t)) = 0, \\ \ddot{\alpha}_2^*(t)^t T(\pi/2)(\alpha_2^*(t) - \alpha_3^*(t)) = 0, \\ \|\alpha_1^*(t) - \alpha_3^*(t)\| = \|\alpha_2^*(t) - \alpha_3^*(t)\| = 1. \end{cases} \tag{2.18}$$

We now show that equation (2.18) is equivalent to the geodesics equation of a suitable Riemannian manifold ([12]). Hence, for any set of initial conditions $\alpha_i^*(t_0), \dot{\alpha}_i^*(t_0)$, $i = 1, 2, 3$, it has a unique solution for $t$ sufficiently close to $t_0$.

First, notice that $\alpha^*$ as a curve in $\mathbb{R}^6$ lies in the submanifold $N$ of $\mathbb{R}^6$ determined by the first and the last equations of (2.18), namely the set of all those points $(x_1, y_1, x_2, y_2, x_3, y_3)$ in $\mathbb{R}^6$ such that $\sum_{i=1}^{3} x_i = \sum_{i=1}^{3} y_i = 0$, $(x_1 - x_3)^2 + (y_1 - y_3)^2 = 1$ and $(x_2 - x_3)^2 + (y_2 - y_3)^2 = 1$. $N$ is a compact two-dimensional

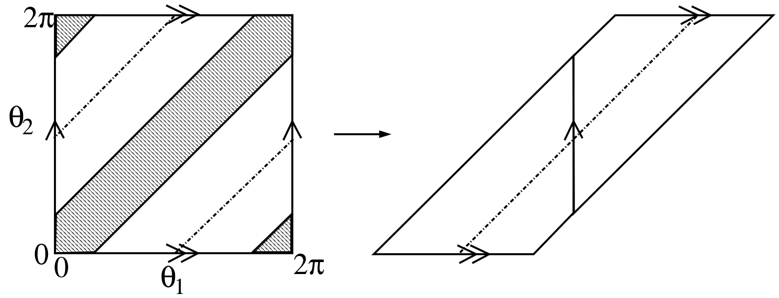


Figure 2.9: $\mathbb{T}^2_0$ as a subset of $\mathbb{T}^2$ in the $(\theta_1, \theta_2)$ coordinate.

submanifold of $\mathbb{R}^6$ and admits a global coordinate $(\theta_1, \theta_2)$ defined by

$$\theta_1 = \arctan \frac{y_1 - y_3}{x_1 - x_3}, \quad \theta_2 = \arctan \frac{y_2 - y_3}{x_2 - x_3}.$$

$(\theta_1, \theta_2)$ takes values in the rectangle $[0, 2\pi] \times [0, 2\pi]$ with opposite edges identified, i.e., the 2-torus $\mathbb{T}^2$. In order to satisfy our assumption that the distance between agent 1 and agent 2 is greater than $r$ during $T$, $\alpha^*$ must lie in an open subset $N_0$ of $N$ consisting of all those points $(x_1, y_1, x_2, y_2, x_3, y_3)$ in $N$ such that $(x_1 - x_2)^2 + (y_1 - y_2)^2 > 1$. In the $(\theta_1, \theta_2)$ coordinate, $N_0$ corresponds to an open subset $\mathbb{T}^2_0$ of $\mathbb{T}^2$ obtained by removing from $\mathbb{T}^2$ the shaded region shown in Figure 2.9. Hence topologically $N_0$ is homeomorphic to $S^1 \times (0, 1)$, an untwisted ribbon whose boundary consists of two disjoint circles.

Each $(\theta_1, \theta_2) \in \mathbb{T}^2$ determines a unique point $f(\theta_1, \theta_2)$ in $N$ by

$$\begin{aligned} f(\theta_1, \theta_2) = \frac{1}{3}(&2\cos\theta_1 - \cos\theta_2, 2\sin\theta_1 - \sin\theta_2, -\cos\theta_1 + 2\cos\theta_2, \\ &-\sin\theta_1 + 2\sin\theta_2, -\cos\theta_1 - \cos\theta_2, -\sin\theta_1 - \sin\theta_2)^t, \end{aligned} \tag{2.19}$$

which is an embedding of $\mathbb{T}^2$ (respectively, $\mathbb{T}^2_0$) into $\mathbb{R}^6$ whose image is $N$ (respectively, $N_0$).

By using $f$ as the coordinate map, it can be verified that in the $(\theta_1, \theta_2)$ coordinate, equation (2.18) is reduced to the following second order ODE:

$$\begin{cases} 2\ddot{\theta}_1 - \cos(\theta_1 - \theta_2)\ddot{\theta}_2 = \sin(\theta_1 - \theta_2)(\dot{\theta}_2)^2 \\ 2\ddot{\theta}_2 - \cos(\theta_1 - \theta_2)\ddot{\theta}_1 = -\sin(\theta_1 - \theta_2)(\dot{\theta}_1)^2. \end{cases} \tag{2.20}$$

Equation (2.20) is the geodesics equation of $\mathbb{T}^2$ with a suitably chosen metric. In fact, let $\mathbb{R}^6$ be equipped with the standard Riemannian metric. $N$ as a submanifold inherits from $\mathbb{R}^6$ a metric by restriction. Let $g$ be the corresponding metric on $\mathbb{T}^2$ obtained by pulling back the metric on $N$ via $f$, so that $f$ becomes an isometry. It will be proved in the following that (2.20) is indeed the equation for geodesics of $\mathbb{T}^2$ under the metric $g$. As a result, each solution $\alpha^*$ of equation (2.18) is a geodesic of $N$, which is not surprising by Remark 1. Since $\mathbb{T}^2$ (hence $N$) is compact, a solution to equation (2.18) is defined for all duration of time, provided that it stays inside $N_0$. Equation (2.20) can be solved by two integrals (see [24] for details).

Deeper optimality conditions of conflict-free maneuvers can be obtained in this interpretation. To this end, we first compute several geometrical quantities of the Riemannian manifold $(\mathbb{T}^2, g)$.

### 2.5.1 Geometry of $(\mathbb{T}^2, g)$

At each point $(\theta_1, \theta_2) \in \mathbb{T}^2$, a basis $\frac{\partial}{\partial \theta_1}$ and $\frac{\partial}{\partial \theta_2}$ of the tangent space of $\mathbb{T}^2$ is mapped by the differential of the coordinate map $f$ defined in (2.19) to

$$\begin{cases} df(\frac{\partial}{\partial \theta_1}) = \frac{1}{3}(-2\sin\theta_1, 2\cos\theta_1, \sin\theta_1, -\cos\theta_1, \sin\theta_1, -\cos\theta_1, )^T, \\ df(\frac{\partial}{\partial \theta_2}) = \frac{1}{3}(\sin\theta_2, -\cos\theta_2, -2\sin\theta_2, 2\cos\theta_2, \sin\theta_2, -\cos\theta_2)^T, \end{cases} \tag{2.21}$$

which form a basis of the tangent space of $N$ at $f(\theta_1, \theta_2)$. Here we have identified the tangent space of $\mathbb{R}^6$ at $f(\theta_1, \theta_2)$ with $\mathbb{R}^6$ itself, thus the tangent space of $N$ at $f(\theta_1, \theta_2)$ becomes a subspace of $\mathbb{R}^6$. The standard metric of $\mathbb{R}^6$ induces by $f$ isometrically the metric $g$ on $\mathbb{T}^2$ of the form:

$$g = \begin{bmatrix} g_{11} & g_{12} \\ g_{21} & g_{22} \end{bmatrix} = \frac{1}{3} \begin{bmatrix} 2 & -\cos(\theta_1 - \theta_2) \\ -\cos(\theta_1 - \theta_2) & 2 \end{bmatrix}, \tag{2.22}$$

where $g_{ij} \triangleq \langle \frac{\partial}{\partial \theta_i}, \frac{\partial}{\partial \theta_j} \rangle$ for $i, j = 1, 2$. The inverse of $g$ can be written as

$$g^{-1} = \begin{bmatrix} g^{11} & g^{12} \\ g^{21} & g^{22} \end{bmatrix} = \frac{3}{4 - \cos^2(\theta_1 - \theta_2)} \begin{bmatrix} 2 & \cos(\theta_1 - \theta_2) \\ \cos(\theta_1 - \theta_2) & 2 \end{bmatrix}.$$

The covariant derivative $\nabla$ of $\mathbb{T}^2$ with respect to the Levi-Civita connection is defined by ([12])

$$\nabla_{\frac{\partial}{\partial \theta_i}} \frac{\partial}{\partial \theta_j} = \sum_{m=1}^{2} \Gamma_{ij}^m \frac{\partial}{\partial \theta_m}, \quad \forall 1 \le i, j \le 2,$$

where $\Gamma_{ij}^m$, $1 \le i, j, m \le 2$, are the *Christoffel symbols* that can be computed by

$$\Gamma_{ij}^m = \frac{1}{2} \sum_{l=1}^{2} \{ \frac{\partial g_{jl}}{\partial \xi_i} + \frac{\partial g_{li}}{\partial \xi_j} - \frac{\partial g_{ij}}{\partial \xi_l} \} g^{lm}, \qquad 1 \le i, j, m \le 2.$$

It is easy to verify that

$$\Gamma_{11}^1 = -\Gamma_{22}^2 = \frac{\sin(\theta_1 - \theta_2)\cos(\theta_1 - \theta_2)}{4 - \cos^2(\theta_1 - \theta_2)}, \quad \Gamma_{11}^2 = -\Gamma_{22}^1 = \frac{2\sin(\theta_1 - \theta_2)}{4 - \cos^2(\theta_1 - \theta_2)},$$

and $\Gamma_{12}^m = \Gamma_{21}^m = 0$ for $m = 1, 2$. The equations for geodesics in $\mathbb{T}^2$ are $\ddot{\xi}_m + \sum_{i,j} \Gamma_{ij}^m \dot{\xi}_i \dot{\xi}_j = 0$, $m = 1, 2$, which yield

$$[4 - \cos^2(\theta_1 - \theta_2)]\ddot{\theta}_1 = -\sin(\theta_1 - \theta_2)\cos(\theta_1 - \theta_2)(\dot{\theta}_1)^2 + 2\sin(\theta_1 - \theta_2)(\dot{\theta}_2)^2,$$

$$[4 - \cos^2(\theta_1 - \theta_2)]\ddot{\theta}_2 = -2\sin(\theta_1 - \theta_2)(\dot{\theta}_1)^2 + \sin(\theta_1 - \theta_2)\cos(\theta_1 - \theta_2)(\dot{\theta}_2)^2.$$

The above equations are readily seen to be equivalent to equation (2.20).

Next, we will compute the curvature of $\mathbb{T}^2$. Let $R$ be the curvature tensor of $\mathbb{T}^2$. Let $R_{ijml}$ be its value in basis $\frac{\partial}{\partial\theta_1}, \frac{\partial}{\partial\theta_2}$ defined by ([12])

$$\begin{aligned} R_{ijml} &\triangleq \langle R(\frac{\partial}{\partial\theta_i}, \frac{\partial}{\partial\theta_j})\frac{\partial}{\partial\theta_m}, \frac{\partial}{\partial\theta_l}\rangle \\ &= \langle(\nabla_{\frac{\partial}{\partial\theta_j}}\nabla_{\frac{\partial}{\partial\theta_i}} - \nabla_{\frac{\partial}{\partial\theta_i}}\nabla_{\frac{\partial}{\partial\theta_j}} + \nabla_{[\frac{\partial}{\partial\theta_i},\frac{\partial}{\partial\theta_j}]})\frac{\partial}{\partial\theta_m}, \frac{\partial}{\partial\theta_l}\rangle, \end{aligned}$$

for all $1 \leq i, j, m, l \leq 2$. Then $R_{ijml} = \sum_{s=1}^{2} R_{ijm}^s g_{sl}$, where $R_{ijm}^s$ can be computed by

$$R_{ijm}^s = \sum_{p=1}^{2} \Gamma_{im}^p \Gamma_{jp}^s - \sum_{p=1}^{2} \Gamma_{jm}^p \Gamma_{ip}^s + \frac{\partial}{\partial\theta_j}\Gamma_{im}^s - \frac{\partial}{\partial\theta_i}\Gamma_{jm}^s.$$

In our case, calculation shows that

$$R_{121}^1 = R_{122}^2 = \frac{-3\cos^2(\theta_1-\theta_2)}{[4-\cos^2(\theta_1-\theta_2)]^2}, \quad R_{121}^2 = R_{122}^1 = \frac{-6\cos(\theta_1-\theta_2)}{[4-\cos^2(\theta_1-\theta_2)]^2},$$

and $R_{21m}^s = -R_{12m}^s$, $R_{11m}^s = R_{22m}^s = 0$ for all $1 \leq m, s \leq 2$. Hence,

$$R_{1212} = \frac{-\cos(\theta_1-\theta_2)}{4-\cos^2(\theta_1-\theta_2)}.$$

Therefore, the sectional curvature of $\mathbb{T}^2$ is

$$K = \frac{R_{1212}}{g_{11}g_{22} - g_{12}^2} = \frac{-9\cos(\theta_1-\theta_2)}{[4-\cos^2(\theta_1-\theta_2)]^2}. \tag{2.23}$$

$K$ depends only on $\theta_1 - \theta_2$ since the map $(\theta_1, \theta_2) \mapsto (\theta_1 + \xi, \theta_2 + \xi) \bmod 2\pi$ is an isometry of $\mathbb{T}^2$ for each $\xi$. In the special case when $\theta_1 - \theta_2 = \pi$, we have $K = 1$.

Now consider the curve $\theta$ in $\mathbb{T}^2$ defined by $\theta(t) = (\theta_1(t), \theta_2(t)) = (t, \pi + t)$ for $t \in [0, \tau]$, where $\tau$ is positive. $\theta$ is a trivial solution to (2.20), hence a geodesic of $\mathbb{T}^2$ that is contained completely in $\mathbb{T}_0^2$. $\theta$ determines a 3-maneuver $\alpha^* = f \circ \theta$, i.e.,

$$\alpha_1^*(t) = (\cos t, \sin t)^t,\ \alpha_2^*(t) = (-\cos t, -\sin t)^t,\ \alpha_3^*(t) = (0,0)^t,\ t \in [0, \tau]. \tag{2.24}$$

In the motions specified by $\alpha^*$, agent 3 stays at the origin, while agent 1 and agent 2 are at unit distance from agent 3 but on the opposite side of it so that three of them are always collinear, and both agent 1 and agent 2 rotate at the same constant angular velocity around agent 3. $\alpha^*$ thus defined is a solution to equation (2.18). An application of Proposition 4 implies that $\alpha^*$ is no longer optimal if $\tau > \pi$, for otherwise a better maneuver can be obtained by rotating agent 1 and agent 2 the opposite way around agent 3. The following proposition improves this result.

**Proposition 8** *Maneuver $\alpha^*$ defined by (2.24) is not optimal if $\tau > \frac{\sqrt{2}}{2}\pi$.*

**Proof:** Since $f$ is an isometry, we need only to prove that the geodesic $\theta$ is no longer distance-minimizing between its end points $\theta(0) = (0, \pi)$ and $\theta(\tau) = (\tau, \pi + \tau)$ once $\tau > \tau_0 = \frac{\sqrt{2}}{2}\pi$. To this end, it suffices to prove that $\theta(\tau_0)$ is a conjugate point of $\theta(0)$ along $\theta$, in other words, there exists a nontrivial Jacobi field $X$ along $\theta$ that vanishes at both $\theta(0)$ and $\theta(\tau_0)$ ([33]).

Define two vector fields along $\theta$ by $X_1 = \frac{\partial}{\partial\theta_1} + \frac{\partial}{\partial\theta_2}$ and $X_2 = \frac{\partial}{\partial\theta_1} - \frac{\partial}{\partial\theta_2}$. Then, it is easy to verify that $X_1$ and $X_2$ are orthogonal, and that $X_1$ coincides with the velocity field $\dot{\theta}$ of the geodesic $\theta$. Moreover, using the Christoffel symbols, we conclude that $\nabla_{\dot{\theta}} X_2 \equiv 0$; hence, $X_2$ is parallel along $\theta$.

A Jacobi field $X$ along $\theta$ and orthogonal to $\dot{\theta}$ is necessarily of the form $X(t) = h(t)X_2(t)$ for some function $h$ defined on $[0, \tau]$, and satisfies the Jacobi equation $\nabla_{\dot{\theta}}\nabla_{\dot{\theta}} X + R(\dot{\theta}, X)\dot{\theta} = 0$, where $R$ is the curvature tensor of $\mathbb{T}^2$. Since $\nabla_{\dot{\theta}}\nabla_{\dot{\theta}} X = \ddot{h}X_2$ and $R(\dot{\theta}, X)\dot{\theta}$ are both orthogonal to $\dot{\theta}$, the Jacobi equation is equivalent to $\langle \ddot{h}X_2, X_2\rangle + \langle R(\dot{\theta}, hX_2)\dot{\theta}, X_2\rangle = 0$. By (2.23), the sectional curvature $K$ of $\mathbb{T}^2$ along $\theta$ is constant 1. Using the relation $\langle R(\dot{\theta}, hX_2)\dot{\theta}, X_2\rangle = hK[\langle\dot{\theta}, \dot{\theta}\rangle\langle X_2, X_2\rangle - \langle\dot{\theta}, X_2\rangle^2]$, we have $\ddot{h} + 2h = 0$. A solution of $h$ vanishing at 0 is $h(t) = \sin(\sqrt{2}t)$, so

$X(t) = \sin(\sqrt{2}t)X_2(t)$ is an Jacobi field along $\theta$ vanishing at $t = 0$ and $t = \frac{\sqrt{2}}{2}\pi = \tau_0$. Therefore, $\theta(\tau_0)$ is a conjugate point of $\theta(0)$ along $\theta$. ■

A more intuitive way of obtaining the conclusion of Proposition 8 is through variational analysis of $\alpha^*$ using perturbations of the following form. Recall that $\theta(t) = (\theta_1(t), \theta_2(t)) = (t, \pi + t)$, $t \in T = [0, \tau]$ is the curve in $\mathbb{T}_0^2$ that $\alpha^*$ corresponds to. Let $\xi_1 : T \times (-\epsilon, \epsilon) \to \mathbb{R}$ be a *proper variation* of the map $\theta_1 : T \to \mathbb{R}$, i.e., $\xi_1$ is a smooth map such that $\xi_1(t, 0) = \theta_1(t)$, $\xi_1(0, s) = \theta_1(0)$, $\xi_1(\tau, s) = \theta_1(\tau)$ for $t \in T$ and $s \in (-\epsilon, \epsilon)$, where $\epsilon$ is a small positive number. Let $\xi_2 : T \times (-\epsilon, \epsilon) \to \mathbb{R}$ be a proper variation of the map $\theta_2 : T \to \mathbb{R}$. Consider joint maneuvers $\beta_s$ defined in $(\theta_1, \theta_2)$ coordinate by $(\xi_1(\cdot, s), \xi_2(\cdot, s))$ for $s \in (-\epsilon, \epsilon)$, which all start from $\alpha^*(0)$ and end in $\alpha^*(\tau)$. In the braid representation, $\hat{\beta}_s$ is obtained from $\hat{\alpha}^*$ by rotating the strings $\hat{\alpha}_1^*$ and $\hat{\alpha}_2^*$ by certain angles with respect to the string $\hat{\alpha}_3^*$ and then re-align the three strings to the origin. $\beta_s$ is conflict-free if the variations $\xi_1$ and $\xi_2$ are small enough. Then, a necessary condition for $\alpha^*$ to be optimal is that the energy of $\beta_s$ is minimized at $s = 0$ for all possible $\xi_1$ and $\xi_2$. After a lengthy calculation, this will lead to the conclusion of Proposition 8.

If we consider only conflict-free maneuvers with this particular formation pattern, then it is proved in [30] that, after $\tau$ passes the critical value $\frac{\sqrt{2}}{2}\pi$, the optimal conflict-free maneuver from $\alpha^*(0)$ to $\alpha^*(\tau)$ bifurcates from $\alpha^*$ into two conflict-free maneuvers with identical energy. Shown in the first row of Figure 2.10 are the plots of $\alpha^*$ for some $\tau > \frac{\sqrt{2}}{2}\pi$. The middle column is its plot in $(\theta_1, \theta_2)$ coordinate, and the right column is its braid representation. In the second and third rows, we plot by numerical simulations the two bifurcated optimal conflict-free maneuvers with this formation pattern, which in $(\theta_1, \theta_2)$ coordinate are mirror image of each other with

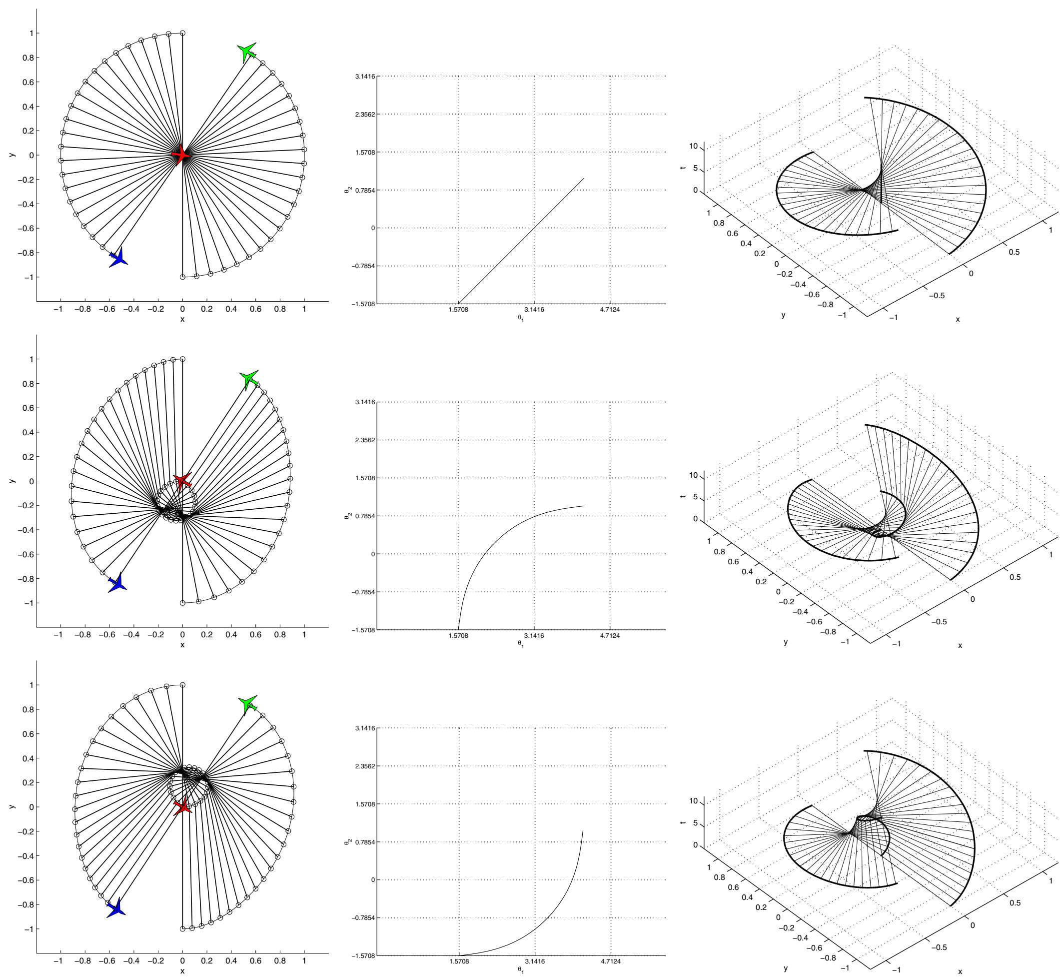

Figure 2.10: Bifurcation of minimizing geodesics in $\mathbb{T}^2$. Left column: 3-maneuvers; Middle column: $(\theta_1, \theta_2)$ phase plots; Right column: braids.

respect to the line $\theta_1 - \theta_2 = \frac{\pi}{2}$. For more details on the above claims and the general problem of conjugate points in manifolds with boundary, see [30].

One can also consider $k \geq 3$ agents with equal priorities, which are originally in a straight line with distance between successive agents being 1, and which rotate at a constant angular velocity around their centroid. This defines a geodesic in a certain submanifold of $\mathbb{R}^{2k}$ as we have discussed before. The maximal angle they can rotate before the first conjugate point of this geodesic is encountered in the submanifold is denoted by $\tau_k^*$. It can be expected that $\tau_k^*$ decreases with $k$. In [27] we prove that

$$\tau_k^* = \frac{\pi}{\sqrt{\frac{k(k-1)}{2} - 1}}.$$

It is worthwhile at this point to summarize the optimality conditions we have derived so far. All of them, with the exception of Proposition 4 and Proposition 8, are *local* in the sense that they can be obtained by using spike-like perturbations in the variational analysis, which only change maneuvers in a neighborhood of a fixed time epoch. Proposition 8 is *semi-global* in that its conclusion can only be reached by perturbations that change maneuvers throughout a subinterval of the encounter with positive length. Proposition 4 is a global one, in the sense that it enables us to compare the performance of maneuvers belonging to different homotopy types.

## 2.6 Two mechanical analogies

We now give two mechanical analogies of our results. Note that they serve only as analogies to gain more insights into the results obtained, and are not rigorous proofs themselves.

First, consider the following experiment. Instead of $k$ agents, we have $k$ particles of mass $\lambda_1, \ldots, \lambda_k$ on a horizontal plane with no external forces acting on them. At time $t_0$, they are at the initial positions $a_1, \ldots, a_k$ with certain initial velocities. Each particle $i$ moves with constant velocity until the distance between it and some other particle $j$ becomes $r$. Then a rigid rod of zero mass is introduced between particle $i$ and particle $j$ to prevent their distance from further decreasing, and the two particles move together with the rod at velocities determined by the law of conservation of momentum and angular momentum. We refer to the above process where a rigid rod is introduced between two particles as a (two-particle) *join*. There are two types of joins: *tangential* and *non-tangential*. A join is tangential if the time derivative of the distance between the two particles at the time of join is zero, otherwise the join is non-tangential. It is evident that some kinetic energy is lost for a non-tangential join since there is a collision between the two particles along the direction of the rod. As time goes on, more particles can join to form larger groups. In addition to joins, a group of particles connected by rods can *split* at any time, in the sense that some or all of the rods disappear instantly at that time. So when a split occurs, neither the positions nor the velocities of the particles change, but the group separates into several independent subgroups.

It is claimed that by appropriately choosing the initial velocities, time and order of the joins and splits, one can get from such an experiment the optimal maneuver $\alpha^*$. In fact, during any time interval $I$ in which there are neither joins nor splits, the system of particles naturally corresponds to a formation pattern with edges between vertices representing rods between particles. Moreover, if $I$ is sufficiently small, the motions of the particles correspond to the optimal conflict-free maneuver associated with such a formation pattern. To see this, recall that by the principle of least action ([3]), the motion of the interconnected particles system is an extremal of the action integral $\int_I (E - U)\, dt$. Here $E = \frac{1}{2}\sum_{i=1}^{k} \lambda_i v_i^2$ represents the kinetic energy, and $U$ is the potential, which is zero by our assumption on the absence of external forces. So, for sufficiently small time interval $I$, the motions of the interconnected particles minimize $\frac{1}{2}\sum_{i=1}^{k} \lambda_i \int_I v_i^2\, dt$; hence they specify precisely the optimal maneuver over $I$ by definition. Equation (2.18) determines, for example, the motions of three particles connected by two rigid rods with zero masses. For discussions on the general problem of kinematically coupled structures composed of rigid and flexible bodies, see [36] and other references in the same book.

In this mechanical interpretation, the conclusion of Proposition 2 is simply the invariance of the motions of a mechanical system with respect to changes of inertial coordinates. Since the total momentum and the total angular momentum of the system are conserved in each time interval with constant configuration (formation pattern) and do not change during joins or splits, they are constant during the whole time interval $T$, which are the conclusions of Corollary 1 and Proposition 4, respectively. Proposition 4 further imposes an upper bound on the total angular momentum, implying that the whole system cannot spin "too fast". In addition, the assertion in Section 2.4.5 that $\alpha^*$ is $C^1$ implies that all the joins should be tangential; hence there is no kinetic energy lost during joints and splits and the total kinetic energy $\frac{1}{2}\sum_{i=1}^{k} \lambda_i v_i^2$ is also conserved, as it is shown in [22] by using a reparameterization operator.

In mechanics, there is a systematic way of using symmetry on the configuration space to reduce the degree of freedom ([3, 45]). In our case, the symmetry is

$\mathbf{SE}_2$, the group of rigid body motions in $\mathbb{R}^2$, acting on $\mathbb{R}^2$. Hence the analysis leading to Corollary 1 and Proposition 4 (except the bound in Proposition 4) is simply the application of the symmetry reduction method uniformly to all the configuration spaces of a system with time-varying configurations. Compared with more advanced techniques such as those based on the Hamiltonian, symplectic, and Poisson viewpoints, our approach, which is Lagrangian in nature, deals with the nonsmoothness of the boundary constraints directly, thus avoiding the trouble of solving for each smooth component of the boundary constraints individually before piecing them together properly to get the final solution. In Chapter 3, the corresponding method is generalized to an arbitrary Riemannian manifold with a group of isometries. For application of Lagrangian reduction to holonomic and nonholonomic mechanical systems, see [34].

A major drawback of the above mechanical model is that it is local, hence little insights can be obtained about the global optimality conditions. In this sense, the second model we are going to present is more "faithful", and once again demonstrates the advantage of adopting the braid point of view. As we have shown in Section 2.2, each conflict-free maneuver $\alpha$ of the $k$ agents corresponds to a $k$-braid $\hat{\alpha}$, whose intersection with any horizontal plane $t = \tau$ ($\tau \in T$) consists of $k$ points satisfying the $r$-separation property. Therefore, if we enlarge the radius of strings in $\hat{\alpha}$ to $r/2$, or more precisely, if we think of each of the $k$ strings in $\hat{\alpha}$ as consisting of an infinite number of horizontal disks of radius $r/2$ and height 0 mounting vertically, with each disk confined to move in a fixed horizontal plane $t = \tau$ for some $\tau \in T$, then the condition that $\alpha$ is conflict-free is equivalent to that the $k$ enlarged strings in $\hat{\alpha}$ do not overlap. Examples of such enlarged braids are shown in Figure 2.11 for

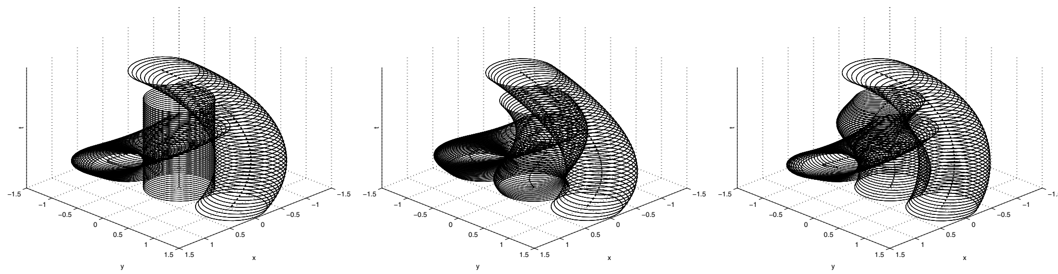

Figure 2.11: Examples of elastic (enlarged) braids in equilibrium positions. Left: unstable; Center and right: stable.

the three conflict-free maneuvers in Figure 2.10.

Assume that, for each $i = 1, \ldots, k$, the enlarged string $\hat{\alpha}_i$ in $\hat{\alpha}$ is elastic with elasticity coefficient $\lambda_i$, and has smooth surface so that any two strings can slide along each other without friction. Under these assumptions, the elastic energy of this $k$-string system is proportional to the energy of the corresponding conflict-free maneuver. If we fix the strings in $\hat{\alpha}$ at both the bottom ($t = t_0$) and the top ($t = t_1$) horizontal planes and leave free the remaining parts, then for certain choices of $\alpha$ this elastic $k$-string system will be in an equilibrium (stationary) position. The optimal conflict-free maneuvers have minimal energy, hence necessarily correspond to equilibrium positions.

Suppose that $\hat{\alpha}$ is in an equilibrium position. Pick any disk in $\hat{\alpha}$ that belongs to the string $\hat{\alpha}_i$ and lies on the horizontal plane $t = \tau$ for some $i = 1, \ldots, k$ and $t_0 < \tau < t_1$. Denote this disk by $D_i(\tau)$. Then $D_i(\tau)$ is subject to two types of forces: forces enacted by disks in the same string that are immediately above and below $D_i(\tau)$, i.e., $D_i(\tau^+)$ and $D_i(\tau^-)$; and forces enacted by disks in the same horizontal plane $t = \tau$ but belonging to different strings, i.e., $D_j(\tau)$ with $j \neq i$. Since $D_i(\tau)$ is confined to move on the plane $t = \tau$, we are concerned with only the projection of the forces onto this plane. The contribution of the forces of the first type is easily seen to be proportional to $\lambda_i \ddot{\alpha}_i(\tau)$. As for the forces of the second type, say, the force enacted by disk $D_j(\tau)$ ($j \neq i$) that contacts $D_i(\tau)$, by our assumption of no frictions, this force is directed from the center of $D_j(\tau)$ to the center of $D_i(\tau)$, i.e., from $(\alpha_j(\tau), \tau)$ to $(\alpha_i(\tau), \tau)$. Now the conclusion of Proposition 7 can be explained as follows. Let $\mathcal{I}$ be a subset of $\{1, \ldots, k\} \backslash \{i\}$ that corresponds to a maximal connected component of the graph obtained by removing node $i$ and all the edges connected with it from the formation pattern of $\alpha$ at time $\tau$. Since $\hat{\alpha}$ is in an equilibrium position, the subsystem $D_{\mathcal{I}}(\tau)$ consisting of disks $D_j(\tau)$ for $j \in \mathcal{I}$ is stationary. So the total moment (torque) of external forces acting on $D_{\mathcal{I}}(\tau)$ is zero, which is exactly the conclusion of Proposition 7. Note that here we choose $(\alpha_i(\tau), \tau)$ as the origin and use the fact that torque of forces enacted by $D_i(\tau)$ on disks in $D_{\mathcal{I}}(\tau)$ is zero by our above analysis.

Other optimality conditions can also be explained in this model. For example, the conclusion of Corollary 1 is, after differentiation with respect to $t$ twice, simply that on any horizontal plane $t = \tau \in T$ the combined external forces acting on the subsystem consisting of disks $D_i(\tau)$, $i = 1, \ldots, k$, is zero. For the example in Section 2.5, the semi-global conclusion of Proposition 8 can be intuitively understood as that, after a rotation of more than $\frac{\pi}{\sqrt{2}}$, the cumulative force of the two neighboring strings on the central one exceeds a critical value so that the equilibrium position of $\hat{\alpha}^*$ becomes unstable. Any slight perturbation will then render the system to settle in one of the two bifurcated positions with minimal elastic energy (see Figure 2.11), provided that there exists very small but nonzero air frictions to avoid persistent oscillation.

## 2.7 Optimal multi-legged conflict-free maneuvers

Due to the difficulty in computing analytically the optimal conflict-free maneuver when the number $k$ of agents is large, we now restrict our attention to those maneuvers specified by a set of waypoints, which might well be the only feasible form of joint maneuvers that a central controller can specify to the participating agents in practice.

To be precise, consider $k$ agents with starting position $\mathbf{a} = \langle a_i \rangle_{i=1}^k$ and destination position $\mathbf{b} = \langle b_i \rangle_{i=1}^k$. Assume that a set of epochs $\{s_j\}_{j=0}^m$, $s_0 = t_0 < s_1 < \cdots < s_{m-1} < s_m = t_1$, where $m$ is a positive integer, has been fixed. For each agent $i$, choose a set of waypoints $\{c_{i,j}\}_{j=0}^m$ in $\mathbb{R}^2$ such that $c_{i,0} = a_i$ and $c_{i,m} = b_i$. Then, an *$m$-legged maneuver* of agent $i$ is a maneuver consisting of $m$ stages, where at each stage $j \in \{0, 1, \ldots, m-1\}$, agent $i$ starts from $c_{i,j}$ at time $s_j$ and reaches $c_{i,j+1}$ at time $s_{j+1}$ with constant velocity. Denote by $\mathbf{P}_i^m$ the set of all $m$-legged maneuvers of agent $i$, and by $\mathbf{P}^m(\mathbf{a}, \mathbf{b}) = \prod_{i=1}^k \mathbf{P}_i^m$ the set of all $m$-legged joint maneuvers. In the braid representation, an $m$-legged joint maneuver corresponds to $k$ strings, each one consisting of $m$ line segments pieced together. The set of *$m$-legged conflict-free maneuvers* consists of all elements of $\mathbf{P}^m(\mathbf{a}, \mathbf{b})$ with MSE at least $r$ and is denoted by $\mathbf{P}^m(r, \mathbf{a}, \mathbf{b})$.

In this section, we shall try to solve the following version of problem (2.4):

$$\text{minimize } J(\alpha) \text{ subject to } \alpha \in \mathbf{P}^m(r, \mathbf{a}, \mathbf{b}). \tag{2.25}$$

By using similar arguments, one can show that some of the optimality conditions in Section 2.4, such as Corollary 1, still apply for solutions to problem (2.25). In general, a solution to problem (2.25) is only suboptimal for problem (2.4).

### 2.7.1 Optimal 2-legged conflict-free maneuver for two agents

We start from the simplest case when $k = 2$ and $m = 2$. Consider two agents with starting position $\mathbf{a} = (a_1, a_2)$ and destination position $\mathbf{b} = (b_1, b_2)$. Let $\alpha = (\alpha_1, \alpha_2)$ be a 2-legged conflict-free maneuver in $\mathbf{P}^2(r, \mathbf{a}, \mathbf{b})$ with three waypoints $c_{i,j}$, $j = 0, 1, 2$, for each agent $i = 1, 2$. Since $c_{i,0} = a_i$ and $c_{i,2} = b_i$ are fixed for each agent $i$, the middle waypoints $c_{i,1}$ will be denoted by $c_i$ to simplify the notations. Let $t_c \in (t_0, t_1)$ be the epoch corresponding to the middle waypoints. Then, the motions of the two agents are described by

$$\alpha_i(t) = \begin{cases} a_i + (c_i - a_i)\frac{t-t_0}{t_c-t_0}, & t_0 \leq t \leq t_c \\ b_i + (c_i - b_i)\frac{t-t_1}{t_c-t_1}, & t_c \leq t \leq t_1 \end{cases}, \quad i = 1, 2.$$

After some calculations, the energy of a maneuver $\alpha \in \mathbf{P}^2(\mathbf{a}, \mathbf{b})$ as the function of $c_1$ and $c_2$ can be expressed as follows

$$J(\alpha) = \frac{t_1 - t_0}{(t_1 - t_c)(t_c - t_0)}[\lambda_1 \|c_1 - c_1^u\|^2 + \lambda_2 \|c_2 - c_2^u\|^2] + C\,, \tag{2.26}$$

where $C$ is a constant and $c_i^u$, $i = 1, 2$, are defined by

$$c_i^u = \frac{(t_1 - t_c)a_i + (t_c - t_0)b_i}{t_1 - t_0}, \quad i = 1, 2. \tag{2.27}$$

Note that $c_1^u$ and $c_2^u$ are the optimal waypoints when minimizing $J(\alpha)$ without the MSE constraint. In the braid representation, $c_1^u$ and $c_2^u$ correspond to the intersections of the plane $t = t_c$ with the lines joining $(a_i, t_0)$ to $(b_i, t_1)$, for $i = 1$ and 2, respectively.

The MSE constraint can be simplified as well. The minimal distance $d_l$

between the two agents during the time interval $[t_0, t_c]$ is given by

$$d_l = \begin{cases} \|c_1 - c_2\|, & \text{if } u_0 < -\|c_1 - c_2 - a_1 + a_2\|^2 \\ \sqrt{\|a_1 - a_2\|^2 - u_0^2/\|c_1 - c_2 - a_1 + a_2\|^2}, & \text{if } -\|c_1 - c_2 - a_1 + a_2\|^2 \leq u_0 \leq 0 \\ \|a_1 - a_2\|, & \text{if } u_0 > 0, \end{cases}$$

where $u_0 \triangleq (a_1 - a_2)^t(c_1 - c_2 - a_1 + a_2)$. Note that $d_l$ is a function of the relative positions $a_1 - a_2$ and $c_1 - c_2$ only and is independent of the epoch $t_c$. We then use $d_l(a_1 - a_2, c_1 - c_2)$ to denote it explicitly. Similarly, the minimum distance between the two agents during the time interval $[t_c, t_1]$ is $d_l(c_1 - c_2, b_1 - b_2)$.

For $\alpha$ to be a conflict-free maneuver, both $d_l(a_1 - a_2, c_1 - c_2)$ and $d_l(c_1 - c_2, b_1 - b_2)$ have to be at least $r$, yielding two constraints on $c_1 - c_2$. Depending on the relative position of $a_1 - a_2$ and $b_1 - b_2$, the feasible set $A$ for $c_1 - c_2$ has four possible configurations, which are numbered from 1 to 4 and represented by shaded regions in Figure 2.12. Notice that $A$ consists of two connected components in configuration 1 and 3, which correspond to the two fundamental types of the conflict-free maneuvers. In configurations 2 and 4, however, only one fundamental type can be achieved by 2-legged maneuvers.

**Remark 4** *The feasible set $A$ for $c_1 - c_2$ can be characterized as the subset of $\mathbb{R}^2$ consisting of all those points that are "visible" to both $a_1 - a_2$ and $b_1 - b_2$ in the presence of the open disk $B(0, r)$ as obstacle. In fact, by applying an appropriate tilt operator $\mathcal{T}_w$ that preserves the MSE and $c_1 - c_2$, one can assume that $c_2 = a_2$, i.e., agent 2 stays at $a_2$ during $[t_0, t_c]$. Thus the MSE constraint during $[t_0, t_c]$ is equivalent to the constraint that the line segment from $a_1$ to $c_1$ does not intersect $B(a_2, r)$, or alternatively, the line segment from $a_1 - a_2$ to $c_1 - c_2$ does not intersect*

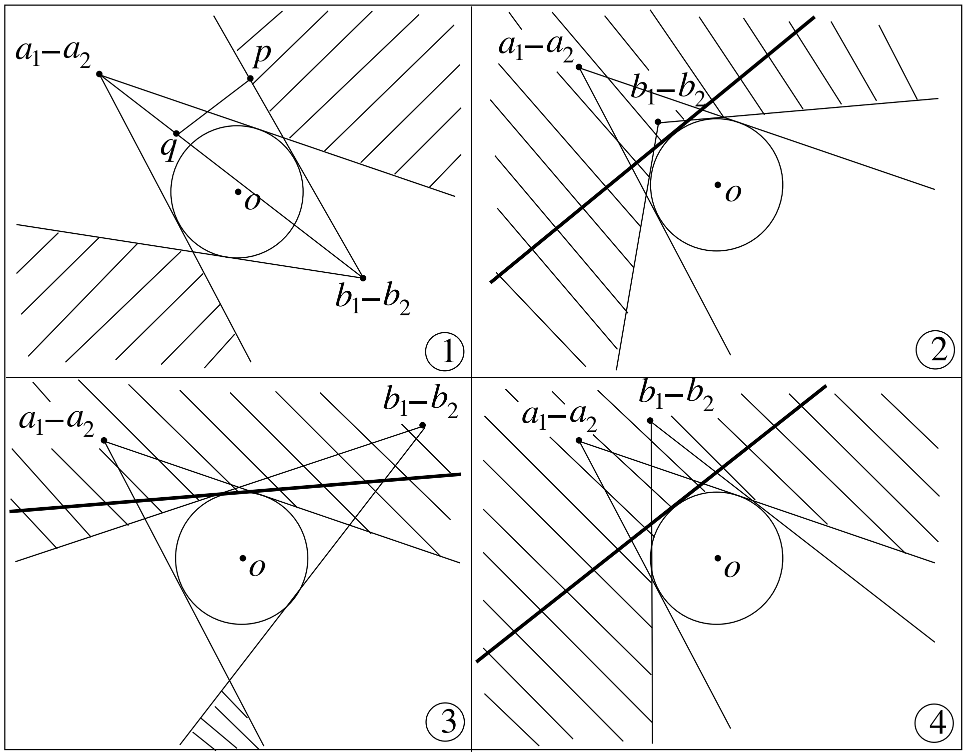


Figure 2.12: The four configurations of the feasible set $A$ for $c_1 - c_2$.

*$B(0, r)$. Similar arguments apply to the second stage of $\alpha$.*

As a result of the above simplifications, problem (2.25) is reduced to

$$\text{minimize } \lambda_1\|c_1 - c_1^u\|^2 + \lambda_2\|c_2 - c_2^u\|^2 \text{ subject to } c_1 - c_2 \in A. \tag{2.28}$$

**Theorem 3** *Define $q \triangleq c_1^u - c_2^u = \frac{t_1 - t_c}{t_1 - t_0}(a_1 - a_2) + \frac{t_c - t_0}{t_1 - t_0}(b_1 - b_2)$. Let $p$ be a point in $A$ at minimum distance from $q$. An optimal solution to problem (2.28) is then given by*

$$c_1^* = \lambda_1 c_1^u + \lambda_2 c_2^u + \lambda_2 p, \quad c_2^* = \lambda_1 c_1^u + \lambda_2 c_2^u - \lambda_1 p.$$

*Moreover, if problem (2.28) is restricted to one of the two fundamental types of* *conflict-free maneuvers that is achievable by 2-legged maneuvers, then* $c_1^*$ *and* $c_2^*$ *are unique.*

**Proof:** Set $\Delta c = c_1 - c_2$. Then we have

$$
\begin{aligned}
&\min\{\lambda_1\|c_1 - c_1^u\|^2 + \lambda_2\|c_2 - c_2^u\|^2 : c_1, c_2 \text{ such that } \Delta c \in A\} \\
=& \min_{\Delta c \in A} \min_{c_2} \{\lambda_1\|c_2 + \Delta c - c_1^u\|^2 + \lambda_2\|c_2 - c_2^u\|^2\} \\
=& \min_{\Delta c \in A} \min_{c_2} \{\|c_2 - \lambda_1(c_1^u - \Delta c) - \lambda_2 c_2^u\|^2 + \lambda_1\lambda_2\|c_1^u - c_2^u - \Delta c\|^2\} \\
=& \min_{\Delta c \in A} \lambda_1\lambda_2\|q - \Delta c\|^2 \\
=&\lambda_1\lambda_2\|q - p\|^2,
\end{aligned}
$$

where the last two equalities follow by choosing $c_2 = \lambda_1(c_1^u - \Delta c) + \lambda_2 c_2^u$ and $\Delta c = p$. Together they imply the desired expressions of $c_1^*$ and $c_2^*$. The uniqueness of $c_1^*$ and $c_2^*$ given a particular fundamental type is a consequence of the fact that $p$ is unique, since either the connected component of $A$ corresponding to that type is convex, or $q$ is contained in it since it lies on the line segment connecting $a_1 - a_2$ to $b_1 - b_2$. ■

Note that in configuration 2, 3, and 4, $p = q$ since $q$ lies on the line segment connecting $a_1 - a_2$ and $b_1 - b_2$ that is contained entirely in $A$. Hence $c_1^*$ and $c_2^*$ are equal to $c_1^u$ and $c_2^u$, respectively. In configuration 1, the set $A$ is the union of two disjoint convex sets, so there might be up to two points in $A$ nearest to $q$, with two being the case when there is an exact collision for the unconstrained optimal joint maneuver. In this case, we can choose either of the two points as $p$.

Figure 2.13 shows the optimal 2-legged conflict-free maneuvers for some typical 2-agent encounters when the agents have equal priorities. In each plot, the starting points are marked with stars and the ending points with diamonds. The circles are the waypoints specified by Theorem 3.

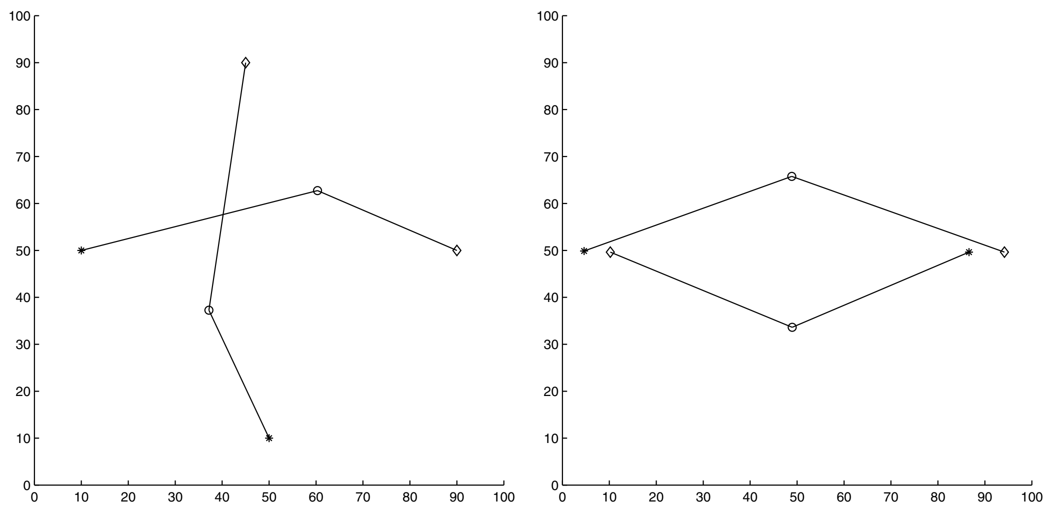


Figure 2.13: 2-legged optimal conflict-free maneuvers for 2-agent encounters ($\lambda_1 = \lambda_2 = 0.5$, $r = 30$).

### 2.7.2 Optimal 2-legged conflict-free maneuver for multiple agents

Consider the case $m = 2$ and $k \geq 3$. Roughly speaking, the nature of problem (2.25) is mainly combinatorial in that the major task is to choose the type of conflict-free maneuvers in which one can find the optimal solution. In this section, we deal only with the problem of finding the optimal conflict-free maneuver within a *given* type. We postpone to Section 2.7.4 the discussion on how to choose the maneuver type.

Fix $t_c \in (t_0, t_1)$ and denote by $A_{ij}$ the feasible set for $c_i - c_j$ when only the agent pair $(i, j)$ is present. $A_{ij}$ is computed as set $A$ in the last subsection with $a_i, b_i, a_j, b_j$ in the place of $a_1, b_1, a_2, b_2$. Suppose that we have chosen a type of conflict-free maneuvers. Then, the problem is to find the waypoints $c_1, \ldots, c_k$ that

$$\text{minimize} \sum_{i=1}^{k} \lambda_i \|c_i - c_i^u\|^2 \text{ subject to } c_i - c_j \in A_{ij}^{\pm}, \quad 1 \leq i < j \leq k, \tag{2.29}$$

where $c_i^u$ is defined as in (2.27) for $i = 1, \ldots, k$, and $A_{ij}^{\pm}$ denotes the connected component of the set $A_{ij}$ matching the desired type. Note that only a finite subset of types of conflict-free maneuvers can be represented in this way, and we assume that the given type belongs to this subset.

Notice that in all but the first configuration shown in Figure 2.12 representing $A_{ij}$ for $i = 1$ and $j = 2$, one of the connected components of $A_{ij}$ is nonconvex, posing great challenge for the efficient solution of problem (2.29). Therefore, in configuration 2, 3, and 4, we linearize the nonconvex component of $A_{ij}$ by using a half space inner approximation, as it is shown in Figure 2.12 by the black lines tangential to the boundary of $B(0, r)$. The choice of the black line may not be unique, and it is preferable that the inner approximated feasible region of $c_i - c_j$ contains the unconstrained optimal value $c_i^u - c_j^u$.

**Remark 5** *Problem 2.29 is a linearly constrained convex optimization problem in the special case when any pair of agents is in the first configuration, i.e., when the unconstrained optimal joint maneuver will cause a conflict between any pair of agents. Therefore, our linear approximation scheme is tight for the most critical encounters.*

After the linearization, if necessary, we have a linearly constrained quadratic optimization problem that can be solved efficiently. In the case when the number of agents is relatively small, we can afford the luxury of running the optimization algorithm for each type achievable by 2-legged maneuvers so as to find the globally optimal 2-legged conflict-free maneuver. Simulation results using MATLAB are shown in Figure 2.14 for two 3-agent encounters ($\lambda_1 = \lambda_2 = 0.5$, $r = 20$). In both cases, each pair of agents is in the first configuration, so linearizations are not necessary and the obtained maneuvers are actually the globally optimal 2-legged conflict-free

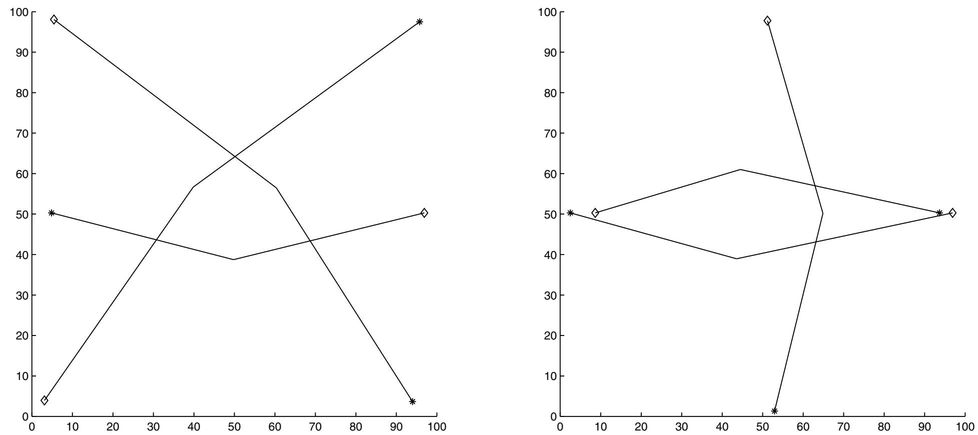

Figure 2.14: Globally optimal 2-legged conflict-free 3-maneuvers.

maneuvers.

### 2.7.3 Optimal $m$-legged conflict-free maneuver for multiple agents

The algorithm described in Section 2.7.2 can be used in an iterative way in the general case when the number $m$ of legs is greater than two. Fix a set of epochs $s_0 = t_0 < s_1 < \cdots < s_{m-1} < s_m = t_1$. A necessary condition for a set of waypoints $c_{i,j}$, $i = 1, \ldots, k$, $j = 0, \ldots, m$, with $c_{i,0} = a_i$, $c_{i,m} = b_i$ to be an optimal solution to problem (2.25) is that

$$c_{i,j} = c_i^*(\langle c_{i,j-1}\rangle_{i=1}^k, \langle c_{i,j+1}\rangle_{i=1}^k, s_{j-1}, s_j, s_{j+1}) \tag{2.30}$$

for $1 \le j \le m-1$. Here $c_i^*(\langle c_{i,j-1}\rangle_{i=1}^k, \langle c_{i,j+1}\rangle_{i=1}^k, s_{j-1}, s_j, s_{j+1})$ denotes the waypoint of agent $i$ for the optimal 2-legged maneuver when the starting and destination positions of the agents are $\langle c_{i,j-1}\rangle_{i=1}^k$ and $\langle c_{i,j+1}\rangle_{i=1}^k$, and the starting, middle and ending epochs are $s_{j-1}, s_j, s_{j+1}$, respectively. This condition inspires the following

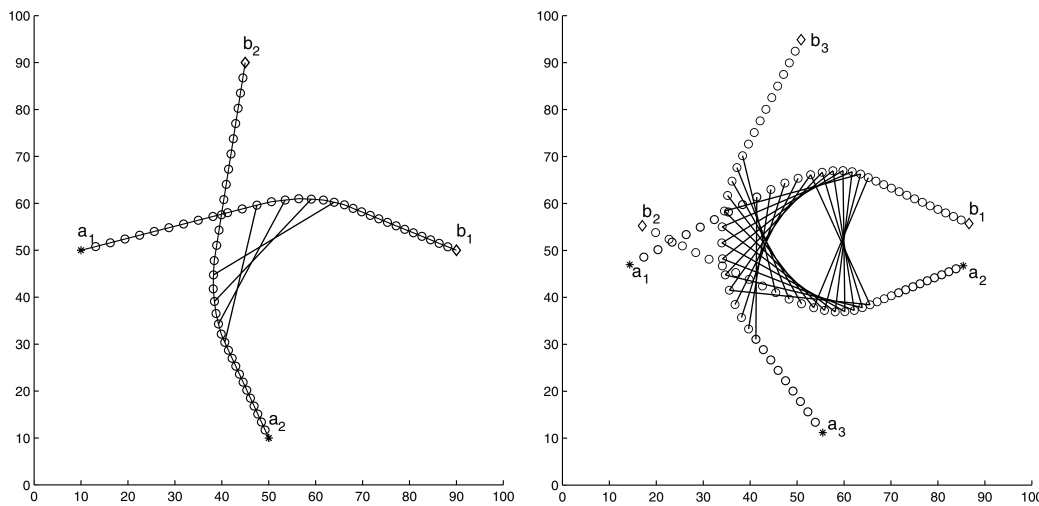


Figure 2.15: Simulation results of Algorithm 1 for two and three agents encounters ($r = 30$).

algorithm.

**Algorithm 1** *1. Let $l = 0$. Pick any feasible set of waypoints $c_{i,j}^{(0)}$, $1 \leq i \leq k$, $0 \leq j \leq m$, such that $c_{i,0}^{(0)} = a_i, c_{i,m}^{(0)} = b_i$ for $1 \leq i \leq k$ and such that the MSE constraint is satisfied over $T$.*

*2. For $j = 1, \ldots, m-1$ compute for $i = 1, \ldots, k$*

$$c_{i,j}^{(l+1)} = c_i^*(\langle c_{i,j-1}^{(l)} \rangle_{i=1}^k, \langle c_{i,j+1}^{(l)} \rangle_{i=1}^k, s_{j-1}, s_j, s_{j+1}).$$

*3. Repeat procedure 2 with $l := l + 1$ until the decrease in energy is below some threshold $\varepsilon$.*

It is easily seen that the energy of the conflict-free maneuvers obtained by Algorithm 1 is non-increasing as a function of the iteration number $l$, and is strictly decreasing whenever condition (2.30) is not satisfied. Therefore, the iteration procedure converges asymptotically to a conflict-free maneuver satisfying condition (2.30). A convergence analysis of Algorithm 1 is yet to be achieved. Besides the issue of local minima suggested by the example in Section 2.5, the situation is further complicated by the fact that the convex optimization procedure introduced in Section 2.7.2 only yields an approximation of $c_i^*$. Another open issue is the sub-optimality of optimal $m$-legged maneuvers in $\mathbf{P}^m(r, \mathbf{a}, \mathbf{b})$ with respect to optimal solutions in $\mathbf{P}(r, \mathbf{a}, \mathbf{b})$. Although in theory the performance gap decreases to zero as $m \to \infty$, in practice, it is not easy to quantify the performance degradation for a finite $m$.

In Figure 2.15, some simulation results for Algorithm 1 when the agents have identical priorities and $r = 30$ are shown. The epochs are chosen to evenly divide $[t_0, t_1]$, and the corresponding waypoints are marked with small circles. In the plots, whenever two agents are at distance $r$, their positions are joined by a line segment. Note that the result shown in the left figure is a good approximation to the optimal maneuvers plotted in Figure 2.6.

### 2.7.4 Randomized optimization

In [22, 59], a decentralized algorithm for multi-agent conflict resolution is proposed in the context of air traffic control. By modeling the agent motion as a Brownian motion with drift, the probability of conflict between two agents is estimated and then used to generate repulsive forces between the agents, inspired by the potential and vortex field methodology for path planning ([46, 62]). Compared with traditional potential field methods that use only the positions of the agents, this algorithm considers also their headings and speeds, and hence generates maneuvers

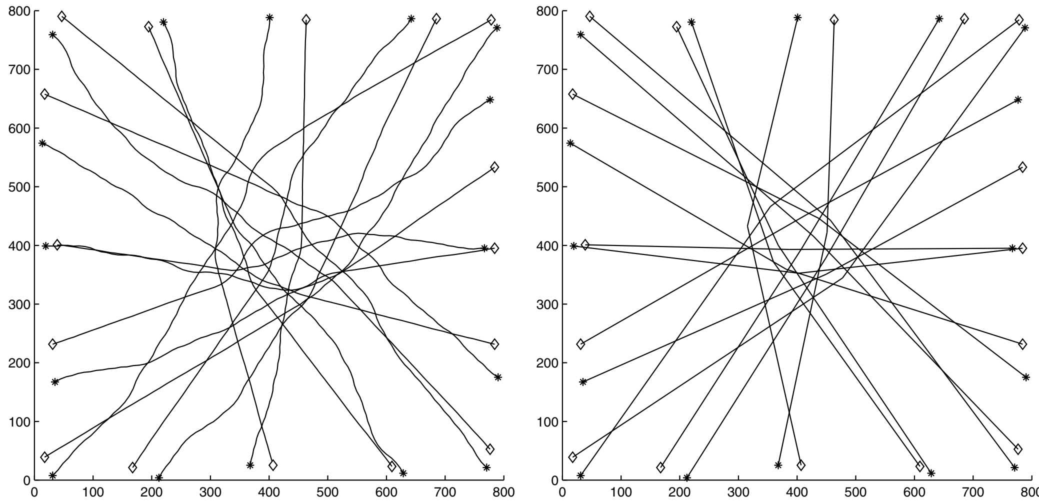


Figure 2.16: 16-maneuvers generated by stochastic (left) and convex optimization algorithm (right).

with less abrupt turns.

Although the stochastic algorithm can be run in real time regardless of the number $k$ of agents involved, one of its drawbacks is that absolute safety cannot be guaranteed with probability one. On the other hand, the convex optimization algorithm we propose in this section can ensure absolute safety, but it cannot handle the explosively increasing number of types when $k$ is large. We then suggest a solution that combines the positive features of these two algorithms, hence it both guarantees safety and is computationally feasible. The proposed algorithm uses the stochastic algorithm as the random "type chooser". More specifically, for a given multi-agent encounter, first the stochastic algorithm is run to generate a joint maneuver corresponding to a particular type, and then the convex optimization algorithm is utilized to obtain an approximation of the optimal multi-legged maneuver within the type selected by the stochastic algorithm.

Simulation results for a 16-agent symmetric encounter are shown in Figure 2.16, in which 16 agents with identical priorities pass approximatively through a common point at angles evenly distributed in $[0, 2\pi]$ and $r = 30$. The one on the left is the joint maneuver generated by the stochastic algorithm, whereas the one on the right is the optimal 2-legged conflict-free maneuver within this type generated by the convex optimization algorithm.

**Remark 6** *When the number of agents is small, say, $k = 2, 3$, experiments show that the stochastic algorithm tends to choose with higher probability those types with lower energy. However, when $k$ is large such as in the previous example, it is hard to evaluate the performance of the randomized algorithm, since currently no theoretical result exists that can exhaust the explosively increasing number of resolution types and find the optimal one (or ones). Much more work is needed in this respect.*

## 2.8 Summary of contributions

In this chapter the problem of optimal coordinated motion planning for multiple agents moving on a plane is studied. After a classification of the homotopy types of conflict-free maneuvers, a weighted energy is proposed as the cost function to select the optimal one. Various local and global optimality conditions are derived. For two-agent encounters, analytical solutions are obtained both for the optimal continuous and piecewise-$C^2$ maneuvers and the optimal 2-legged maneuvers. For the general multi-agent case, a randomized convex optimization algorithm is proposed to find the optimal multi-legged maneuvers numerically.

# Chapter 3

# Three Dimensional Aircraft Conflict Resolution

## 3.1 Introduction

In this chapter, we study the problem of finding optimal conflict-free maneuvers for multiple agents moving in three dimensional Euclidean space. Compared with Chapter 2, in this chapter we focus on the specific problem of aircraft conflict resolution, where a group of aircraft flying in a certain region of the airspace tries to avoid conflicts by employing maneuvers that change not only their headings and speeds, but also their altitudes. The protection zone surrounding each aircraft is now a cylinder instead of a disk in the 2D case. The goal is still to find the conflict-free maneuvers with the minimal weighted energy, where, in defining the energy, we penalize vertical maneuvers with respect to horizontal ones for the sake of passenger comfort.

We stress the numerical aspect in solving the problem. In particular, a geometric construction and a numerical algorithm for computing the optimal resolution maneuvers are given in the two aircraft case. For the multi-aircraft case, an approximation scheme is proposed to compute a suboptimal two-legged solution. Simulation results are also presented to illustrate the effectiveness of the proposed algorithms.

This chapter is organized as follows. First in Section 3.2 we formulate the optimal conflict resolution problem in 3D airspace. An energy function is proposed as the cost, which takes into consideration different priorities of the aircraft, as well as penalty for vertical maneuvers over horizontal ones. Then in Section 3.3 some necessary conditions for optimal conflict-free maneuvers are derived. These enable us to propose in Section 3.4 a geometric characterization of the optimal resolution maneuvers in the two aircraft case and a numerical procedure to compute them. For the multiple aircraft case, in Section 3.5 the original constrained optimization problem is approximated by a finite dimensional convex optimization problem. Simulation results for some typical multi-aircraft encounters are presented.

The proposed approaches have some limitations. Specifically, constraints on the aircraft dynamics are not taken into account and the adopted model is simple. However, we discuss some methods that can be adopted to alleviate these limitations. In particular, we introduce additional (convex) constraints so as to restrict the sharp turns near the waypoints that would make the two-legged maneuvers not flyable in practice.

## 3.2 Problem formulation

Consider a group of aircraft, numbered from 1 to $k$, flying in a certain region of the airspace that have been isolated so that only conflicts among aircraft in this group need to be considered during the time interval of interest $T = [t_0, t_1]$. Suppose that each aircraft, say, aircraft $i$, starts at time $t_0$ at $a_i \in \mathbb{R}^3$ and is destined to reach $b_i \in \mathbb{R}^3$ at time $t_1$. Similarly as in Chapter 2, we denote by $\mathbf{P}_i$ the set of all *maneuvers* for aircraft $i$, where a maneuver $\alpha_i$ for aircraft $i$ is a continuous and piecewise $C^2$ map from $T$ to $\mathbb{R}^3$ satisfying $\alpha_i(t_0) = a_i$ and $\alpha_i(t_1) = b_i$. The *energy* of a maneuver $\alpha_i$ for aircraft $i$ is defined as

$$J(\alpha_i) = \frac{1}{2} \int_{t_0}^{t_1} ||\dot{\alpha}_i(t)||^2 \, dt. \tag{3.1}$$

Let $\mathbf{P}(\mathbf{a}, \mathbf{b}) \triangleq \mathbf{P}_1 \times \cdots \times \mathbf{P}_k$ be the set of all joint maneuvers (or $k$-maneuvers), where $\mathbf{a} = \langle a_i \rangle_{i=1}^k$ and $\mathbf{b} = \langle b_i \rangle_{i=1}^k$ are the starting and destination positions of the $k$-aircraft system, respectively. A joint maneuver $\alpha = \langle \alpha_i \rangle_{i=1}^k \in \mathbf{P}(\mathbf{a}, \mathbf{b})$ is said to be *conflict-free* if during the time interval $T$ none of the aircraft enters the cylindrical protection zone of radius $r$ and height $2h$ surrounding another aircraft. If for an arbitrary $c \in \mathbb{R}^3$ we denote by $c_{xy} \in \mathbb{R}^2$ and $c_z \in \mathbb{R}$ its components on the horizontal $xy$ plane and the vertical $z$-axis, respectively, then the conflict-free condition is equivalent to the condition that there is no pair of indices $(i, j)$, $1 \leq i < j \leq k$, such that $\|\alpha_{i,xy}(t) - \alpha_{j,xy}(t)\| < r$ and $|\alpha_{i,z}(t) - \alpha_{j,z}(t)| < h$ for some $t \in T$.

We denote with $\mathbf{P}(r, h; \mathbf{a}, \mathbf{b})$ the set of all *conflict-free (joint) maneuvers* with starting position $\mathbf{a}$ and destination position $\mathbf{b}$ for the $k$-aircraft system. We shall occasionally call conflict-free maneuvers *resolution maneuvers.* We assume that each pair of points in the $k$-tuple $\mathbf{a}$ satisfies either the horizontal or the vertical separation condition so that there is no conflict for the $k$-aircraft system at time $t_0$. Similarly for $\mathbf{b}$. As a result, the set $\mathbf{P}(r, h; \mathbf{a}, \mathbf{b})$ is nonempty.

The performance of a $k$-maneuver $\alpha = \langle \alpha_i \rangle_{i=1}^{k} \in \mathbf{P}(\mathbf{a}, \mathbf{b})$ is characterized in terms of its (weighted) energy (or $\lambda$-energy) defined as

$$J(\alpha) \triangleq \sum_{i=1}^{k} \lambda_i J(\alpha_i), \tag{3.2}$$

where $\lambda_1, \ldots, \lambda_k$ are positive real numbers adding up to 1. By an appropriate choice of these numbers, one can assign different priorities to the $k$ aircraft. In particular, one can associate smaller $\lambda_i$ to those aircraft with higher maneuverability so that they will assume a larger responsibility in resolving the conflict.

In this chapter we try to solve the following problem:

$$\text{Minimize } J(\alpha) \text{ subject to } \alpha \in \mathbf{P}(r, h; \mathbf{a}, \mathbf{b}). \tag{3.3}$$

Solutions to problem (3.3) are called *optimal (resolution) maneuvers.*

In this formulation, it can be expected that the optimal resolution maneuvers will mainly utilize the vertical dimension for almost all encounters since the minimum allowed vertical distance $h$ is typically much smaller than the minimum allowed horizontal distance $r$. However, vertical maneuvers are usually the least comfortable ones for passengers. This is the reason why we now redefine the energy of a maneuver $\alpha_i$ in equation (3.1) as follows:

$$J(\alpha_i) = \frac{1}{2} \int_{t_0}^{t_1} [\|\dot{\alpha}_{i,xy}(t)\|^2 + \eta^2 |\dot{\alpha}_{i,z}(t)|^2] \, dt, \tag{3.4}$$

where $\eta \geq 1$ is a coefficient introduced to penalize the vertical maneuvers. The $\lambda$-energy of a joint maneuver $\alpha$ is then defined by (3.2) with $J(\alpha_i)$ given by (3.4) instead of by (3.1).

This modification does not add further difficulties to the solution of problem (3.3), since the minimization of the new cost function can be easily reduced to the previous one without penalty by scaling the $z$-axis by a factor of $\eta$. After the scaling, the starting and destination positions $\mathbf{a}$ and $\mathbf{b}$ of the $k$-aircraft system become $\tilde{\mathbf{a}}$ and $\tilde{\mathbf{b}}$, while the radius and the height of the protection zone become $r$ and $2\eta h$, respectively. Each conflict-free maneuver $\alpha \in \mathbf{P}(r, h; \mathbf{a}, \mathbf{b})$ is scaled to a conflict-free maneuver $\tilde{\alpha}$ in $\mathbf{P}(r, \eta h; \tilde{\mathbf{a}}, \tilde{\mathbf{b}})$, and the $\lambda$-energy with penalty $\eta$ of $\alpha$ is in fact equal to the $\lambda$-energy without penalty of $\tilde{\alpha}$. Therefore, optimal solutions to the original problem can be obtained by first minimizing $J(\tilde{\alpha})$ subject to $\tilde{\alpha} \in \mathbf{P}(r, \eta h; \tilde{\mathbf{a}}, \tilde{\mathbf{b}})$ with no penalty on the vertical maneuvers, and then mapping the obtained solutions to $\mathbf{P}(r, h; \mathbf{a}, \mathbf{b})$ by scaling the $z$-coordinates back by a factor of $1/\eta$. Note that the protection zone of the scaled problem is a cylinder of radius $r$ and height $2\eta h$. Hence for larger $\eta$ horizontal resolution maneuvers are more likely to be invoked. In particular, in the case where all the starting and destination positions are on the same horizontal plane, if $\eta \to \infty$ the problem degenerates into the 2D problem studied in the previous chapter.

From the above discussions, we can assume without loss of generality that $\eta = 1$. Thus the $\lambda$-energy of a joint maneuver $\alpha$ is given by (3.2) with $J(\alpha_i)$ still defined by (3.1).

## 3.3 The $\lambda$-alignment condition

The starting and destination positions $\mathbf{a}$ and $\mathbf{b}$ of a $k$-aircraft system are said to be $\lambda$-*aligned* if they have the same $\lambda$-centroid, i.e., if $\sum_{i=1}^{k} \lambda_i a_i = \sum_{i=1}^{k} \lambda_i b_i$.

For each $w \in \mathbb{R}^3$ we denote by $\mathbf{b} + w$ the $k$-tuple $\langle b_i + w \rangle_{i=1}^{k}$, which can be thought of as a new destination position of the $k$-aircraft system.

**Definition 9** *The tilt operator* $\mathcal{T}_w : \mathbf{P}(r,h;\mathbf{a},\mathbf{b}) \to \mathbf{P}(r,h;\mathbf{a},\mathbf{b}+w)$ *is a map such that for any* $\alpha \in \mathbf{P}(r,h;\mathbf{a},\mathbf{b})$*,* $\beta = \mathcal{T}_w(\alpha) \in \mathbf{P}(r,h;\mathbf{a},\mathbf{b}+w)$ *is defined by* $\beta_i(t) = \alpha_i(t) + \frac{t-t_0}{t_1-t_0}w$*,* $\forall t \in T,\ i = 1,\ldots,k$*.*

Following similar steps as in the previous chapter, we can prove the following two propositions.

**Proposition 9** *Suppose that* $\alpha^* \in \mathbf{P}(r,h;\mathbf{a},\mathbf{b})$ *is an optimal solution to problem (3.3). Then* $\beta^* = \mathcal{T}_w(\alpha^*)$ *minimizes* $J(\beta)$ *subject to* $\beta \in \mathbf{P}(r,h;\mathbf{a},\mathbf{b}+w)$*.*

For arbitrary $\mathbf{a}$ and $\mathbf{b}$, set $\mathbf{b}' = \mathbf{b} + w$ where $w = \sum_{i=1}^k \lambda_i(a_i - b_i)$. Then $\mathbf{a}$ and $\mathbf{b}'$ are $\lambda$-aligned. By Proposition 9, solving problem (3.3) for the $\lambda$-aligned $\mathbf{a}$ and $\mathbf{b}'$ is equivalent to solving problem (3.3) for the original $\mathbf{a}$ and $\mathbf{b}$. Therefore, we can focus on the $\lambda$-aligned case.

**Proposition 10** *Assume that* $\alpha^* \in \mathbf{P}(r,h;\mathbf{a},\mathbf{b})$ *is an optimal solution to problem (3.3). Then*

$$\sum_{i=1}^k \lambda_i \alpha_i^*(t) = \sum_{i=1}^k \lambda_i a_i + \frac{t-t_0}{t_1-t_0}\Big(\sum_{i=1}^k \lambda_i b_i - \sum_{i=1}^k \lambda_i a_i\Big), \quad \forall t \in T, \tag{3.5}$$

*which in the case of $\lambda$-aligned* $\mathbf{a}$ *and* $\mathbf{b}$ *reduces to*

$$\sum_{i=1}^k \lambda_i \alpha_i^*(t) = \sum_{i=1}^k \lambda_i a_i = \sum_{i=1}^k \lambda_i b_i, \quad \forall t \in T.$$

## 3.4 Optimal maneuvers for two-aircraft encounters

In this section we describe how optimal resolution maneuvers for two-aircraft encounters can be constructed. The approach closely parallels that in Section 2.4.2 in the 2D case. This construction will be used in Section 3.5 to determine an approximate solution to problem (3.3) in the multiple aircraft case.

Assume that $\mathbf{a} = (a_1, a_2)$ and $\mathbf{b} = (b_1, b_2)$ are $\lambda$-aligned and denote with $c$ their common $\lambda$-centroid, i.e., $c = \lambda_1 a_1 + \lambda_2 a_2 = \lambda_1 b_1 + \lambda_2 b_2$. By Proposition 10, an optimal 2-maneuver $\alpha^* = (\alpha_1^*, \alpha_2^*) \in \mathbf{P}(r, h; \mathbf{a}, \mathbf{b})$ satisfies

$$\alpha_1^*(t) - c = -\frac{\lambda_2}{\lambda_1}(\alpha_2^*(t) - c), \quad \forall t \in T, \tag{3.6}$$

from which it easily follows that the energies of $\alpha_1^*$ and $\alpha_2^*$ are related by $\lambda_1^2 J(\alpha_1^*) = \lambda_2^2 J(\alpha_2^*)$. Hence the problem becomes finding among all conflict-free maneuvers satisfying equation (3.6) the one that minimizes the energy of the maneuver for a single aircraft, say, aircraft 1. By equation (3.6), the separation constraint is equivalent to that the curve $\alpha_1^*(\cdot)$ never enters the open cylinder $W_\lambda$ of radius $r_\lambda = \lambda_2 r$ and height $2h_\lambda = 2\lambda_2 h$ centered symmetrically around $c$.

As a result, problem (3.3) is equivalent to:

$$\text{minimize } J(\alpha_1) \text{ subject to } \alpha_1 \in \mathbf{P}_1, \text{ and } \alpha_1(t) \in \mathbb{R}^3 \setminus W_\lambda \text{ for all } t \in T, \tag{3.7}$$

which consists in finding minimum energy maneuvers of a single aircraft in the presence of the static obstacle $W_\lambda$. So a solution to problem (3.7) is a constant-speed motion along a shortest curve joining $a_1$ to $b_1$ while avoiding the obstacle $W_\lambda$. Under the feasibility assumption, both $a_1$ and $b_1$ belong to $\mathbb{R}^3 \setminus W_\lambda$, and such a curve can be computed efficiently by an algorithm whose description is postponed to Section 3.4.2 due to its technicality. Once $\alpha_1^*$ is computed, $\alpha_2^*$ can be obtained from $\alpha_1^*$ through equation (3.6), thus concluding the discussions on the $\lambda$-aligned case.

For the general case when $\mathbf{a}$ and $\mathbf{b}$ are not necessarily $\lambda$-aligned, by Propo-

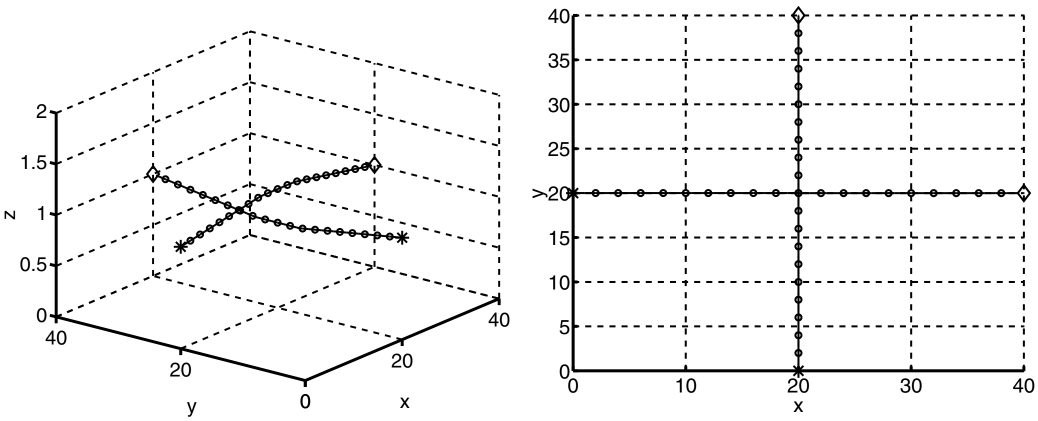


(a) (b)

Figure 3.1: An optimal resolution maneuver for an orthogonal two-aircraft encounter ($\eta = 5$ and $\lambda_1 = \lambda_2 = 0.5$): (a) three dimensional representation; (b) top view.

sition 9, an optimal solution $\alpha^* \in \mathbf{P}(r, h; \mathbf{a}, \mathbf{b})$ to problem (3.3) is given by:

$$\begin{cases} \alpha_1^*(t) = \gamma_1^*(\mathbf{a}, \mathbf{b} + w)(t) - \frac{t - t_0}{t_1 - t_0} w \\ \alpha_2^*(t) = \gamma_2^*(\mathbf{a}, \mathbf{b} + w)(t) - \frac{t - t_0}{t_1 - t_0} w \end{cases}, \quad \forall t \in T, \tag{3.8}$$

where $(\gamma_1^*(\mathbf{a}, \mathbf{b} + w), \gamma_2^*(\mathbf{a}, \mathbf{b} + w))$ denotes an optimal conflict-free maneuver in $\mathbf{P}(r, h; \mathbf{a}, \mathbf{b} + w)$ with $w = \lambda_1 a_1 - \lambda_1 b_1 + \lambda_2 a_2 - \lambda_2 b_2$ (note that $\mathbf{a}$ and $\mathbf{b} + w$ are $\lambda$-aligned).

### 3.4.1 Some examples of optimal 2-maneuvers

In this section, we present some examples of two-aircraft encounters, and discuss the influence of various factors on the corresponding optimal resolution maneuvers. In all of the examples, the coordinates of the aircraft positions are measured in nmi, with $r = 5$ nmi and $h = 0.3292$ nmi.

We start by considering a two-aircraft encounter where $a_1 = (0, 20, 1)$, $b_1 =$

$(40, 20, 1)$, and $a_2 = (20, 0, 1)$, $b_2 = (20, 40, 1)$, so that the two straight lines each connecting the starting and destination positions of an aircraft are on the same horizontal plane and cross each other at a right angle. These two lines are the *ideal trajectories* of the two aircraft.

Figure 3.1 shows an optimal maneuver in the case when the two aircraft have the same priority ($\lambda_1 = \lambda_2 = 0.5$) and $\eta = 5$. Starting and destination positions of the two aircraft are marked with stars and diamonds, respectively, whereas the circles represent the aircraft positions at equally spaced time instants. Hence the denser the circles, the slower the motions. The top view in (b) shows that the conflict is resolved by vertical deviations from the ideal trajectories.

We now study the effect of the priority coefficients on the optimal resolution maneuvers. Plotted in Figure 3.2 are optimal resolution maneuvers for the same two-aircraft orthogonal encounter under three different sets of aircraft priorities and the same $\eta$ ($\eta = 5$). Although the optimal maneuvers in all three cases have the same top view (shown in the right-hand side of Figure 3.1), the vertical deviation of aircraft 1 from its ideal trajectory decreases as its priority increases. In other words, aircraft 2 with smaller priority will assume more responsibility in resolving the conflict. In the extreme case when $\lambda_1 = 1$ and $\lambda_2 = 0$, the optimal resolution maneuver will be such that aircraft 1 flies along its ideal trajectory, while aircraft 2 assumes all the responsibility of avoiding conflicts with aircraft 1. These conclusions hold in general for multi-aircraft encounters.

As for the effect of the vertical penalty factor, note that in Figure 3.1 where $\eta = 5$ and $\lambda_1 = \lambda_2 = 0.5$, the conflict is resolved using only vertical deviations from the ideal trajectories. In contrast, in the case shown in Figure 3.3 where $\eta$ is set equal

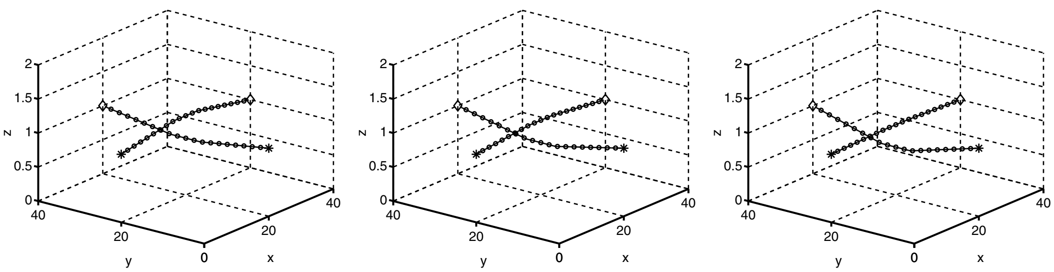


(a) (b) (c)

Figure 3.2: Optimal resolution maneuvers for the orthogonal two-aircraft encounter under three different sets of aircraft priorities ($\eta = 5$): (a) $\lambda_1 = 0.5$, $\lambda_2 = 0.5$; (b) $\lambda_1 = 0.7$, $\lambda_2 = 0.3$; (c) $\lambda_1 = 0.9$, $\lambda_2 = 0.1$.

to 15 ($\lambda_1 = \lambda_2 = 0.5$), the conflict is resolved using only horizontal deviations. The explanation is that, in order to obtain the optimal resolution maneuvers, we have to scale the $z$-axis by a factor of $\eta$. When $\eta$ is so large that the height of the cylindrical obstacle becomes much larger than its radius, a shortest curve between two points across the cylinder is more likely to be a curve around the side of the cylinder than around its top or bottom. Therefore, the larger the vertical penalty factor $\eta$, the more likely it is that an optimal resolution maneuver will consist of horizontal deviations from the ideal trajectories. In general, for encounters involving two or more aircraft, there are two extreme cases: When $\eta$ is very large and the aircraft initial and destination positions are all at about the same altitude, the problem degenerates into a planar conflict resolution problem, where only horizontal deviations are allowed in resolving the conflict; When $\eta$ is close to 0, then only vertical deviations are used in the optimal resolution maneuvers and their top views consist of straight line segments.

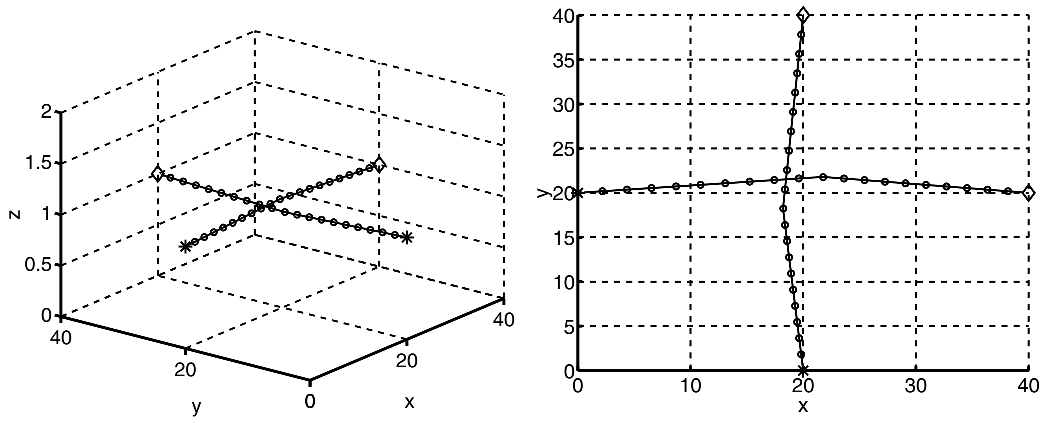


(a) (b)

Figure 3.3: An optimal resolution maneuver for the orthogonal two-aircraft encounter with larger $\eta = 15$ ($\lambda_1 = \lambda_2 = 0.5$): (a) three dimensional representation; (b) top view.

### 3.4.2 Shortest curve between two points in $\mathbb{R}^3$ avoiding a cylindrical obstacle

In this section we address the problem of computing a shortest curve in $\mathbb{R}^3$ connecting two points while avoiding a cylindrical obstacle. This is to complete the solution to problem (3.3) in the two aircraft case (i.e., problem (3.7)).

Consider a cylinder of radius $r$ and height $2h$ centered at the origin:

$$D = \{(x, y, z) \in \mathbb{R}^3 : \; x^2 + y^2 < r^2 \text{ and } |z| < h\}.$$

Given two points $a$ and $b$ in $\mathbb{R}^3 \setminus D$, we wish to

$$\text{find a shortest curve in } \mathbb{R}^3 \setminus D \text{ connecting } a \text{ and } b. \tag{3.9}$$

Problem (3.9) is a special instance of the general problem of finding distance-minimizing geodesics in manifolds with (nonsmooth) boundary. Determining shortest curves in the presence of geometric obstacles is a well studied problem in computational geometry. See the surveys [51, 52]. Here we study a very special case.

It is obvious that when $a$ and $b$ are *visible* to each other in the sense that the line segment joining $a$ and $b$ does not intersect the obstacle $D$, the shortest curve we are looking for is the straight line segment joining $a$ and $b$; hence, the solution to problem (3.9) is trivial. Suppose now that $a$ and $b$ are not visible to each other.

Since the cylinder $D$ is convex, a shortest curve in $\mathbb{R}^3 \setminus D$ connecting two points on its boundary $\partial D$ is contained entirely in $\partial D$, and is a distance-minimizing geodesic of $\partial D$ in its own geometry. For general $a$ and $b$ not necessarily belonging to $\partial D$, we have that

**Proposition 11** *A shortest curve in $\mathbb{R}^3 \setminus D$ connecting $a$ and $b$ can be decomposed into three segments: a straight line segment from $a$ to a point $p \in \partial D$, a geodesic segment of $\partial D$ from $p$ to a point $q \in \partial D$, and a straight line segment from $q$ to $b$. Moreover, the two line segments are contained entirely in the interior of $\mathbb{R}^3 \setminus D$ except for their end points $p$ and $q$.*

If the shortest curve between $a$ and $b$ is viewed as a path traveled from $a$ to $b$, then Proposition 11 says that the curve will enter and exit $\partial D$ exactly once, at positions $p$ and $q$, respectively. We then call $p$ and $q$ *entry point* and *exit point*, respectively. As a result of Proposition 11, solving problem (3.9) is equivalent to determining the entry point $p$, the exit point $q$, and the distance-minimizing geodesic segment on $\partial D$ between $p$ and $q$. In the case when $a \in \partial D$, $p = a$ and the first line segment degenerates into a single point. Similarly for the second line segment if $b \in \partial D$. The middle geodesic segment in $\partial D$ degenerates into a single point if $p = q$, in which case the two straight line segments are not collinear since $a$ and $b$

are assumed to be not visible to each other.

There are certain restrictions on the possible locations of $p$ and $q$ in $\partial D$. Denote with $\partial D_T$ and $\partial D_B$ the closed disks of radius $r$ constituting respectively the top and bottom surfaces of the cylinder $D$. Denote with $\partial D_S$ the side surface of $D$ (boundary included). Then $\partial D = \partial D_T \cup \partial D_B \cup \partial D_S$. The entry point $p$ and the exit point $q$ must satisfy the following conditions. First of all, $p$ is visible to $a$ and $q$ visible to $b$. Moreover, if $a$ (respectively, $b$) is in the interior of $\mathbb{R}^3 \setminus D$, then $p$ (respectively, $q$) belongs to the *contour* of $D$ with respect to a viewer situated at $a$ (respectively, $b$). In particular, this implies that $p \in \partial D_S$ unless $a$ is in the interior of $\partial D_T$ or $\partial D_B$, and $q \in \partial D_S$ unless $b$ is in the interior of $\partial D_T$ or $\partial D_B$.

Notice that $D$ is a subset of the whole cylinder $Q$ defined by $Q = \{(x, y, z) \in \mathbb{R}^3 : \; x^2 + y^2 < r^2\}$. We can then distinguish the following three cases:

**Case 1.** Both $a$ and $b$ are outside of $Q$, and at least one of them has $z$-coordinate in $[-h, h]$;

**Case 2.** Both $a$ and $b$ are outside of $Q$, and neither of them has $z$-coordinate in $[-h, h]$;

**Case 3.** At least one of $a$ and $b$ belongs to $Q$.

In each one of these cases solutions to problem (3.9) can assume only a finite number of possible configurations. We shall describe in the following a numerical procedure to compute a shortest curve for each such configuration. Although in general it is difficult to obtain an analytic solution, one can reduce the problem to a finite number of simple optimization problems, each over a compact region of $\mathbb{R}^1$ or at most $\mathbb{R}^2$.

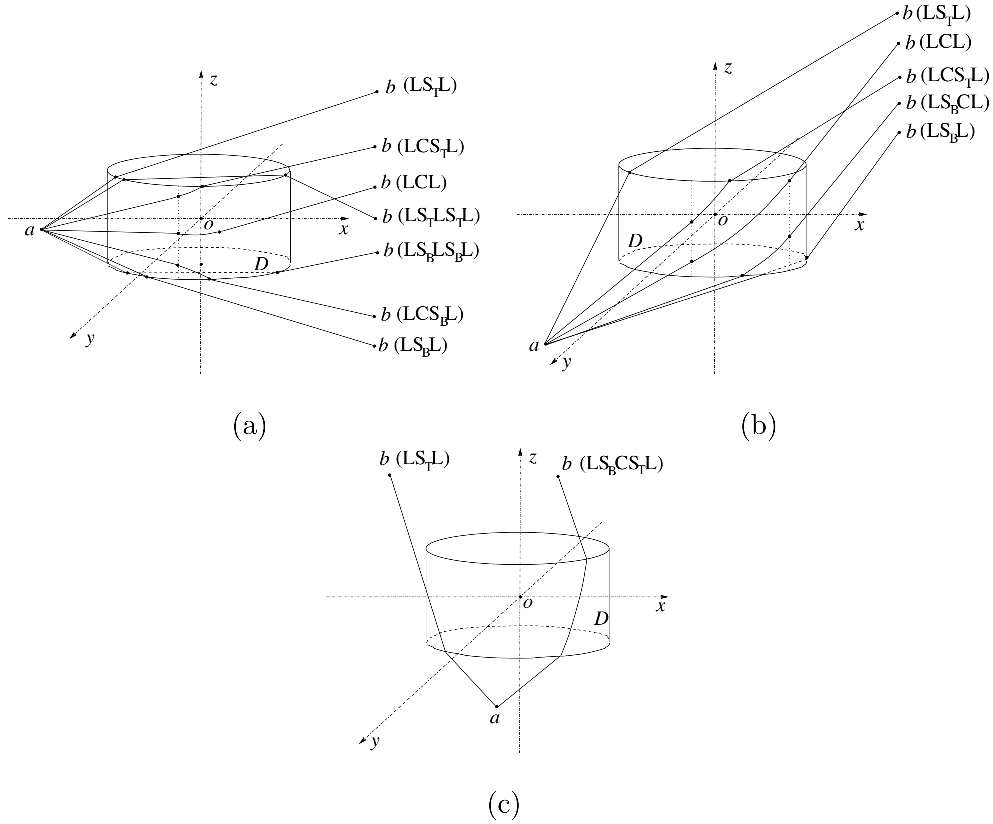


Figure 3.4: Possible configurations for the solutions in (a) case 1; (b) case 2; (c) case 3.

**Case 1** By the symmetry of $D$, we consider only the case when both $a = (a_x, a_y, a_z)$ and $b = (b_x, b_y, b_z)$ are outside of $Q$ and $|a_z| \leq h$. The case when $|b_z| \leq h$ is similar. Without loss of generality we can assume that $a_y = 0$, $a_x \leq -r$, and $b_y \geq 0$. To find a shortest curve in $\mathbb{R}^3 \setminus D$ between $a$ and $b$, we need to focus only on those curves contained in $\{(x, y, z) : y \geq 0\}$. Specifically, solutions to problem (3.9) may have the following possible configurations:

- $LS_TL$: a line segment from $a$ to $p \in \partial D_T \cap \partial D_S$ followed by a line segment from $p$ to $b$;

- $LS_TLS_TL$: a line segment from $a$ to $p \in \partial D_T \cap \partial D_S$, then a line segment from $p$ to $q \in \partial D_T \cap \partial D_S$ in $\partial D_T$, and finally a line segment from $q$ to $b$;
- $LCS_TL$: a line segment from $a$ to $p \in \partial D_S$, then a helix on $\partial D_S$ from $p$ to $q \in \partial D_T \cap \partial D_S$, and finally a line segment from $q$ to $b$;
- $LCL$: a line segment from $a$ to $p \in \partial D_S$ followed by a helix from $p$ to $q \in \partial D_S$, and finally a line segment from $q$ to $b$;
- $LCS_BL$: mirror image of configuration $LCS_TL$ across the $xy$-plane, i.e., a line segment from $a$ to $p \in \partial D_S$, then a helix on $\partial D_S$ from $p$ to $q \in \partial D_B \cap \partial D_S$, and finally a line segment from $q$ to $b$;
- $LS_BLS_BL$: mirror image of configuration $LS_TLS_TL$ across the $xy$-plane;
- $LS_BL$: mirror image of configuration $LS_TL$ across the $xy$-plane.

See Figure 3.4 (a) for the plots of these configurations. In some degenerate cases, one solution may belong to two configurations at the same time.

Depending on the specific position of $b$, only a subset of the configurations should be considered. For example, if $b$ has $z$-coordinate $b_z > h$, then only configurations $LS_TL$, $LCS_TL$, and $LCL$ are possible. If $|b_z| \leq h$, then possible configurations are $LS_TLS_TL$, $LCL$, and $LS_BLS_BL$. If $b_z < -h$, then only configurations $LS_BL$, $LCS_BL$, and $LCL$ should be considered.

Given $a$ and $b$, we can find a shortest curve in each one of the possible configurations. A global solution is the shortest one of them. We now show how to compute a shortest curve for some typical configurations.

Consider the case when $b_z > h$. Then the optimal entry point $p$ in configuration $LS_TL$ can be obtained by solving the following optimization problem:

$$\text{minimize } \|a - (r\cos\theta, r\sin\theta, h)\| + \|b - (r\cos\theta, r\sin\theta, h)\| \tag{3.10}$$

for $\theta$ subject to the constraint that $(r\cos\theta, r\sin\theta, h)$ is visible to $a$, which translates into $\theta \in [\theta_-, \theta_+]$ for some $\theta_-$ and $\theta_+$ with $\theta_- \le \theta_+$. This optimization problem can be solved by many standard numerical algorithms efficiently. In most practical situations, the existence of local minima is not a problem since the cost function (3.10) either has a unique interior minimum, or has a minimum at the boundary $\theta_-$ or $\theta_+$, which is a hint that the corresponding neighboring configuration can provide even better solutions. This phenomenon is typical for other configurations as well.

Another possible configuration when $b_z > h$ is $LCS_TL$. In this case, denote $p = (r\cos\theta_0, r\sin\theta_0, z)$ for some $z \in [-h, h]$, where $\theta_0$ is determined by the contour of $D$ for a viewer sitting at $a$ (shown in Figure 3.4 (a) by the vertical dotted line), and let $q = (r\cos\theta, r\sin\theta, h)$ for some $\theta$ such that $q$ is visible to $b$ and $|\theta - \theta_0| \le \pi$. Then the optimal $p$ and $q$ are obtained by solving the following problem:

$$\begin{aligned}\text{minimize } &\|a - (r\cos\theta_0, r\sin\theta_0, z)\| + \sqrt{(h-z)^2 + r^2(\theta_0 - \theta)^2} \\ &+ \|b - (r\cos\theta, r\sin\theta, h)\|.\end{aligned}$$

Note that the feasible region of $(z, \theta)$ is a compact rectangle, thus the above optimization problem admits a solution, which can be computed by using, for example, the 'fminsearch' function in MATLAB.

Other configurations can be solved similarly. It should be pointed out that configuration $LCL$ is the only one for which an analytic solution exists, which can be obtained by a simple geometric construction (unwrapping the cylinder).

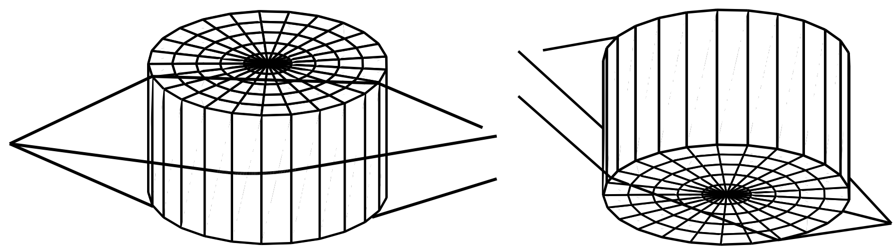


Figure 3.5: Three configurations of case 1 viewed from two different angles ($r = 5$, $h = 3$).

Shortest curves assuming different configurations in case 1 are shown in Figure 3.5 with one end point fixed and the other one assuming various positions.

**Case 2** We now study the case when both $a = (a_x, a_y, a_z)$ and $b = (b_x, b_y, b_z)$ are outside of $Q$ and neither of them has $z$-coordinate in $[-h, h]$. Since $a$ and $b$ are supposed to be not visible to each other, one of them has $z$-coordinate smaller than $-h$, and the other has $z$-coordinate greater than $h$. We assume without loss of generality that $a_z < -h$ and $b_z > h$. As in case 1, we assume that the coordinate axes are properly chosen such that $a_y = 0$, $a_x \leq -r$, and $b_y \geq 0$, so that we can focus on the curves contained in $\{(x, y, z) : y \geq 0\}$.

The five possible configurations for a shortest curve in $\mathbb{R}^3 \setminus D$ connecting $a$ and $b$ are plotted in Figure 3.4 (b). They include three configurations $LS_TL$, $LCS_TL$, and $LCL$ already introduced in case 1, and two new configurations $LS_BCL$ and $LS_BL$. Configuration $LS_BCL$ consists of first a line segment from $a$ to $p \in \partial D_B \cap \partial D_S$, then a helix on $\partial D_S$ from $p$ to $q \in \partial D_S$, and finally a line segment from $q$ to $b$. Configuration $LS_BL$ consists of two line segments with a turning point belonging to $\partial D_B \cap \partial D_S$. The process of obtaining a shortest curve joining $a$ and $b$

for each configuration is entirely analogous to case 1, hence it is omitted.

**Case 3** Finally, consider the case when at least one of $a$ and $b$ (say, $a$) belongs to $Q$. By a possible reflection across the $xy$-plane, we assume $a_z \leq -h$. Then depending on the location of $b$, there are two possible configurations for a shortest curve in $\mathbb{R}^3 \setminus D$ between $a$ and $b$, which are plotted in Figure 3.4 (c).

- $LS_BL$: two line segments with a turning point at $p = q \in \partial D_B \cap \partial D_S$;

- $LS_BCS_TL$: A helix on $\partial D_S$ sandwiched by two line segments such that $p \in \partial D_B \cap \partial D_S$ and $q \in \partial D_T \cap \partial D_S$.

If $b$ belongs to $Q$, then only configuration $LS_BCS_TL$ is possible. Otherwise both of the two configurations have to be considered. A shortest curve in each configuration is obtained in the same way as before. However, it should be pointed out here that for configuration $LS_BCS_TL$, unlike the previous cases, the existence of local minima does pose some problems, since the optimization is over the product of two circles $\partial D_T \cap \partial D_S$ and $\partial D_B \cap \partial D_S$, i.e., a torus. We suggest to partition each of the two circles into several segments, solve the optimization problem in each segment, and then choose the best one. We shall not go into further details since they are irrelevant to the main development.

This complete our discussion on how to compute a solution to problem (3.7), which in turn solves problem (3.3) in the two-aircraft case.

## 3.5 Optimal two-legged maneuvers for multiple aircraft

The approach adopted in the previous sections cannot be easily generalized to the multiple aircraft case since there are too many configurations to be considered. In this section we simplify the problem by considering two-legged maneuvers specified by a set of waypoints.

Consider a $k$-aircraft system with starting position $\mathbf{a} = \langle a_i \rangle_{i=1}^{k}$ and destination position $\mathbf{b} = \langle b_i \rangle_{i=1}^{k}$. Fix an epoch $t_c \in T$ such that $t_0 < t_c < t_1$. For each aircraft $i$, $i = 1, \ldots, k$, choose a waypoint $c_i \in \mathbb{R}^3$. A *two-legged maneuver* with waypoint $c_i$ for aircraft $i$ is a maneuver consisting of two stages: first from $a_i$ at time $t_0$ to $c_i$ at time $t_c$, and then from $c_i$ at time $t_c$ to $b_i$ at time $t_1$, moving at constant velocity in both stages. Denote with $\mathbf{P}_i^2$ the set of all two-legged maneuvers of aircraft $i$, and with $\mathbf{P}^2(\mathbf{a}, \mathbf{b}) = \mathbf{P}_1^2 \times \cdots \times \mathbf{P}_k^2$ the set of all *two-legged joint maneuvers* of the $k$-aircraft system. Denote with $\mathbf{P}^2(r, h; \mathbf{a}, \mathbf{b})$ the subset of $\mathbf{P}^2(\mathbf{a}, \mathbf{b})$ consisting of all those elements of $\mathbf{P}^2(\mathbf{a}, \mathbf{b})$ that are conflict-free. We assume that the epoch $t_c$ is fixed, so that each maneuver in $\mathbf{P}^2(\mathbf{a}, \mathbf{b})$ (and hence in $\mathbf{P}^2(r, h; \mathbf{a}, \mathbf{b})$) is uniquely specified by the waypoints $\langle c_i \rangle_{i=1}^{k}$. The choice of a uniform $t_c$ for all of the aircraft is for the sake of simplicity. It is possible to extend our approach to allow for different $t_c$ for the aircraft, though at the cost of increased complexity.

Now we try to solve the following problem:

$$\text{minimize } J(\alpha) \text{ subject to } \alpha \in \mathbf{P}^2(r, h; \mathbf{a}, \mathbf{b}). \tag{3.11}$$

One reason why one should study problem (3.11) instead of the general problem (3.3) is due to the ATM practice: it is far simpler for the central controller to transmit the aircraft trajectory information in the form of waypoints and times to reach these waypoints rather than continuous trajectories.

By using exactly the same arguments leading to Proposition 10, one can prove that the $\lambda$-alignment condition holds also for the two-legged case.

**Proposition 12** *Suppose that a solution $\alpha^* \in \mathbf{P}^2(r,h;\mathbf{a},\mathbf{b})$ to problem (3.11) has waypoints $\langle c_i^* \rangle_{i=1}^k$. Then*

$$\sum_{i=1}^k \lambda_i c_i^* = \sum_{i=1}^k \lambda_i a_i + \frac{t_c - t_0}{t_1 - t_0}\Big(\sum_{i=1}^k \lambda_i b_i - \sum_{i=1}^k \lambda_i a_i\Big), \tag{3.12}$$

*which in the case of $\lambda$-aligned* $\mathbf{a}$ *and* $\mathbf{b}$ *reduces to*

$$\sum_{i=1}^k \lambda_i c_i^* = \sum_{i=1}^k \lambda_i a_i = \sum_{i=1}^k \lambda_i b_i.$$

This condition is not sufficient for deriving the solutions to problem (3.11) when there are more than two aircraft involved. However, in the two-legged case, both the cost function and the constraints in problem (3.11) can be simplified, and a solution - though suboptimal in general - can be computed. We start by considering the cost function, and postpone the discussion on the constraints to a later section.

Let $\alpha$ be a two-legged joint maneuver in $\mathbf{P}^2(\mathbf{a},\mathbf{b})$ with waypoints $\langle c_i \rangle_{i=1}^k$. Then $\alpha$ is specified by

$$\alpha_i(t) = \begin{cases} a_i + (c_i - a_i)\frac{t-t_0}{t_c-t_0}, & t_0 \le t \le t_c \\ b_i + (c_i - b_i)\frac{t-t_1}{t_c-t_1}, & t_c < t \le t_1 \end{cases}, \quad i = 1, \dots, k. \tag{3.13}$$

Similarly as in the 2D case, it can be shown that problem (3.11) in the case of $\eta = 1$ is equivalent to

$$\text{minimize} \sum_{i=1}^k \lambda_i \|c_i - c_i^u\|^2 \text{ subject to } \alpha \in \mathbf{P}^2(r,h;\mathbf{a},\mathbf{b}) \text{ with waypoints } \langle c_i \rangle_{i=1}^k, \tag{3.14}$$

where

$$c_i^u = \frac{(t_1 - t_c)a_i + (t_c - t_0)b_i}{t_1 - t_0}, \quad i = 1, \dots, k, \tag{3.15}$$

are the optimal waypoints when minimizing $J(\alpha)$ without the conflict-free constraint. Note that the cost function to be optimized in problem 3.14 is quadratic in the optimization variables $\langle c_i \rangle_{i=1}^k$.

### 3.5.1 Constraints on the waypoints

The condition that the two-legged joint maneuver $\alpha \in \mathbf{P}^2(\mathbf{a}, \mathbf{b})$ with waypoints $\langle c_i \rangle_{i=1}^k$ is conflict-free can be expressed in terms of constraints on $\langle c_i \rangle_{i=1}^k$. These constraints are in general nonconvex. We now study how they can be simplified and approximated by appropriate linear constraints.

Since $\alpha \in \mathbf{P}^2(r, h; \mathbf{a}, \mathbf{b})$ is equivalent to the condition that there is no conflict between any aircraft pair, we focus on aircraft 1 and 2, and temporarily ignore the presence of other aircraft.

**Proposition 13** *The condition that there is no conflict between aircraft 1 and aircraft 2 in $\alpha \in \mathbf{P}^2(\mathbf{a}, \mathbf{b})$ is equivalent to the condition that their waypoints $c_1$ and $c_2$ satisfy the following condition: $c_1 - c_2$ is visible to both $a_1 - a_2$ and $b_1 - b_2$ in $\mathbb{R}^3$ in the presence of the open cylindrical obstacle $W$ of radius $r$ and height $2h$ centered at the origin.*

**Proof:** Notice that for any $w \in \mathbb{R}^3$ and $\alpha \in \mathbf{P}^2(\mathbf{a}, \mathbf{b})$, $\beta = \mathcal{T}_w(\alpha)$ is still a two-legged joint maneuver, though in $\mathbf{P}^2(\mathbf{a}, \mathbf{b} + w)$. Moreover, there is no conflict between aircraft 1 and 2 in $\beta$ if and only if there is no conflict between aircraft 1 and 2 in $\alpha$. We start by considering the first stage of the joint maneuver $\alpha$. By choosing

$w = \frac{t_1 - t_0}{t_c - t_0}(a_2 - c_2)$, the waypoint of aircraft 2 in maneuver $\beta$ becomes $a_2$, and the waypoint of aircraft 1 becomes $a_2 + c_1 - c_2$. So in the first stage of the motions specified by $\beta$, aircraft 2 stays at $a_2$, while aircraft 1 moves at constant velocity from $a_1$ to $a_2 + c_1 - c_2$. Therefore, the condition that there is no conflict between aircraft 1 and aircraft 2 during the first stage of the motions specified by $\beta$ is equivalent to that the line segment from $a_1$ to $a_2 + c_1 - c_2$ does not intersect the cylinder of radius $r$ and height $2h$ centered at $a_2$, or equivalently after a translation of $-a_2$, the line segment from $a_1 - a_2$ to $c_1 - c_2$ does not intersect $W$. Similar arguments can be applied to the second stage of the motions to show that there is no conflict between aircraft 1 and aircraft 2 during the second stage of the motions specified by $\alpha$ if and only if the line segment from $b_1 - b_2$ to $c_1 - c_2$ does not intersect $W$. ■

Set $\Delta a = a_1 - a_2$, $\Delta b = b_1 - b_2$, and $\Delta c = c_1 - c_2$. By Proposition 13 the feasible region of $\Delta c$ consists of those points in $\mathbb{R}^3$ visible to both $\Delta a$ and $\Delta b$ in the presence of the obstacle $W$. Such a region has a complex shape (in general, there is a "hole" in it). In particular it is not convex. Hence problem (3.14) is in essence a nonconvex optimization problem, which is not only difficult to solve, but may also admit multiple solutions. It is then natural to look for some convex approximation of the feasible region.

In safety-critical context such as in ATM systems, it is necessary that the approximation is strictly contained in the original feasible region so as to ensure absolute safety (*inner approximation*). On the other hand, the approximation should be as tight as possible so that the computed solutions are close to be optimal. The approximation scheme introduced below satisfies these requirements. Moreover, since it only uses the fact that $W$ is convex, it can be easily generalized to the case when the protection zone has an arbitrary convex shape, not necessarily cylindrical.

In the following we assume that both $\Delta a$ and $\Delta b$ belong to the interior of $\mathbb{R}^3 \setminus W$, which is satisfied in all situations in practice. We then distinguish two different cases depending on whether $\Delta a$ and $\Delta b$ are visible to each other in the presence of the obstacle $W$.

**$\Delta a$ and $\Delta b$ are visible to each other.** Suppose that the line segment joining $\Delta a$ and $\Delta b$ does not intersect $W$. In this case there is no conflict between aircraft 1 and aircraft 2 if they both fly at constant speed along their ideal trajectories, which correspond to the two-legged joint maneuver with waypoints $c_1^u$ and $c_2^u$ defined in (3.15). Notice that $\Delta c^u = c_1^u - c_2^u$ is on the line segment between $\Delta a$ and $\Delta b$, hence outside of $W$. From this it follows that the approximated feasible region of $\Delta c$ should include $\Delta c^u$ and as much region in $\mathbb{R}^3$ as possible, provided it is visible to both $\Delta a$ and $\Delta b$. One such choice is described next.

Let $L_{ab}$ be the line segment between $\Delta a$ and $\Delta b$ (end points included), and let $\overline{W}$ be the closure of $W$, which is a closed cylinder. Since both $L_{ab}$ and $\overline{W}$ are compact and convex subsets of $\mathbb{R}^3$, there exists a point $u$ in $L_{ab}$ and a point $v$ in $W$ such that $\|u - v\| = \inf\{\|x - y\| : x \in L_{ab}, y \in \overline{W}\}$. If $u \neq v$, then through point $v$ there is a unique plane $P$ orthogonal to the straight line between $u$ and $v$. $P$ divides $\mathbb{R}^3$ into two closed half spaces which intersect each other at $P$. The definition of $u$ and $v$ together with the convexity of $L_{ab}$ and $\overline{W}$ implies that $L_{ab}$ is contained in one half space, while $\overline{W}$ is contained in the other half space. We denote by $P^+$ the closed half space containing $L_{ab}$. If $u = v$, then $u$ (hence $v$) is located on $\partial W$. In this case we can choose any tangent plane to $\partial W$ at $u$ that separates $L_{ab}$ and $\overline{W}$, and define $P^+$ to be the side of it containing $L_{ab}$. Note that here we use the term

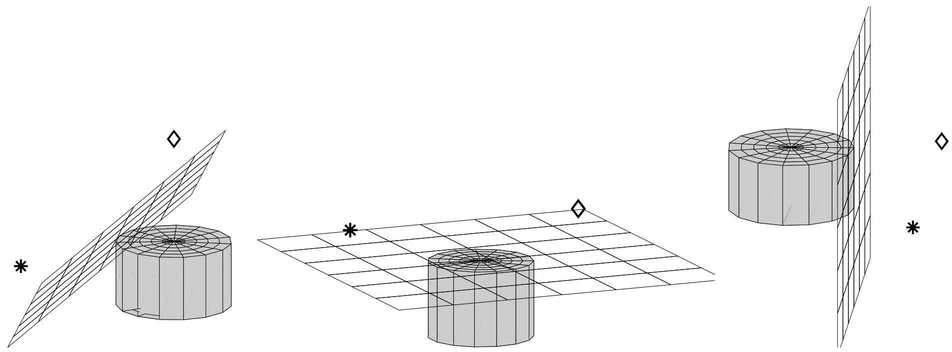

(a) (b) (c)

Figure 3.6: Approximated feasible region for $\Delta c$ when $\Delta a$ and $\Delta b$ are visible to each other.

"tangent planes" of $\partial W$ in its generalized sense, i.e., those planes which intersect $\partial W$ and have $W$ on one side exclusively. In the special case when $u = v$ and $u$ is on the sharp edges of $\partial W$, there might be a family of such tangent planes, and we can choose any one of them in defining $P^+$, provided it separates $L_{ab}$ and $\overline{W}$.

The closed half space $P^+$ thus obtained satisfies the condition that it contains $\Delta c^u$ and that all of its points are visible to both $\Delta a$ and $\Delta b$. Therefore, we can use $P^+$ as the approximated feasible region of $\Delta c$. This in essence imposes a single linear constraint on $c_1$ and $c_2$.

The points $u$ and $v$ can be computed by using standard optimization algorithms. Some results are shown in Figure 3.6. In each case, $\Delta a$ is marked with a star, and $\Delta b$ with a diamond. The three plots correspond to the cases when $v$ is on a sharp edge, the top, and the side surface of the cylinder, respectively.

**$\Delta a$ and $\Delta b$ are not visible to each other.** Let $p$ and $q$ be the entry point and the exit point of a shortest curve in $\mathbb{R}^3 \setminus W$ from $\Delta a$ to $\Delta b$ as defined after

Proposition 11.

Since $\Delta a$ is in the interior of $\mathbb{R}^3 \setminus W$ by assumption, $p$ is located on the contour of $W$ with respect to a viewer situated at $\Delta a$. Among all the planes that are tangent to $\partial W$ at $p$, let $P_a$ be the one which passes through $\Delta a$. The choice of $P_a$ is unique unless $p$ is on the sharp edges of $\partial W$ *and* $\Delta a$ has the same $z$-coordinate as $p$. In the latter case, we can choose an arbitrary tangent plane. Let $P_a^+$ be the closed half space determined by the side of $P_a$ that does not contain $W$. Points in $P_a^+$ are visible to $\Delta a$. In a similar way we can define $P_b^+$ based on the tangent plane $P_b$ to $\partial W$ at $q$ that passes through $\Delta b$. Points in $P_b^+$ are visible to $\Delta b$. Therefore, points in $P^+ \triangleq P_a^+ \cap P_b^+$ are visible to both $\Delta a$ and $\Delta b$, and can be used as the approximated feasible set of $\Delta c$. This translates into two linear constraints on $c_1$ and $c_2$.

Some typical examples are plotted in Figure 3.7, where in each case $\Delta a$ is marked with a star and $\Delta b$ a diamond, and the solid line is a shortest curve in $\mathbb{R}^3 \setminus W$ connecting $\Delta a$ and $\Delta b$.

In summary, given $\Delta a$ and $\Delta b$, one or two linear inequalities can be used to approximate the constraint that $\Delta c$ is visible to both $\Delta a$ and $\Delta b$ in the presence of the obstacle $W$. Such a linear approximation should be carried out for all aircraft pairs, thus leading to the following approximated version of problem (3.14):

$$\text{minimize} \sum_{i=1}^{k} \lambda_i \|c_i - c_i^u\|^2 \text{ subject to } c_i - c_j \in P_{ij}^+,\ 1 \le i < j \le k, \tag{3.16}$$

where $P_{ij}^+$ is the linear approximation of the feasible set for $c_i - c_j$ computed based on $a_i - a_j$ and $b_i - b_j$ as described above. Problem (3.16) is a linearly constrained quadratic programming problem, which can be efficiently solved by many existing software packages.

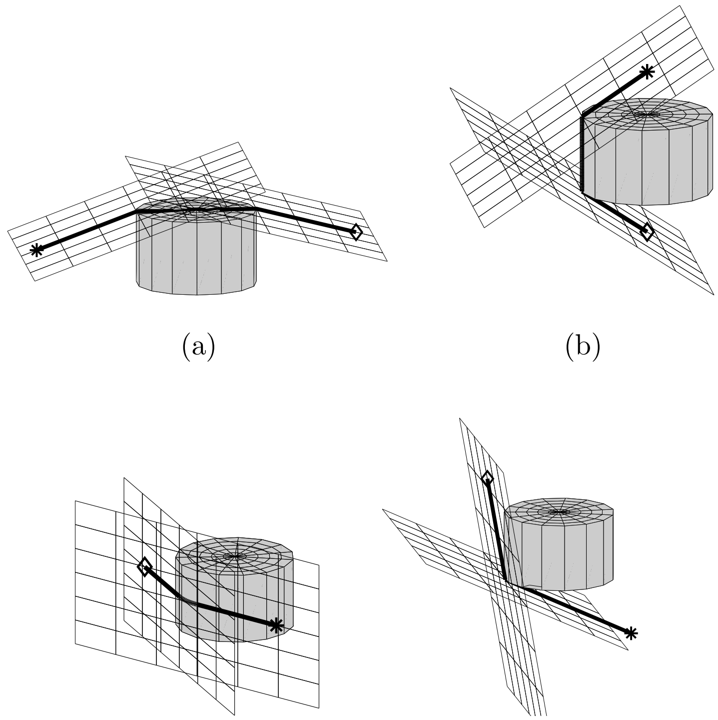

(a) (b)

(c) (d)

Figure 3.7: Approximated feasible region for $\Delta c$ when $\Delta a$ and $\Delta b$ are not visible to each other.

### 3.5.2 Some examples of multi-aircraft encounters

Consider a three-aircraft encounter where $a_1 = (0, 50, 4)$, $b_1 = (100, 50, 4)$, $a_2 = (50, 0, 4)$, $b_2 = (50, 100, 4)$, $a_3 = (100, 100, 5)$, and $b_3 = (0, 0, 3)$, i.e., aircraft 1 and aircraft 2 are flying at the same altitude with cross-path angle of 90°, whereas aircraft 3 dives across that altitude and has a path angle of 135° with both aircraft 1 and aircraft 2. All three aircraft have the same priority and $t_c = (t_0 + t_1)/2$. We choose a larger $r$ ($r = 10$ nmi) to make the resolution maneuvers evident. $h$ is chosen

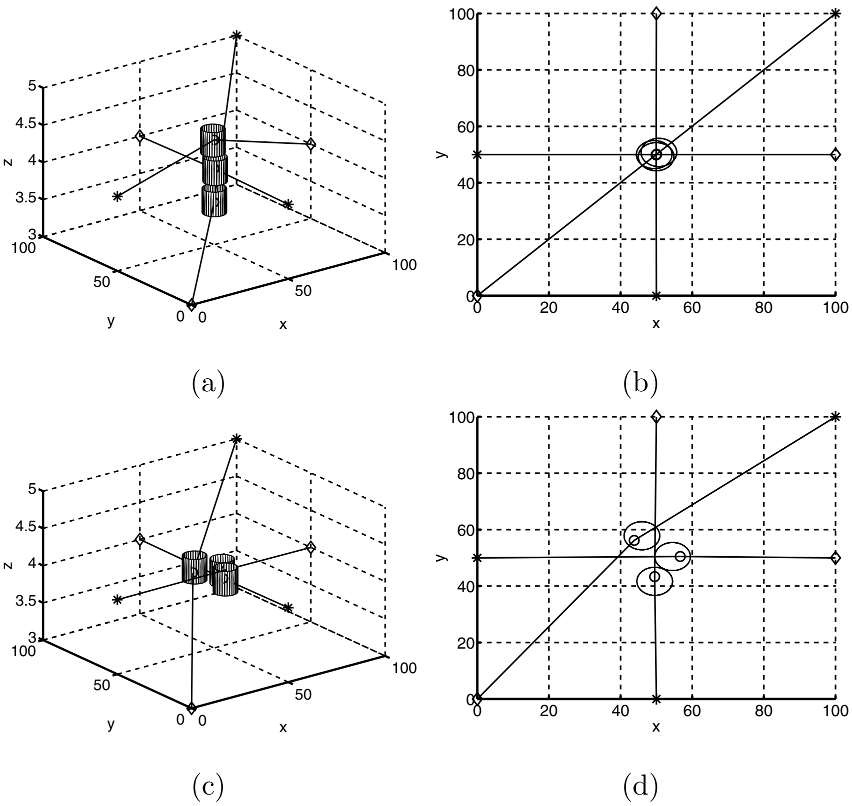


Figure 3.8: Two-legged resolution maneuvers for a three-aircraft encounter ($\lambda_1 = \lambda_2 = \lambda_3 = 1/3$): (a) three dimensional representation and (b) top view in the case $\eta = 5$; (c) three dimensional representation and (d) top view in the case $\eta = 50$.

to be 0.3292 nmi. In Figure 3.8 the solutions to problem (3.16) corresponding to two different values of $\eta$ are shown. Plotted in (a) is the snapshot at a time instant near $t_c$ of the two-legged joint maneuver that is a solution to problem (3.16) with $\eta = 5$. Its top view is shown in (b). The cylinders in (a) represent *half* the size of the protection zones surrounding the aircraft, i.e., they are (open) cylinders of radius $r/2$ and height $h$. Therefore, two aircraft are in a conflict situation if and only if the corresponding cylinders intersect each other. Similarly, (c) and (d) plot a

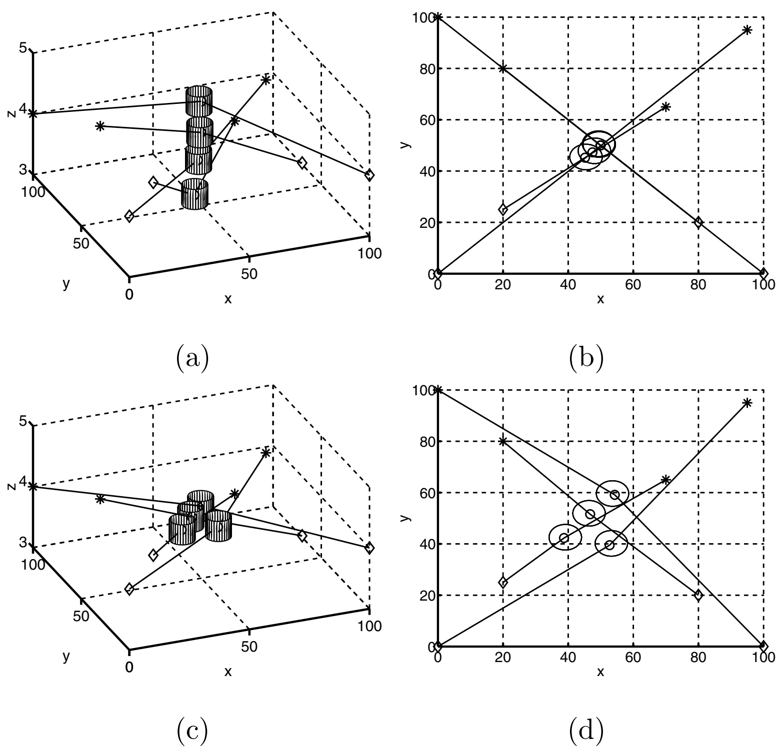


Figure 3.9: Two-legged resolution maneuvers for a four-aircraft encounter ($\lambda_1 = \lambda_2 = \lambda_3 = \lambda_4 = 1/4$): (a) three dimensional representation and (b) top view in the case $\eta = 5$; (c) three dimensional representation and (d) top view in the case $\eta = 50$.

snapshot of a solution to problem (3.16) with $\eta = 50$. As in the case of two-aircraft encounters, a larger value of $\eta$ will force the aircraft to adopt horizontal maneuvers to resolve the conflict.

Figure 3.9 shows the simulation results for a four-aircraft encounter with $a_1 = (0, 100, 4)$, $b_1 = (100, 0, 4)$, $a_2 = (20, 80, 4)$, $b_2 = (80, 20, 4)$, $a_3 = (95, 95, 4)$, $b_3 = (0, 0, 4)$, $a_4 = (70, 65, 4)$, and $b_4 = (20, 25, 4)$. The four aircraft are divided into two groups, each consisting of two aircraft one overtaking the other, with the path angle between the two groups being $90°$. We choose $r = 10$ nmi, $h = 0.3292$ nmi,

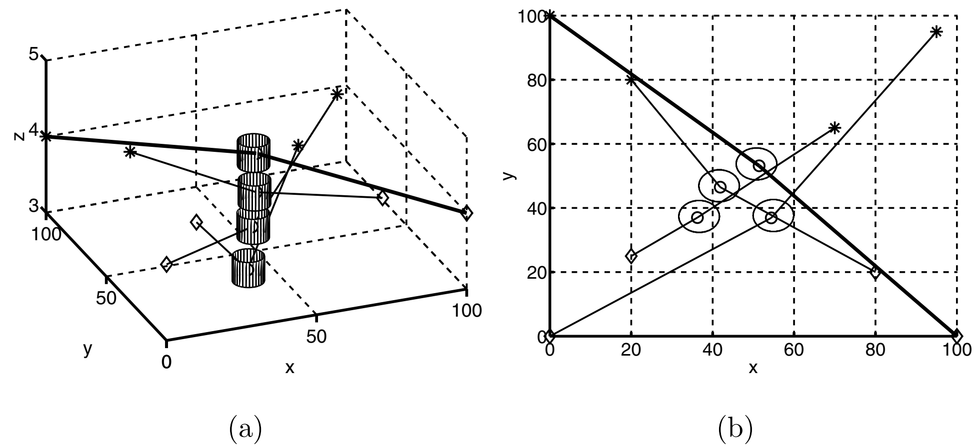


Figure 3.10: Two-legged resolution maneuvers for the four-aircraft encounter ($\lambda_1 = 0.7$, $\lambda_2 = \lambda_3 = \lambda_4 = 0.1$): (a) three dimensional representation in the case $\eta = 5$; (b) top view in the case $\eta = 50$.

and $t_c = (t_0 + t_1)/2$. All aircraft have equal priority. (a) and (b) plot the snapshot of a solution at a time instant near $t_c$ when $\eta = 5$, (c) and (d) plot a snapshot of a solution when $\eta = 50$. (c) and (d) can be thought of as the restricted solution to problem (3.16) when the motion of each aircraft is required to be contained in the plane of altitude 4. If we increase the priority of aircraft 1 such that $\lambda_1 = 0.7$, $\lambda_2 = \lambda_3 = \lambda_4 = 0.1$, we obtain the results shown in (a) and (b) of Figure 3.10 for $\eta = 5$ and $\eta = 50$, respectively. Compared with (a) and (d) of Figure 3.9, the motions of aircraft 1 (shown in Figure 3.10 by the heavy lines) are closer to the straight line motions, forcing other aircraft to "bend" more.

As the number of aircraft involved gets larger, the resolution maneuver becomes more complicated. An example is shown in Figure 3.11 for an eight-aircraft encounter, which is obtained by adding to the four-aircraft encounter in Figures 3.9 and 3.10 four more aircraft with $a_5 = (55, 0, 3.7)$, $b_5 = (50, 80, 3.7)$, $a_6 = (55, 20, 3.7)$,

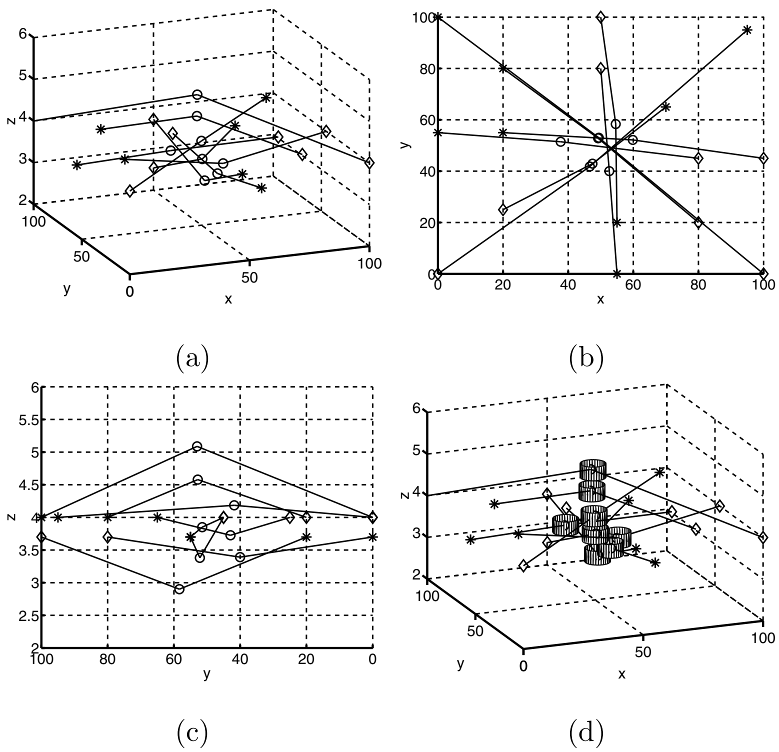


Figure 3.11: A two-legged resolution maneuver for an eight-aircraft encounter ($\lambda_i = 1/8$, $i = 1, \ldots, 8$, $\eta = 20$).

$b_6 = (50, 100, 3.7)$, $a_7 = (0, 55, 3.7)$, $b_7 = (80, 45, 4)$, $a_8 = (20, 55, 3.7)$, and $b_8 = (100, 45, 4)$. By choosing identical priority and $\eta = 20$, the obtained solution to problem (3.16) consists of both horizontal and vertical resolution motions. (a), (b), and (c) are views of the solution from different viewpoints, (d) is its snapshot at a certain time instant.

In each simulation, a large portion of the computational time is spent on linearizing the feasible region, which is very sensitive to the configuration of the starting and destination positions of the aircraft. On a desktop PC with 450 MHz Pentium III processor, the computational time for the previous 3, 4, and 8 aircraft examples (implemented in MATLAB) is 4.7500, 3.9370, and 26.1720 seconds, respectively. These times could be significantly reduced by writing the code in programming languages more efficient than MATLAB, thus making the algorithm suitable for real-time implementations.

### 3.5.3 Further constraints on the waypoints for the maneuver feasibility

So far we have assumed that the two-legged maneuver obtained by solving the optimization problem (3.16) is flyable. In practice, this is usually not the case because of the abrupt turn and the change of speed when an aircraft passes through its waypoint. In the following we shall propose practical constraints on the waypoints to alleviate such drawbacks, at least to a certain extent. In order for the optimization problem to be computationally tractable, it is important that the introduced constraints are convex.

We start by considering the speed constraint. Suppose that the speed of each aircraft during both stages of its maneuver cannot exceed a certain threshold $v_{max}$. Recall that $t_c$ is the time epoch corresponding to the middle waypoints. Then the speed constraint can be expressed as:

$$\|a_i - c_i\| \leq v_{max}(t_c - t_0), \quad \|b_i - c_i\| \leq v_{max}(t_1 - t_c), \quad i = 1, \ldots, k. \tag{3.17}$$

For a single aircraft, say, aircraft $i$, constraint (3.17) implies that $c_i$ must belong to the intersection of two balls, one centered at $a_i$ and the other centered at $b_i$. Hence the speed constraint is convex. Instead of a common $v_{max}$, one can also impose different speed upper bounds for different aircraft in the two stages.

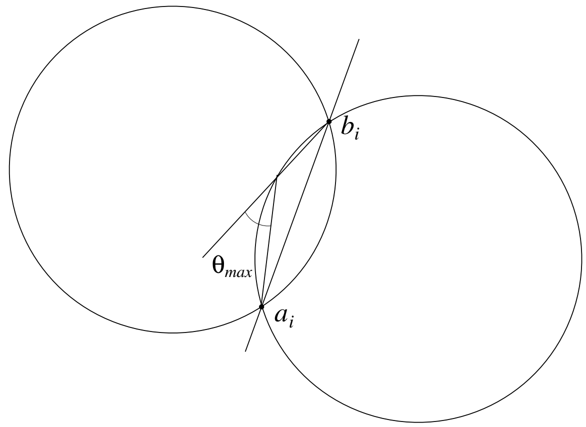


Figure 3.12: Turning angle constraint on waypoints.

A further practical constraint is the turning angle constraint. Suppose that the angle each aircraft turns at a waypoint cannot exceed a certain threshold $\theta_{max}$. For aircraft $i$, this constraint specifies that its waypoint $c_i$ must lie in a convex region of $\mathbb{R}^3$ that is invariant under rotations around the axis $\overline{a_i b_i}$, where $\overline{a_i b_i}$ denotes the straight line passing through $a_i$ and $b_i$. The intersection of this convex region with any plane through $\overline{a_i b_i}$ is plotted in Figure 3.12. It is the intersection of two disks with properly chosen centers and radii.

Note that each of the two constraints above can be expressed as *second order cone constraints* of the form (assume $s$ is the optimization variable)

$$\|\hat{A}s + \hat{b}\| \leq \hat{c}s + \hat{d}, \tag{3.18}$$

for some matrix $\hat{A}$, vectors $\hat{b}$, $\hat{c}$, and constant $\hat{d}$, of suitable dimensions. Although the turning angle constraint is actually equivalent to an infinite number of second order cone constraints, one can, for example, impose upper bounds on the turning angles for the projections of the maneuver onto the plane $xy$, $xz$, and $yz$, respectively, thus

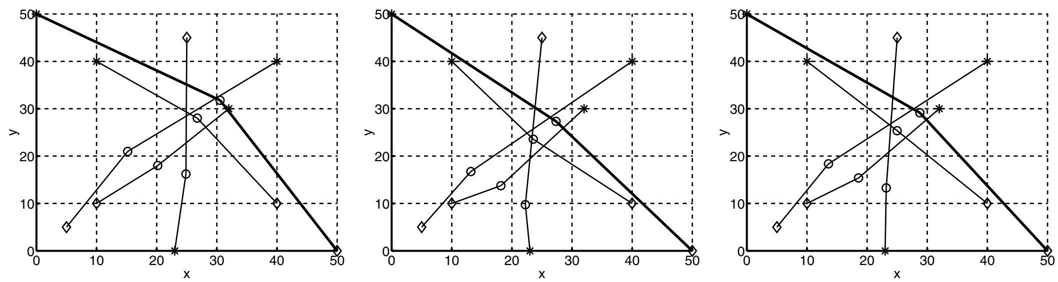


(a) (b) (c)

Figure 3.13: Two-legged resolution maneuvers for a five-aircraft encounter ($\lambda_1 = \lambda_2 = \lambda_3 = \lambda_4 = \lambda_5 = 1/5$, $\eta = 50$): (a) no additional constraint; (b) speed constraint with $v_{max} = 7.102$ nmi/min; (c) turning angle constraint with $\theta_{max} = \pi/10$.

leading to three second order cone constraints. Therefore, the optimization problem (3.16) together with the speed and the simplified turning angle constraints becomes a Second Order Cone Programming (SOCP) problem, which can be solved by using software such as SOCP [43]. Note that as before, the vertical penalty factor $\eta$ can be incorporated into these two constraints.

Figure 3.13 shows the effect of the speed and the turning angle constraints by considering a five-aircraft encounter. Here we choose $t_0 = 0$ min, $t_1 = 10$ min, $t_c = 5$ min, $\eta = 50$, $r = 5$ nmi, $h = 0.3292$ nmi, and we assign the same priority to all of the aircraft. The solution to problem (3.16) without any additional constraint is shown in (a), the solution with the speed constraint of $v_{max} = 7.102$ nmi/min is shown in (b), whereas the solution with the turning angle constraint $\theta_{max} = \pi/10$ on the $xy$ plane projection is plotted in (c). As expected, the aircraft that possesses the largest speed and turning angle in case (a) (whose trajectory is highlighted by a heavy line) tends to have a straighter and smoother motion under the additional constraints on either the speed or the turning angle.

Further adjustments can be introduced to improve the flyability of the generated maneuvers. For example, one can consider multi-legged maneuvers and adopt an iterative procedure to get an approximated optimal solution for the multi-legged version of the conflict resolution problem. Furthermore, to avoid sharp turns at time $t_0$, one can choose the starting epoch to be $t_0 + \Delta$ for some positive $\Delta$, and use the time interval $[t_0, t_0 + \Delta]$ as a buffer for possible heading adjustments. Much more work is still needed in this respect in order to actually implement our algorithms in practical situations.

## 3.6 Summary of contributions

The problem of designing optimal conflict-free maneuvers for multi-aircraft encounters in three dimensional airspace is studied. Numerical algorithms for solving the problem are introduced based on a simplified model of the aircraft dynamics, and their effectiveness is shown by extensive simulations. The proposed algorithms rest on a geometric interpretation of the solutions, and possess some features that make them attractive for practical implementation. For example, aircraft may have different priorities; vertical maneuvers are penalized; and the maximum speed and turning angle constraints can be introduced so as to improve path flyability.

# Chapter 4

# Optimal Collision Avoidance and Formation Switching on Riemannian Manifolds

## 4.1 Introduction

As a generalization of the problems studied in the previous two chapters, we consider next the problems of optimal collision avoidance and optimal formation switching for multiple agents moving on a Riemannian manifold. Based on the assumption that the manifold admits a group of symmetries, various optimality conditions are obtained that generalize the results in Chapter 2 and Chapter 3.

The main contribution of this chapter consists in

- the extension of the Noether theorem to OCA and OFS problems with nonsmooth boundaries;

- the introduction of bounds on the conserved quantities that apply uniformly to solutions to all OCA and OFS problems. Some of these bounds can be further improved by exploiting the structure of the specific problem under consideration;
- the generalization of the obtained results to OCA and OFS problems for bodies with arbitrary shapes.

For simplicity, we assume in this chapter that solutions to the OCA and OFS problems belong to the class of continuous and piecewise smooth trajectories, a reasonable assumption in most of the practical applications. However, even when the underlying manifold is simple, it is a nontrivial task to prove that a solution exists in this class for arbitrary starting and destination positions of the agents. Therefore, all the results obtained should be understood to hold under the provision that a solution does exist in the class of continuous and piecewise smooth trajectories for the considered starting and destination positions.

This chapter is organized as follows. In Section 4.2, we formulate the OCA and OFS problems for multiple agents moving on a Riemannian manifold, and introduce the symmetry assumption on this manifold used throughout the chapter. In Section 4.3, we derive various necessary conditions that apply uniformly to solutions to all OCA and OFS problems. In particular, using some preliminary results in Section 4.3.1, we show in Section 4.3.2 that a version of the classical Noether theorem, namely, the preservation of momentum maps, still apply in our problems that are nonsmooth in nature. Bounds on the momentum maps are derived in Sections 4.3.2 and 4.3.5 through a second variational analysis and a topological analysis, respectively. Section 4.4 contains a natural generalization of our results to the case of agents of arbitrary shape. Finally, in Section 4.5, some conclusions and possible future directions of research are outlined.

Throughout this chapter, the results are illustrated using several recurrent examples: the Euclidean space $\mathbb{R}^n$, the sphere $\mathbf{S}^n$, a group $G$ with a bi-invariant metric, the Grassmann and the Stiefel manifolds.

## 4.2 Problem formulation

In this section, we formulate the OCA and OFS problems on Riemannian manifolds. First of all, we need to introduce some notations and recall a few concepts in differential geometry.

Let $M$ be a $C^\infty$ Riemannian manifold. For each $q \in M$, we denote by $\langle \cdot, \cdot \rangle_q$ and $\|\cdot\|_q$ (or simply $\langle \cdot, \cdot \rangle$ and $\|\cdot\|$) the Riemannian metric and the corresponding norm on the tangent space $T_qM$, respectively. Fix $t_0, t_1 \in \mathbb{R}$ with $t_0 < t_1$, and consider a curve $\gamma : [t_0, t_1] \to M$. The arc length of $\gamma$ is defined as $l_\gamma = \int_{t_0}^{t_1} \|\dot{\gamma}(t)\| \, dt$. Note that, unless otherwise stated, we shall always assume that curves in $M$ are continuous and piecewise $C^\infty$. For this class of curves the arc length is well defined. The distance $d_M(q_0, q_1)$ between two arbitrary points $q_0$ and $q_1$ in $M$ is by definition the infimum of the arc length of all curves connecting $q_0$ and $q_1$: $d_M(q_0, q_1) = \inf\{l_\gamma : \ \gamma : [t_0, t_1] \to M, \ \gamma(t_0) = q_0, \ \gamma(t_1) = q_1\}$. A geodesic in $M$ is a locally distance-minimizing curve. More precisely, $\gamma : [t_0, t_1] \to M$ is a geodesic if and only if for any $t \in (t_0, t_1)$, there exists an $\epsilon > 0$ small enough such that the arc length of $\gamma$ restricted on $[t - \epsilon, t + \epsilon]$ is equal to $d_M(\gamma(t - \epsilon), \gamma(t + \epsilon))$. In this chapter, we assumed that $M$ is connected and complete, and that all geodesics in $M$ are parameterized proportionally to arc length.

Let $L : TM \to \mathbb{R}$ be a *Lagrangian function*, i.e., a smooth function defined on the tangent bundle $TM = \{T_qM : \ q \in M\}$ of $M$ that is nonnegative and convex on each fiber $T_qM$, $q \in M$. For each curve $\gamma : [t_0, t_1] \to M$, we define the *energy* of $\gamma$ as

$$J(\gamma) = \int_{t_0}^{t_1} L[\dot{\gamma}(t)]\, dt. \tag{4.1}$$

The curves joining two fixed points in $M$ with minimal energy are extremals of the functional $J$, and in any canonical local coordinates of $TM$, $(x_1, \ldots, x_n, \dot{x}_1, \ldots, \dot{x}_n)$, $n = \dim(M)$, they are characterized by the Euler-Lagrange equations [3]:

$$\frac{d}{dt}\frac{\partial L}{\partial \dot{x}_i} = \frac{\partial L}{\partial x_i}, \quad i = 1, \ldots, n.$$

As an example one can take $L = \frac{1}{2}\|\cdot\|^2$, i.e., $L(v) = \frac{1}{2}\|v\|_q^2$, $\forall v \in T_qM, q \in M$. In this case the Euler-Lagrange equations describe the geodesics in $M$.

Consider an ordered $k$-tuple of points of $M$, $\langle q_i \rangle_{i=1}^k$, where $k$ is a positive integer. We say that $\langle q_i \rangle_{i=1}^k$ satisfies the *$r$-separation condition* for some positive $r$ if $d_M(q_i, q_j) \geq r$ for all $i \neq j$. Let $\langle a_i \rangle_{i=1}^k$ and $\langle b_i \rangle_{i=1}^k$ be two $k$-tuples of points of $M$, each of which satisfies the $r$-separation condition. $\langle a_i \rangle_{i=1}^k$ is called the *starting position* and $\langle b_i \rangle_{i=1}^k$ the *destination position*.

Let $\gamma = \langle \gamma_i \rangle_{i=1}^k$ be a $k$-tuple of curves in $M$ defined on $[t_0, t_1]$ such that $\gamma_i(t_0) = a_i, \gamma_i(t_1) = b_i$, for $i = 1, \ldots, k$. One can interpret $\gamma$ as the joint trajectory of $k$ agents moving on $M$ that start from $\langle a_i \rangle_{i=1}^k$ at time $t_0$ and end at $\langle b_i \rangle_{i=1}^k$ at time $t_1$. $\gamma$ is said to be *collision-free* if the $k$-tuple $\langle \gamma_i(t) \rangle_{i=1}^k$ satisfies the $r$-separation condition for each $t \in [t_0, t_1]$. Equivalently, if the agents are Riemannian disks of radius $r/2$ in $M$ whose centers follow $\gamma$, then $\gamma$ is collision-free if and only if no two agents overlap during $[t_0, t_1]$. Naturally, $r$ must be small enough so that it is possible to pack $k$ disks of radius $r/2$ in $M$.

Using these notations, we can now formulate the first problem we are going to study.

**Problem 1 (Optimal Collision Avoidance (OCA))** *Among all collision-free $\gamma$ that start from $\langle a_i \rangle_{i=1}^k$ at time $t_0$ and end at $\langle b_i \rangle_{i=1}^k$ at time $t_1$, find the ones that minimize the energy*

$$J(\gamma) = \sum_{i=1}^{k} \lambda_i J(\gamma_i), \tag{4.2}$$

*where $\langle \lambda_i \rangle_{i=1}^k$ is a $k$-tuple of positive real numbers and $J(\gamma_i)$ is defined as in (4.1).*

The $k$-tuple $\langle \lambda_i \rangle_{i=1}^k$ of weighting coefficients in the overall energy $J(\gamma)$ represents the priorities of the $k$ agents, with a larger $\lambda_i$ corresponding to a higher priority for agent $i$.

The OCA problem can be formulated in an alternative way by viewing each $k$-tuple of points of $M$ as a single point in $M^{(k)} = M \times \cdots \times M$. According to this interpretation, $\gamma$ becomes a curve in $M^{(k)}$ starting from $(a_1, \ldots, a_k)$ at time $t_0$ and ending at $(b_1, \ldots, b_k)$ at time $t_1$, while avoiding the obstacle

$$W = \cup_{i \neq j} \{(q_1, \ldots, q_k) \in M^{(k)} : d_M(q_i, q_j) < r\}. \tag{4.3}$$

As a result, solutions to the OCA problem are energy-minimizing curves in $M^{(k)} \setminus W$ connecting two fixed points. In particular, if $L = \frac{1}{2}\| \cdot \|^2$, then these solutions are geodesics in $M^{(k)} \setminus W$ with a proper choice of metric.

To define the OFS problem we need to introduce some further notions. Given a $k$-tuple $\langle q_i \rangle_{i=1}^k$ of points of $M$ satisfying the $r$-separation condition, we define the *formation pattern* of $\langle q_i \rangle_{i=1}^k$ as a graph $(\mathcal{V}, \mathcal{E})$ whose set of vertices $\mathcal{V}$ is given by $\mathcal{V} = \{1, \ldots, k\}$ and whose set of edges $\mathcal{E}$ contains the edge $(i, j)$ between

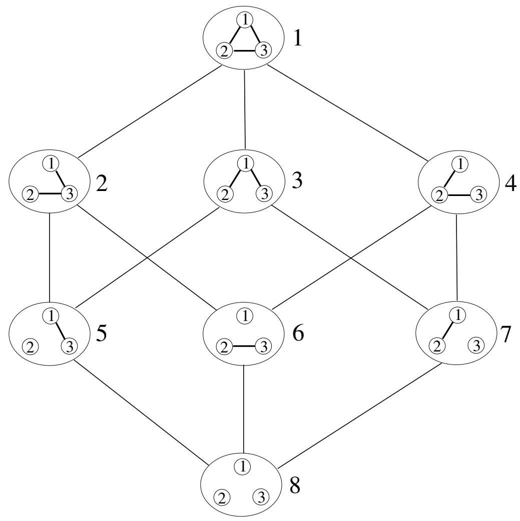


Figure 4.1: Hasse diagram of $\mathcal{F}$ when $M = \mathbb{R}^2$ and $k = 3$.

vertex $i$ and vertex $j$ if and only if $d_M(q_i, q_j) = r$. Let $\gamma = \langle \gamma_i \rangle_{i=1}^k$ be a collision-free $k$-tuple of curves in $M$ defined on $[t_0, t_1]$. Then, for each $t \in [t_0, t_1]$, the formation pattern of $\gamma$ at time $t$ is defined to be the formation pattern of the $k$-tuple of points $\langle \gamma_i(t) \rangle_{i=1}^k$.

**Remark 7** *For given $M, r$ and $k$, not all graphs with $k$ vertices can represent the formation pattern of some $k$-tuple of points of $M$ satisfying the $r$-separation condition. For example, if $M = \mathbb{R}^2$ and $k = 4$, the complete graph with four vertices is not the formation pattern of any $\langle q_i \rangle_{i=1}^4$ satisfying the $r$-separation condition, regardless of $r > 0$. In fact, each formation pattern $(\mathcal{V}, \mathcal{E})$ corresponds to a nonempty subset of $M^{(k)} \setminus W$, namely, those $(q_1, \ldots, q_k) \in M^{(k)} \setminus W$ satisfying $d_M(q_i, q_j) = r$ if $(i, j) \in \mathcal{E}$ and $d_M(q_i, q_j) > r$ otherwise. In particular, if $\mathcal{E}$ contains no edges, then $(\mathcal{V}, \mathcal{E})$ corresponds to the interior of $M^{(k)} \setminus W$.*

Denote by $\mathcal{F}$ the set of all formation patterns. A partial order $\prec$ is defined on $\mathcal{F}$ such that two formation patterns $(\mathcal{V}_1, \mathcal{E}_1)$ and $(\mathcal{V}_2, \mathcal{E}_2)$ satisfy $(\mathcal{V}_1, \mathcal{E}_1) \prec (\mathcal{V}_2, \mathcal{E}_2)$ if and only if $(\mathcal{V}_1, \mathcal{E}_1)$ is a subgraph of $(\mathcal{V}_2, \mathcal{E}_2)$. Based on this partial order relation, $\mathcal{F}$ can be rendered graphically as a *Hasse diagram* ([63]). In this diagram, each element of $\mathcal{F}$ is represented by a node on a plane at a certain position such that the node corresponding to $(\mathcal{V}_1, \mathcal{E}_1)$ is placed at a lower position than the node corresponding to $(\mathcal{V}_2, \mathcal{E}_2)$ if $(\mathcal{V}_1, \mathcal{E}_1) \prec (\mathcal{V}_2, \mathcal{E}_2)$, and a line segment is drawn upward from node $(\mathcal{V}_1, \mathcal{E}_1)$ to node $(\mathcal{V}_2, \mathcal{E}_2)$ if and only if $(\mathcal{V}_1, \mathcal{E}_1) \prec (\mathcal{V}_2, \mathcal{E}_2)$ and there exists no other $(\mathcal{V}, \mathcal{E}) \in \mathcal{F}$ such that $(\mathcal{V}_1, \mathcal{E}_1) \prec (\mathcal{V}, \mathcal{E})$ and $(\mathcal{V}, \mathcal{E}) \prec (\mathcal{V}_2, \mathcal{E}_2)$. As an example, Figure 4.1 plots the Hasse diagram of $\mathcal{F}$ in the case $M = \mathbb{R}^2$ and $k = 3$.

Now we can define the OFS problem.

**Problem 2 (Optimal Formation Switching (OFS))** *Suppose that $\tilde{\mathcal{F}}$ is a subset of $\mathcal{F}$ such that the formation patterns of both $\langle a_i \rangle_{i=1}^k$ and $\langle b_i \rangle_{i=1}^k$ belong to $\tilde{\mathcal{F}}$. Among all collision-free $\gamma = \langle \gamma_i \rangle_{i=1}^k$ that start from $\langle a_i \rangle_{i=1}^k$ at time $t_0$ and end at $\langle b_i \rangle_{i=1}^k$ at time $t_1$, find the ones minimizing the energy (4.2) and satisfying the constraint that the formation pattern of $\gamma$ at any time $t \in [t_0, t_1]$ belongs to $\tilde{\mathcal{F}}$.*

The OFS problem is a natural generalization of the OCA problem: the OFS problem reduces to the OCA problem if $\tilde{\mathcal{F}} = \mathcal{F}$. Regarded as a curve in $M^{(k)} \setminus W$, a solution $\gamma$ to the OFS problem can only lie in a *subset* of $M^{(k)} \setminus W$ obtained by piecing together cells of various dimensions, one for each formation pattern in $\tilde{\mathcal{F}}$. Depending on $\tilde{\mathcal{F}}$, this union of cells can be highly complicated. In the example shown in Figure 4.1, one can choose $\tilde{\mathcal{F}}$ to consist of formation patterns 1, 2, 3, and 4, thus requiring that every two agents “contact” each other either directly or indirectly via the third agent at all time. This makes sense in practical situations where the three agents have to share data among one another and information exchange is possible only at the minimum allowed distance. As another example, $\tilde{\mathcal{F}}$ can be chosen to consist of formation patterns 1, 3, 4, and 7. In this case agent 1 and agent 2 are required to be bound together during the whole time interval $[t_0, t_1]$; and the OFS problem can be viewed as the OCA problem between agent 3 and this two-agent subsystem.

**Remark 8** *Solutions to the OCA and OFS problems may not exist. The OCA problem of two agents on a line trying to switch positions is one such example. As another example, consider the OFS problem in Figure 4.1, with $\tilde{\mathcal{F}}$ consisting of only formation pattern 8. Regarded as a curve in $M^{(k)} \setminus W = \mathbb{R}^6 \setminus W$, a solution $\gamma$ has to lie in the interior of $\mathbb{R}^6 \setminus W$. If the starting and destination positions correspond to two points in int$(\mathbb{R}^6 \setminus W)$ that are 'invisible' to each other, i.e., if the line segment connecting them intersects the obstacle $W$, then the OFS problem does not admit a solution. In general, to ensure that a solution to the OFS problem exists, it is sufficient (though not necessary) to require that the subset of $M^{(k)} \setminus W$ corresponding to $\tilde{\mathcal{F}}$ is closed and that the two points corresponding to the starting and destination positions are in the same connected component of this subset. The first requirement translates into the following property of $\tilde{\mathcal{F}}$: for each $(\mathcal{V}, \mathcal{E}) \in \tilde{\mathcal{F}}$, any formation pattern $(\mathcal{V}_1, \mathcal{E}_1)$ such that $(\mathcal{V}, \mathcal{E}) \prec (\mathcal{V}_1, \mathcal{E}_1)$ is also an element of $\tilde{\mathcal{F}}$. This is automatically satisfied in the OCA problem because $\tilde{\mathcal{F}} = \mathcal{F}$. The second requirement is satisfied if there exists at least one collision-free $\langle \gamma_i \rangle_{i=1}^k$ from the starting to the destination position whose formation pattern is always in $\tilde{\mathcal{F}}$.*

In this chapter, we focus on the OCA and OFS problems on certain Riemannian manifolds satisfying the following assumptions, whose implications will be detailed next.

**Assumption 1 (Symmetry)** *There is a Lie group $G$ such that*

1. *$G$ acts on $M$ from the left by isometries (denote by $\Phi : G \times M \to M$ this $C^\infty$ action);*

2. *the Lagrangian function $L$ is $G$-invariant.*

We now explain the meaning of these assumptions. For brevity, we write $gq$ for $\Phi(g, q)$, $g \in G$ and $q \in M$. For each $g \in G$, define $\Phi_g : M \to M$ to be the map $\Phi_g : q \mapsto gq$, $\forall q \in M$. Similarly, for each $q \in M$, define $\Phi^q : G \to M$ to be the map $\Phi^q : g \mapsto gq$, $\forall g \in G$. Both $\Phi_g$ and $\Phi^q$ are $C^\infty$ maps since $\Phi$ is $C^\infty$. $\Phi$ being a left action on $M$ is equivalent to that i) $\Phi_{g_1 g_2} = \Phi_{g_1} \circ \Phi_{g_2}$ for $g_1, g_2 \in G$, where $\circ$ denotes composition of maps, and ii) $\Phi_e(q) = q$, $\forall q \in M$, where $e$ is the identity element of $G$. For each $g \in G$, the first assumption implies that $\Phi_g$ is an isometry of $M$, i.e., $\Phi_g : M \to M$ is a map preserving the metric $\langle \cdot, \cdot \rangle$ (hence the distance) on $M$, while the second assumption implies that $L \circ d\Phi_g = L$, where $d\Phi_g : TM \to TM$ is the tangent map of $\Phi_g$. If in particular $L = \frac{1}{2}\| \cdot \|^2$, then the second assumption is a direct consequence of the first one.

We now give a few simple examples of $M$ and $G$ satisfying the above assumptions. More examples will be presented later.

**Example 2 (Euclidean space)** *A classical example is the Euclidean space $M = \mathbb{R}^n$, which is the manifold of interest in many practical applications, for example, those studied in Chapter 2 and Chapter 3. Elements of $\mathbb{R}^n$ are thought of as column vectors. The tangent space of $\mathbb{R}^n$ at any point can be identified with $\mathbb{R}^n$ itself and is* *equipped with the standard Euclidean metric. Let* $L = \frac{1}{2}\|\cdot\|^2$*. Then the energy of a k-tuple of curves* $\gamma = \langle\gamma_i\rangle_{i=1}^k$ *in* $\mathbb{R}^n$ *is* $J(\gamma) = \frac{1}{2}\sum_{i=1}^k \lambda_i \int_{t_0}^{t_1} \|\dot{\gamma}_i(t)\|^2\, dt$*. There are many choices of* $G$ *for which Assumption 1 holds. For example,* $G$ *can be chosen to be* $\mathbb{R}^n$ *itself, with the group operation being vector addition. The action* $\Phi : \mathbb{R}^n \times \mathbb{R}^n \to \mathbb{R}^n$ *is simply the group operation. As another example, consider the group of orientation-preserving n-by-n orthogonal matrices,* $G = \mathbf{SO}_n \triangleq \{A \in \mathbb{R}^{n\times n} : A^t A = I_n, \det A = 1\}$*. The matrix multiplication defines an action of* $\mathbf{SO}_n$ *on* $\mathbb{R}^n$ *that also satisfies Assumption 1.*

**Example 3 (Sphere in $\mathbb{R}^n$)** *Let* $M = \mathbf{S}^{n-1} \triangleq \{(x_1, \ldots, x_n) \in \mathbb{R}^n : x_1^2 + \cdots + x_n^2 = 1\}$ *be the unit* $(n-1)$*-sphere for some* $n \geq 2$*. For each* $q \in \mathbf{S}^{n-1}$*, the tangent space* $T_q\mathbf{S}^{n-1} = \{v \in \mathbb{R}^n : v^t q = 0\} \simeq \mathbb{R}^{n-1}$ *is equipped with the standard Euclidean metric. This metric is the one* $\mathbf{S}^{n-1}$ *inherits from* $\mathbb{R}^n$ *as a submanifold. Let* $L = \frac{1}{2}\|\cdot\|^2$*. Then the action of the matrix group* $G = \mathbf{SO}_n$ *on* $\mathbf{S}^{n-1}$ *by matrix multiplication satisfies Assumption 1.*

**Example 4 (Lie group)** *More abstractly, let* $M = G$ *be a Lie group with a left invariant Riemannian metric, in other words, the left multiplication by* $g$ *defines an isometry of* $G$ *for each* $g \in G$*. Let* $L : TG \to \mathbb{R}$ *be a left invariant Lagrangian function. Such* $L$ *correspond in a one-to-one way with nonnegative and convex functions* $T_eG \to \mathbb{R}$*, where* $e$ *is the identity element of* $G$*. Then the group multiplication* $G \times G \to G$ *is a left action of* $G$ *on itself satisfying Assumption 1.*

In the last example, if in particular the metric on $G$ is also right invariant, i.e., it is *bi-invariant*, the results in this chapter turn out to be especially simple. Lie groups with bi-invariant metric include all compact Lie groups and semi-simple Lie groups (see [12, 20]). Example 2 with $G = M = \mathbb{R}^n$ is an example of a Lie group with a bi-invariant metric. As another example, consider $G = \mathbf{SO}_n$. Its Lie algebra, namely, the tangent space of $\mathbf{SO}_n$ at the identity element, is $\mathfrak{so}_n = \{X \in \mathbb{R}^{n\times n} : X + X^t = 0\}$, the set of skew symmetric $n$-by-$n$ matrices. Denote by $\langle \cdot, \cdot \rangle_F$ the Frobenius inner product on $\mathbb{R}^{n\times n}$ defined by $\langle Y, Z\rangle_F = \mathrm{tr}(Y^t Z)$ for $Y, Z \in \mathbb{R}^{n\times n}$. A left invariant metric on $\mathbf{SO}_n$ can be established by first specifying its restriction on the fiber $\mathfrak{so}_n$ to be $\frac{1}{2}\langle \cdot, \cdot \rangle_F$, and then extending it to all other fibers so that each left multiplication is an isometry. It is easy to see that the metric thus defined is also right invariant, hence bi-invariant.

This last example finds application in surveillance systems. Consider a cluster of cameras monitoring, for instance, a chamber in a museum. Suppose that each camera has a limited angle of view, and is mounted on a ball head that can rotate freely. The configuration space of each camera is $\mathbf{SO}_3$, and we can define two cameras to be in a “collision” if their visibility regions ever overlap. Efficient coordination of the surveillance cameras can then be reformulated as an OCA (or OFS) problem on $\mathbf{SO}_3$. The results proved in this chapter still apply in the case when the visibility regions of the cameras have possibly an irregular shape (see Section 4.4). Similar applications can be found in multiple satellites covering the earth for surveillance/communication purposes.

## 4.3 Necessary conditions for optimality

In this section, we derive necessary conditions for continuous and piecewise smooth curves to be optimal solutions to the OCA and OFS problems on a Riemannian manifold $M$ satisfying Assumption 1. It should be pointed out that some of the results, more specifically those in Section 4.3.3, can be proved using the Hamiltonian or symplectic approach. However, we adopt the more direct (though less elegant) Lagrangian viewpoint for two reasons: it is easier to deal with the nonsmooth nature of the problems addressed; and, as a byproduct, further optimality conditions such as those in Sections 4.3.4 and 4.3.5 can be obtained.

### 4.3.1 Variations of curves in the Lie group G

We first review some notions and results on smooth variations of curves in $G$ that are useful in later sections. All of the results in this section are well known in the literature and can be found in, e.g., [12, 45].

**Definition 10** *Let $h_0 : [t_0, t_1] \to G$ be a $C^\infty$ curve in $G$. A (smooth)* variation *of $h_0$ is a $C^\infty$ map $h : (-\epsilon, \epsilon) \times [t_0, t_1] \to G$ such that $h(0, \cdot) = h_0(\cdot)$, $\epsilon$ being some small positive real number. If in addition $h(\cdot, t_0) \equiv h_0(t_0)$ and $h(\cdot, t_1) \equiv h_0(t_1)$, then the variation $h$ is called* proper.

Let $h$ be a variation of $h_0$ as in Definition 10. For each $s \in (-\epsilon, \epsilon)$, $h(s, \cdot) : [t_0, t_1] \to G$ is a curve in $G$ which we denote by $h_s(\cdot)$ (note that this is consistent with Definition 10, since at $s = 0$ we obtain $h_0$). The variation $h$ can then be equivalently specified by a smoothly varying family of curves $\{h_s\}_{s\in(-\epsilon,\epsilon)}$. Also, the condition that $h$ is a proper variation is equivalent to that all curves in this family have the same starting and ending points.

For each $(s, t) \in (-\epsilon, \epsilon) \times [t_0, t_1]$, we define $\dot{h}(s, t) \triangleq \frac{\partial h}{\partial t}(s, t)$, $h'(s, t) \triangleq \frac{\partial h}{\partial s}(s, t)$, using dot and prime to indicate differentiation with respect to $t$ and $s$, respectively. Both $\dot{h}(s, t)$ and $h'(s, t)$ belong to the tangent space of $G$ at $h(s, t)$. We can pull them back via left multiplication to the tangent space of $G$ at the identity element $e$, i.e., the Lie algebra $\mathfrak{g} = T_e G$ of $G$. Thus we define

$$\xi(s,t) \triangleq h(s,t)^{-1}\dot{h}(s,t) \in \mathfrak{g}, \qquad \eta(s,t) \triangleq h(s,t)^{-1}h'(s,t) \in \mathfrak{g}.$$

Here to simplify the notation we use $h(s,t)^{-1}\dot{h}(s,t)$ to denote $dm_{h(s,t)^{-1}}[\dot{h}(s,t)]$ ($m$ is the action of $G$ on itself defined from the group operation, so that for any $g \in G$, $m_g : G \to G$ stands for the left multiplication by $g$, while $dm_g : TG \to TG$ is its tangent map). Similarly for $h(s,t)^{-1}h'(s,t)$. This kind of notational simplification will be carried out in the following without further explanation.

Define $\dot{\xi}(s,t) = \frac{\partial \xi}{\partial t}(s,t)$ and $\xi'(s,t) = \frac{\partial \xi}{\partial s}(s,t)$, both of which belong to $T_{\xi(s,t)}\mathfrak{g}$. Since $\mathfrak{g}$ is a vector space, we can identify $T_{\xi(s,t)}\mathfrak{g}$ with $\mathfrak{g}$. Hence $\dot{\xi}(s,t)$ and $\xi'(s,t)$ belong to $\mathfrak{g}$. Similarly we can define $\dot{\eta}(s,t)$, $\eta'(s,t) \in \mathfrak{g}$. Denote by $[\cdot,\cdot]$ the Lie bracket of $\mathfrak{g}$. Then

**Lemma 1** *At any* $(s,t) \in (-\epsilon,\epsilon) \times [t_0,t_1]$,

$$\xi'(s,t) = \dot{\eta}(s,t) + [\xi(s,t), \eta(s,t)].$$

**Proof:** Define a $\mathfrak{g}$-valued left invariant 1-form $\omega$ on $G$ by $\omega(v) = g^{-1}v$, $\forall v \in T_g G$, $g \in G$. By the Maurer-Cartan structure equation [67], $d\omega = -[\omega,\omega]$. Pulling this back via the map $h : (-\epsilon,\epsilon) \times [t_0,t_1] \to G$ yields $h^*(d\omega) = -[h^*\omega, h^*\omega]$. Evaluating both sides at the vector fields $\frac{\partial}{\partial s}$ and $\frac{\partial}{\partial t}$, and noting that $\omega(\dot{h}) = \xi$ and $\omega(h') = \eta$ by definition, we obtain

$$\begin{aligned}
-[h^*\omega(\frac{\partial}{\partial s}), h^*\omega(\frac{\partial}{\partial t})] &= -[\omega(dh\frac{\partial}{\partial s}), \omega(dh\frac{\partial}{\partial t})] = -[\omega(h'), \omega(\dot{h})] = -[\eta,\xi] = [\xi,\eta], \\
h^*(d\omega)(\frac{\partial}{\partial s}, \frac{\partial}{\partial t}) &= d(h^*\omega)(\frac{\partial}{\partial s}, \frac{\partial}{\partial t}) \\
&= \frac{\partial}{\partial s}[h^*\omega(\frac{\partial}{\partial t})] - \frac{\partial}{\partial t}[h^*\omega(\frac{\partial}{\partial s})] - h^*\omega([\frac{\partial}{\partial s}, \frac{\partial}{\partial t}]) = \xi' - \dot{\eta}.
\end{aligned}$$

The desired conclusion follows by equating the above two equations. ■

Proofs can also be found in [7], and in the case of matrix Lie groups, in [44].

In line with our previous notations, we define $\dot{h}_s(\cdot) = \dot{h}(s,\cdot)$ and $h'_s(\cdot) = h'(s,\cdot)$, for each $s \in (-\epsilon, +\epsilon)$. We shall also write $\xi_s(\cdot) = \xi(s,\cdot)$, $\dot{\xi}_s(\cdot) = \dot{\xi}(s,\cdot)$, and $\xi'_s(\cdot) = \xi'(s,\cdot)$. Similarly for $\eta_s(\cdot)$, $\dot{\eta}_s(\cdot)$ and $\eta'_s(\cdot)$. Thus the statement in Lemma 1 can be rewritten as

$$\xi'_s = \dot{\eta}_s + [\xi_s, \eta_s], \quad \text{for all } s. \tag{4.4}$$

We now apply Lemma 1 to a very special case. Denote by $c_e$ the constant map that maps every $t \in [t_0, t_1]$ to the identity $e$ in $G$, i.e., $c_e(\cdot) \equiv e$. Suppose that $h$ is a *proper* variation of $h_0 = c_e$. Then $\dot{h}_0(\cdot) \equiv 0$ since $h_0(\cdot) \equiv e$, and therefore $\xi_0(\cdot) \equiv 0$. Since $h$ is a proper variation, we have $h'(\cdot, t_0) = h'(\cdot, t_1) \equiv 0$, hence $\eta(\cdot, t_0) = \eta(\cdot, t_1) \equiv 0$. Define $\chi : [t_0, t_1] \to \mathfrak{g}$ by

$$\chi = \xi'_0. \tag{4.5}$$

$\chi$ is a $C^\infty$ map which, by Lemma 1, satisfies

$$\chi = \dot{\eta}_0 + [\xi_0, \eta_0] = \dot{\eta}_0, \tag{4.6}$$

where the second equality follows from $\xi_0(\cdot) \equiv 0$. Therefore,

$$\int_{t_0}^{t_1} \chi(t)\, dt = \int_{t_0}^{t_1} \dot{\eta}_0(t)\, dt = \eta_0(t_1) - \eta_0(t_0) = 0.$$

Conversely, given any $C^\infty$ map $\chi : [t_0, t_1] \to \mathfrak{g}$ satisfying $\int_{t_0}^{t_1} \chi(t)\, dt = 0$, define $h(s,t) = \exp[s \int_{t_0}^{t} \chi(t)\, dt]$, $\forall (s,t) \in (-\epsilon, \epsilon) \times [t_0, t_1]$, where $\epsilon$ is a positive real number small enough and exp is the exponential map of $G$. One can verify that $h$ is indeed a proper variation of $c_e$ such that $\xi'_0$ coincides with $\chi$. Therefore,

**Lemma 2** *A necessary and sufficient condition for a $C^\infty$ map $\chi : [t_0, t_1] \to \mathfrak{g}$ to be realized as $\chi = \xi_0'$, where $\xi = h^{-1}\dot{h}$ for some $C^\infty$ proper variation $h$ of $h_0 : [t_0, t_1] \to G$ given by $h_0(\cdot) \equiv e$, is*

$$\int_{t_0}^{t_1} \chi(t)\, dt = 0.$$

**Remark 9** *The result in Lemma 2 can also be derived from Proposition 1.14.1 in [13].*

### 4.3.2 Variational analysis

Suppose that $\gamma = \langle \gamma_i \rangle_{i=1}^k$ is an optimal solution to the OCA (or OFS) problem that starts from $\langle a_i \rangle_{i=1}^k$ at time $t_0$ and ends at $\langle b_i \rangle_{i=1}^k$ at time $t_1$. Necessary conditions on $\gamma$ can be derived in the following way. Let $h : (-\epsilon, \epsilon) \times [t_0, t_1] \to G$ be a $C^\infty$ proper variation of the constant map $c_e(\cdot) \equiv e$ for some small $\epsilon > 0$. According to the notations introduced in Section 4.3.1, for each $s \in (-\epsilon, \epsilon)$, $h_s : [t_0, t_1] \to G$ is a $C^\infty$ curve in $G$ both starting and ending at $e$, hence can be used to define a $k$-tuple of perturbed curves $\gamma_s = \langle \gamma_{s,i} \rangle_{i=1}^k$ in $M$ by

$$\gamma_{s,i}(\cdot) = h_s(\cdot)\gamma_i(\cdot), \quad i = 1, \ldots, k,$$

which by the fact that $h_s(t_0) = h_s(t_1) = e$ also starts from $\langle a_i \rangle_{i=1}^k$ at time $t_0$ and ends at $\langle b_i \rangle_{i=1}^k$ at time $t_1$. Note that $\gamma_0 = \gamma$ since $h_0(\cdot) \equiv e$. Moreover, since by Assumption 1 $\Phi_{h_s(t)}$ is an isometry of $M$, $\gamma_s$ is collision-free, and has the same formation pattern as $\gamma$ at any time $t \in [t_0, t_1]$. Define

$$J(s) \triangleq J(\gamma_s), \quad \forall s \in (-\epsilon, \epsilon). \tag{4.7}$$

$J(s)$ is a $C^\infty$ function since $h$ is a $C^\infty$ variation.

For each $(s,t) \in (-\epsilon, \epsilon) \times [t_0, t_1]$ and each $i = 1, \ldots, k$, we have[1]

$$L[\dot{\gamma}_{s,i}] = L[\dot{h}_s\gamma_i + h_s\dot{\gamma}_i] = L[h_s\xi_s\gamma_i + h_s\dot{\gamma}_i] = L[h_s(\xi_s\gamma_i + \dot{\gamma}_i)] = L[\xi_s\gamma_i + \dot{\gamma}_i].$$

Here $\dot{h}_s\gamma_i$ denotes $d\Phi^{\gamma_i}(\dot{h}_s)$, and $h_s\dot{\gamma}_i$ denotes $d\Phi_{h_s}(\dot{\gamma}_i)$, both of which belong to $T_{h_s\gamma_i}M$. In the second equality we use the fact that $\dot{h}_s\gamma_i = h_s\xi_s\gamma_i$, a consequence of the property that $(g_1g_2)q = g_1(g_2q)$, $\forall g_1, g_2 \in G$, $q \in M$. The last equality follows from the $G$-invariance of $L$. The energy of $\gamma_s$ is then

$$J(s) = \sum_{i=1}^{k} \lambda_i \int_{t_0}^{t_1} L[\xi_s\gamma_i + \dot{\gamma}_i]\, dt. \tag{4.8}$$

A necessary condition for $\gamma$ to be optimal is that $J(s)$ assumes its minimum at $s = 0$. In particular, this implies that the derivatives $J'(0) = 0$ and $J''(0) \geq 0$. The implications of these two conditions will be studied in the next two subsections.

### 4.3.3 First variation

For any vector space $V$, denote by $(\cdot,\cdot) : V^* \times V \to \mathbb{R}$ the natural pairing between $V$ and its dual $V^*$, i.e., $\forall \alpha \in V^*$, $v \in V$, $(\alpha, v) = \alpha(v)$ is the value of $\alpha$ on $v$. Differentiating (4.8) with respect to $s$, we have

$$J'(s) = \sum_{i=1}^{k} \lambda_i \int_{t_0}^{t_1} (\mathbb{D}L_{\xi_s\gamma_i + \dot{\gamma}_i}, \xi'_s\gamma_i)\, dt. \tag{4.9}$$

Here we identify the tangent space at $\xi_s\gamma_i + \dot{\gamma}_i$ of $T_{\gamma_i}M$ with $T_{\gamma_i}M$ itself, so $\xi'_s\gamma_i \in T_{\gamma_i}M$; $\mathbb{D}L_{\xi_s\gamma_i+\dot{\gamma}_i}$ is the fiberwise differential of $L$, or more precisely, the differential of $L$ restricted on $T_{\gamma_i}M$ and evaluated at $\xi_s\gamma_i + \dot{\gamma}_i \in T_{\gamma_i}M$. $\mathbb{D}L_{\xi_s\gamma_i+\dot{\gamma}_i}$ can be thought

[1] Since $\gamma_i$ is only piecewise $C^\infty$, this and all equations that follow should be understood to hold only at those $t$ where $\dot{\gamma}_i$'s are well defined. In addition, the parameter $t$ is implicit in these equations for brevity.

of as an element of $T^*_{\gamma_i}M$. At $s = 0$, we have $\xi_0 \equiv 0$ and $\xi_0' = \chi$. Therefore, recalling that $\xi_s'\gamma_i = d\Phi^{\gamma_i}(\xi_s')$, we get

$$J'(0) = \sum_{i=1}^{k} \lambda_i \int_{t_0}^{t_1} (\mathbb{D}L_{\dot{\gamma}_i}, d\Phi^{\gamma_i}(\chi))\, dt = \int_{t_0}^{t_1} (\sum_{i=1}^{k} \lambda_i (d\Phi^{\gamma_i})^* \mathbb{D}L_{\dot{\gamma}_i}, \chi)\, dt, \tag{4.10}$$

where $(d\Phi^{\gamma_i})^* : T^*_{\gamma_i}M \to \mathfrak{g}^*$ is the dual of $d\Phi^{\gamma_i} : \mathfrak{g} \to T_{\gamma_i}M$ defined by

$$((d\Phi^{\gamma_i})^*\alpha, \zeta) = (\alpha, d\Phi^{\gamma_i}(\zeta)), \quad \forall \alpha \in T^*_{\gamma_i}M,\, \zeta \in \mathfrak{g}. \tag{4.11}$$

From (4.10) and Lemma 2, the condition that $J'(0) = 0$ for all proper variations $h$ of the constant map $c_e(\cdot) \equiv e$ is equivalent to

$$\int_{t_0}^{t_1} (\sum_{i=1}^{k} \lambda_i (d\Phi^{\gamma_i})^* \mathbb{D}L_{\dot{\gamma}_i}, \chi)\, dt = 0 \tag{4.12}$$

for all $C^\infty$ map $\chi : [t_0, t_1] \to \mathfrak{g}$ such that $\int_{t_0}^{t_1} \chi(t)\, dt = 0$. Since $\sum_{i=1}^{k} \lambda_i (d\Phi^{\gamma_i})^* \mathbb{D}L_{\dot{\gamma}_i}$ is piecewise $C^\infty$ (though not necessarily continuous) in $\mathfrak{g}^*$, condition (4.12) implies that $\sum_{i=1}^{k} \lambda_i (d\Phi^{\gamma_i})^* \mathbb{D}L_{\dot{\gamma}_i}$ is constant for all $t \in [t_0, t_1]$ where $\dot{\gamma}_i$'s are well defined, because otherwise one can choose a $\chi$ with $\int_{t_0}^{t_1} \chi(t)\, dt = 0$ such that (4.12) fails to hold. This concludes the proof of the following theorem.

**Theorem 4** *Suppose that $\gamma = \langle \gamma_i \rangle_{i=1}^{k}$ is an optimal solution to the OCA (or OFS) problem. Then there exists a constant $\nu_0 \in \mathfrak{g}^*$ such that*

$$\sum_{i=1}^{k} \lambda_i (d\Phi^{\gamma_i})^* \mathbb{D}L_{\dot{\gamma}_i} \equiv \nu_0 \tag{4.13}$$

*for all $t \in [t_0, t_1]$ where $\dot{\gamma}_i$'s are well defined.*

In the following we shall denote by $\nu$ the quantity on the left hand side of (4.13).

**Remark 10** *The action of $G$ on $M$ induces an action of $G$ on $M^{(k)}$ naturally, which can be cotangent lifted to an action of $G$ on $T^*(M^{(k)})$. $\nu$ is the momentum map for this last action evaluated along the curve $(\gamma_1, \ldots, \gamma_k, \lambda_1 \mathbb{D}L_{\dot\gamma_1}, \ldots, \lambda_k \mathbb{D}L_{\dot\gamma_k})$ in $T^*(M^{(k)})$. Theorem 4 thus generalizes the classical Noether theorem ([3, 45]) to the nonsmooth case.*

If $L = \frac{1}{2}\|\cdot\|^2$, then the conclusion of Theorem 4 can be simplified by canonically identifying each $v \in T_{\gamma_i}M$ with the element in $T^*_{\gamma_i}M$ defined by $u \mapsto \langle v, u\rangle$, $\forall u \in T_{\gamma_i}M$. Thus $\mathbb{D}L_{\dot\gamma_i}$ is identified with $\dot\gamma_i$, and (4.13) becomes

$$\sum_{i=1}^{k} \lambda_i (d\Phi^{\gamma_i})^* \dot\gamma_i \equiv \nu_0 \in \mathfrak{g}^*, \tag{4.14}$$

where $(d\Phi^{\gamma_i})^* : T_{\gamma_i}M \to \mathfrak{g}^*$ is now defined by

$$((d\Phi^{\gamma_i})^* v, \zeta) = \langle v, d\Phi^{\gamma_i}(\zeta)\rangle, \quad \forall v \in T_{\gamma_i}M,\, \zeta \in \mathfrak{g}. \tag{4.15}$$

Furthermore, there is occasionally a natural choice for a metric on $\mathfrak{g}$, which can be used to identify $\mathfrak{g}$ and $\mathfrak{g}^*$. In this case, the conserved quantity $\nu$ can be thought of taking values in $\mathfrak{g}$.

**Example 5 ($G = \mathbf{SO}_n$, $M = \mathbb{R}^n$)** *Consider Example 2 with $G = \mathbf{SO}_n$, $M = \mathbb{R}^n$, and $L = \frac{1}{2}\|\cdot\|^2$. The Lie algebra $\mathfrak{g}$ of $\mathbf{SO}_n$ is $\mathfrak{so}_n = \{X \in \mathbb{R}^{n\times n} : X + X^t = 0\}$. Suppose that a $k$-tuple of curves in $\mathbb{R}^n$, $\gamma = \langle\gamma_i\rangle_{i=1}^k$, is an optimal solution to the OCA (or OFS) problem defined on $[t_0, t_1]$. At each time $t \in [t_0, t_1]$, let $v \in T_{\gamma_i}\mathbb{R}^n \simeq \mathbb{R}^n$ and $X \in \mathfrak{so}_n$ be arbitrary. Then*

$$\langle v, d\Phi^{\gamma_i}(X)\rangle = \langle v, X\gamma_i\rangle = v^t X \gamma_i = tr(\gamma_i v^t X) = \langle v\gamma_i^t, X\rangle_F = \frac{1}{2}\langle v\gamma_i^t - \gamma_i v^t, X\rangle_F,$$

*where we recall that* $\langle\cdot,\cdot\rangle_F$ *is the Frobenius inner product on* $\mathbb{R}^{n\times n}$ *defined in Example 4. The last equality follows from the skew-symmetry of* $X$*. So by (4.15),*

$$((d\Phi^{\gamma_i})^* v, X) = \frac{1}{2}\langle v\gamma_i^t - \gamma_i v^t, X\rangle_F, \quad \forall X \in \mathfrak{so}_n.$$

*Note that* $v\gamma_i^t - \gamma_i v^t \in \mathfrak{so}_n$*. So, if* $\mathfrak{so}_n$ *is identified with* $\mathfrak{so}_n^*$ *using the metric* $\frac{1}{2}\langle\cdot,\cdot\rangle_F$*, the above equation implies that* $(d\Phi^{\gamma_i})^* v = v\gamma_i^t - \gamma_i v^t$*. Hence (4.14) becomes*

$$\sum_{i=1}^{k} \lambda_i(\dot\gamma_i\gamma_i^t - \gamma_i\dot\gamma_i^t) \equiv \nu_0 \in \mathfrak{so}_n. \tag{4.16}$$

*Or equivalently,* $\sum_{i=1}^k \lambda_i(\dot\gamma_i \wedge \gamma_i)$ *is constant, where* $\wedge$ *is the wedge product defined on* $\mathbb{R}^n$*. In particular, if* $n = 3$ *(*$G = \mathbf{SO}_3$*,* $M = \mathbb{R}^3$*), equation (4.16) is equivalent to* $\sum_{i=1}^k \lambda_i(\gamma_i \times \dot\gamma_i) \equiv \Omega_0$ *for some* $\Omega_0 \in \mathbb{R}^3$*, where* $\times$ *is the vector product. Therefore, if* $\gamma$ *is thought of as the trajectories of* $k$ *particles moving in* $\mathbb{R}^3$ *with mass* $\lambda_1, \ldots, \lambda_k$*, respectively, then their total angular momentum is preserved along an optimal solution to the OCA (or OFS) problem. The conserved quantity when* $n > 3$ *can also be thought of as the generalized angular momentum for the particle system. Note that (4.16) in the case* $n = 2$ *has been derived in Chapter 2 (Proposition 4).*

**Example 6 (**$G = \mathbf{SO}_n$**,** $M = \mathbf{S}^{n-1}$**)** *Consider Example 3, where* $G = \mathbf{SO}_n$*,* $M = \mathbf{S}^{n-1}$*, and* $L = \frac{1}{2}\|\cdot\|^2$*. Since* $\mathbf{S}^{n-1}$ *is a submanifold of* $\mathbb{R}^n$*, by following the same steps as in Example 5, we conclude that (4.16) still holds for optimal solutions* $\gamma$ *to the OCA (or OFS) problem on* $\mathbf{S}^{n-1}$*.*

**Example 7 (Lie Group with a Bi-Invariant Metric)** *Suppose that* $M = G$ *is a Lie group with a bi-invariant Riemannian metric in Example 4, and* $L = \frac{1}{2}\|\cdot\|^2$*. Let* $\gamma = \langle\gamma_i\rangle_{i=1}^k$ *be a solution to the OCA (or OFS) problem on* $G$*. Then at each time* *t,* $\forall v \in T_{\gamma_i}G$, $\zeta \in \mathfrak{g}$,

$$\langle v, d\Phi^{\gamma_i}(\zeta)\rangle = \langle v, \zeta\gamma_i\rangle = \langle v\gamma_i^{-1}\gamma_i, \zeta\gamma_i\rangle = \langle v\gamma_i^{-1}, \zeta\rangle \quad \Rightarrow \quad ((d\Phi^{\gamma_i})^* v, \zeta) = \langle v\gamma_i^{-1}, \zeta\rangle. \tag{4.17}$$

*Under the canonical identification of* $\mathfrak{g}$ *with* $\mathfrak{g}^*$ *via* $\langle\cdot,\cdot\rangle$*, the right hand side is equivalent to* $(d\Phi^{\gamma_i})^* v = v\gamma_i^{-1} \in \mathfrak{g}$*. Therefore, the conservation law (4.14) is*

$$\sum_{i=1}^{k} \lambda_i \dot{\gamma}_i \gamma_i^{-1} \equiv \nu_0 \in \mathfrak{g}. \tag{4.18}$$

*In the particular case when* $M = G = \mathbb{R}^n$*, (4.18) implies* $\sum_{i=1}^{k} \lambda_i \dot{\gamma}_i \equiv \nu_0 \in \mathbb{R}^n$*. In other words, if* $k$ *particles with mass* $\lambda_1, \ldots, \lambda_k$ *follow the trajectories of* $\gamma$*, then their total linear momentum is preserved. This condition has been derived in Chapter 2 and Chapter 3 from elementary approaches. If we consider* $G = \mathbf{SO}_n$ *with the bi-invariant metric defined in Example 4, and* $L = \frac{1}{2}\|\cdot\|^2$*, then (4.18) holds for solutions* $\gamma = \langle\gamma_i\rangle_{i=1}^k$ *to the OCA (or OFS) problem on* $\mathbf{SO}_n$*, and* $\nu_0 \in \mathfrak{so}_n$ *is now a constant skew symmetric n-by-n matrix.*

A large class of examples can be derived from Example 7 by considering the quotient spaces of $G$ under certain subgroups $H$, i.e., the symmetric spaces $G/H$. We give two of these examples here. The first one is the OCA (or OFS) problem on the Grassmann manifold and has it origin in multi-user wireless communication [75]. In such a scenario, a communication channel is shared by multiple users. Specifically, each user is allocated a $p$-dimensional subspace in the $n$-dimensional signal space used for data transmission. Separation among these subspaces should be maintained to minimize crosstalk and hence guaranteeing a satisfactory signal-to-noise ratio (SNR). Due to the possible changes of user locations and channel conditions, the signal subspaces might need to be re-allocated from time to time in an incremental way, resulting each time in an OCA problem on the Grassmann manifold.

**Example 8 (Grassmann Manifold)** *Suppose that* $\mathbf{SO}_n$ *has the bi-invariant metric described in Example 4. Let* $p$ *be an integer,* $1 \leq p \leq n$. *Denote by* $H_p$ *the subgroup* $\begin{bmatrix} \mathbf{SO}_p & 0 \\ 0 & \mathbf{SO}_{n-p} \end{bmatrix} \simeq \mathbf{SO}_p \times \mathbf{SO}_{n-p}$ *of* $\mathbf{SO}_n$. *Define* $G_{n,p} \triangleq \mathbf{SO}_n / H_p$ *to be the set of left cosets of* $H_p$ *in* $\mathbf{SO}_n$, *and let* $\pi : \mathbf{SO}_n \to G_{n,p}$ *be the natural projection. Elements of* $G_{n,p}$ *are* $\pi(A) = AH_p$, $\forall A \in \mathbf{SO}_n$. *For each* $\pi(A) \in G_{n,p}$, *the subspace of* $\mathbb{R}^n$ *spanned by the first* $p$ *column vectors of* $A$ *is the same for all* $A \in \pi(A)$, *hence there is a one-to-one correspondence between* $G_{n,p}$ *and set of* $p$*-dimensional subspaces of* $\mathbb{R}^n$. *Since* $H_p$ *is a closed subgroup of* $\mathbf{SO}_n$, $G_{n,p}$ *admits a natural differential structure, and is called a* Grassmann manifold. *At each* $A \in \mathbf{SO}_n$, *the tangent space of* $\mathbf{SO}_n$ *has the orthogonal decomposition [14]:*

$$T_A\mathbf{SO}_n = vert_A\mathbf{SO}_n \oplus hor_A\mathbf{SO}_n.$$

*The* vertical space $vert_A\mathbf{SO}_n = A \begin{bmatrix} \mathfrak{so}_p & 0 \\ 0 & \mathfrak{so}_{n-p} \end{bmatrix}$ *is the tangent space of* $AH_p$ *at* $A$*; the* horizontal space $hor_A\mathbf{SO}_n$ *consists of all those matrices of the form* $A \begin{bmatrix} 0 & -X^t \\ X & 0 \end{bmatrix}$ *for some* $X \in \mathbb{R}^{(n-p)\times p}$. *Note that* $d\pi : hor_A\mathbf{SO}_n \to T_{\pi(A)}G_{n,p}$ *is a vector space isomorphism. The restriction of the metric on* $T_A\mathbf{SO}_n$ *defines a metric on* $hor_A\mathbf{SO}_n$ *as*

$$\langle A \begin{bmatrix} 0 & -X_1^t \\ X_1 & 0 \end{bmatrix}, A \begin{bmatrix} 0 & -X_2^t \\ X_2 & 0 \end{bmatrix} \rangle = \langle X_1, X_2 \rangle_F, \quad \forall X_1, X_2 \in \mathbb{R}^{(n-p)\times p}. \tag{4.19}$$

*An important observation is that there is a unique Riemannian metric on $G_{n,p}$ that makes $d\pi : hor_A\mathbf{SO}_n \to T_{\pi(A)}G_{n,p}$ an isometry for each $\pi(A) \in G_{n,p}$, regardless of the choice of $A \in \pi(A)$. Such a metric exists because the metric on $\mathbf{SO}_n$ is right invariant. Moreover, this metric on $G_{n,p}$ is invariant under the induced left action of $\mathbf{SO}_n$ on $G_{n,p}$ since the metric on $\mathbf{SO}_n$ is left invariant. In the terminology of [53], $\pi : \mathbf{SO}_n \to G_{n,p}$ is a* Riemannian submersion*, and when viewed as a principal $H_p$-bundle over $G_{n,p}$, $\mathbf{SO}_n$ has a metric of* constant bi-invariant type*. See [53] for more details on (sub-Riemannian) metrics of principal bundles.*

*Suppose that $L = \frac{1}{2}\|\cdot\|^2$. Let $\gamma = \langle\gamma_i\rangle_{i=1}^k$ be a k-tuple of curves in $G_{n,p}$ that is a solution to the OCA (or OFS) problem. For each $i = 1, \ldots, k$, let $A_i$ be a lifting of $\gamma_i$ in $\mathbf{SO}_n$ in the sense that $\pi(A_i) = \gamma_i$. In other words, the first p column vectors of $A_i \in \mathbf{SO}_n$ span the subspace $\gamma_i \in G_{n,p}$. We can choose $A_i$ to be continuous and piecewise $C^\infty$. At each time t, choose arbitrary $X \in \mathfrak{so}_n$ and $v \in T_{\gamma_i}G_{n,p}$, and let V be the unique element of $hor_{A_i}\mathbf{SO}_n$ such that $d\pi(V) = v$. Then, using the fact that $d\pi : hor_{A_i}\mathbf{SO}_n \to T_{\gamma_i}G_{n,p}$ is an isometry, we have*

$$\langle v, d\Phi^{\gamma_i}(X)\rangle_{T_{\gamma_i}G_{n,p}} = \langle V, P_{A_i}(XA_i)\rangle_{hor_{A_i}\mathbf{SO}_n} = \langle V, XA_i\rangle_{T_{A_i}\mathbf{SO}_n} = \langle VA_i^t, X\rangle_{\mathfrak{so}_n},$$

*where $P_{A_i}$ is the orthogonal projection $T_{A_i}\mathbf{SO}_n \to hor_{A_i}\mathbf{SO}_n$. Here for clarity we indicate in subscript the associated tangent space of each inner product. Therefore, $(d\Phi^{\gamma_i})^*v = VA_i^t \in \mathfrak{so}_n \simeq \mathfrak{so}_n^*$. Finally, notice that $\dot\gamma_i = d\pi[P_{A_i}(\dot A_i)]$. Then (4.14) becomes*

$$\sum_{i=1}^k \lambda_i (d\Phi^{\gamma_i})^*\dot\gamma_i = \sum_{i=1}^k \lambda_i P_{A_i}(\dot A_i)A_i^t \equiv \nu_0 \in \mathfrak{so}_n. \tag{4.20}$$

**Example 9 (Stiefel Manifold)** *Denote by $K_p$ the subgroup $\begin{bmatrix} I_p & 0 \\ 0 & \mathbf{SO}_{n-p} \end{bmatrix}$ of $\mathbf{SO}_n$.*

*Then* $K_p \simeq \mathbf{SO}_{n-p}$ *and the quotient space* $V_{n,p} \triangleq \mathbf{SO}_n/K_p$ *is called a* Stiefel manifold. *Elements in* $V_{n,p}$ *correspond in a one-to-one way to the orthonormal p-frames of* $\mathbb{R}^n$. *At each* $A \in \mathbf{SO}_n$, *the vertical space is now* $A \begin{bmatrix} 0 & 0 \\ 0 & \mathfrak{so}_{n-p} \end{bmatrix}$, *while the horizontal space consists of matrices of the form* $A \begin{bmatrix} Y & -X^t \\ X & 0 \end{bmatrix}$ *for* $X \in \mathbb{R}^{(n-p)\times p}$, $Y \in \mathbb{R}^{p\times p}$, $Y + Y^t = 0$. *The metric on* $\mathbf{SO}_n$ *restricts to a metric on the horizontal space as*

$$\langle A \begin{bmatrix} Y_1 & -X_1^t \\ X_1 & 0 \end{bmatrix}, A \begin{bmatrix} Y_2 & -X_2^t \\ X_2 & 0 \end{bmatrix} \rangle = \langle X_1, X_2 \rangle_F + \frac{1}{2}\langle Y_1, Y_2 \rangle_F,$$

*which can be used to define a Riemannian metric on* $V_{n,p}$ *such that* $d\pi$ *is an isometry from the horizontal space at each* $A \in \mathbf{SO}_n$ *to* $T_{\pi(A)}V_{n,p}$ *(*$\pi$ *is now the natural projection from* $\mathbf{SO}_n$ *to* $V_{n,p}$*). The metric thus defined is invariant under the induced left action of* $\mathbf{SO}_n$ *on* $V_{n,p}$.

*Let* $L = \frac{1}{2}\|\cdot\|^2$. *By similar arguments as in Example 8, we can show that if* $\gamma = \langle \gamma_i \rangle_{i=1}^k$ *is a solution to the OCA (or OFS) problem on* $V_{n,p}$, *and if* $A_i$ *is a lifting of* $\gamma_i$ *in* $\mathbf{SO}_n$, $1 \le i \le k$, *then*

$$\sum_{i=1}^{k} \lambda_i \hat{P}_{A_i}(\dot{A}_i)A_i^t \equiv \nu_0 \in \mathfrak{so}_n. \tag{4.21}$$

*Here* $\hat{P}_{A_i}$ *is the orthogonal projection from* $T_{A_i}\mathbf{SO}_n$ *to the horizontal space of* $\mathbf{SO}_n$ *at* $A_i$.

### 4.3.4 Second variation

Let $J(s)$ be defined as in (4.8). Differentiating equation (4.9) with respect to $s$ at $s=0$, we have

$$\begin{aligned} J''(0) &= \sum_{i=1}^{k} \lambda_i \int_{t_0}^{t_1} [(\mathbb{D}L_{\dot{\gamma}_i}, \xi_0''\gamma_i) + \mathbb{D}^2 L_{\dot{\gamma}_i}(\xi_0'\gamma_i, \xi_0'\gamma_i)]\, dt \\ &= \int_{t_0}^{t_1} (\sum_{i=1}^{k} \lambda_i (d\Phi^{\gamma_i})^* \mathbb{D}L_{\dot{\gamma}_i}, \xi_0'')\, dt + \int_{t_0}^{t_1} \sum_{i=1}^{k} \lambda_i \mathbb{D}^2 L_{\dot{\gamma}_i}(\xi_0'\gamma_i, \xi_0'\gamma_i)\, dt. \end{aligned} \tag{4.22}$$

Here $\xi_0'' \in \mathfrak{g}$, and $\mathbb{D}^2 L_{\dot{\gamma}_i} : T_{\gamma_i}M \times T_{\gamma_i}M \to \mathbb{R}$ is the fiberwise second order derivative (Hessian) of $L$ on $T_{\gamma_i}M$ evaluated at $\dot{\gamma}_i$. By Theorem 4, the first term in (4.22) can be written as $\int_{t_0}^{t_1} (\nu_0, \xi_0'')\, dt$, which can in turn be simplified as

$$\begin{aligned} \int_{t_0}^{t_1} (\nu_0, \xi_0'')\, dt &= \frac{d}{ds}\Big|_{s=0} (\nu_0, \int_{t_0}^{t_1} \xi_s'\, dt) \qquad = \frac{d}{ds}\Big|_{s=0} (\nu_0, \int_{t_0}^{t_1} (\dot{\eta}_s + [\xi_s, \eta_s])\, dt) \\ &= \frac{d}{ds}\Big|_{s=0} (\nu_0, \int_{t_0}^{t_1} [\xi_s, \eta_s]\, dt) = (\nu_0, \int_{t_0}^{t_1} ([\xi_0', \eta_0] + [\xi_0, \eta_0'])\, dt) \\ &= (\nu_0, \int_{t_0}^{t_1} [\dot{\eta}_0, \eta_0]\, dt), \end{aligned} \tag{4.23}$$

where we have used Lemma 1 and the following facts: $\eta_s(t_0) = \eta_s(t_1) = 0$; $\xi_0(\cdot) \equiv 0$; and $\xi_0' = \chi = \dot{\eta}_0$ by equation (4.6). As for the second term in (4.22), define

$$\mathbb{I}_t(\zeta_1, \zeta_2) \triangleq \sum_{i=1}^{k} \lambda_i \mathbb{D}^2 L_{\dot{\gamma}_i(t)}(\zeta_1\gamma_i(t), \zeta_2\gamma_i(t)), \quad \forall \zeta_1, \zeta_2 \in \mathfrak{g}, \tag{4.24}$$

for each $t \in [t_0, t_1]$. Then $\mathbb{I}_t(\cdot,\cdot) : \mathfrak{g} \times \mathfrak{g} \to \mathbb{R}$ is a nonnegative definite quadratic form on $\mathfrak{g}$, since $\lambda_i > 0$ and $L$ is convex on each fiber of $TM$ by assumption. If in particular $L = \frac{1}{2}\|\cdot\|^2$, then $\mathbb{D}^2 L_v(\cdot,\cdot) = \langle\cdot,\cdot\rangle_q$ for any $v \in T_qM$, $q \in M$. Hence $\mathbb{I}_t$ in this case is given by

$$\mathbb{I}_t(\zeta_1, \zeta_2) \triangleq \sum_{i=1}^{k} \lambda_i \langle \zeta_1\gamma_i, \zeta_2\gamma_i \rangle, \quad \forall \zeta_1, \zeta_2 \in \mathfrak{g}. \tag{4.25}$$

In mechanics, $\mathbb{I}_t$ defined in (4.25) is called the *moment of inertia tensor* ([45, 53]) for the action of $G$ on $M^{(k)}$ (with the metric $\prod_{i=1}^k \lambda_i\langle\cdot,\cdot\rangle$) evaluated at $(\gamma_1, \ldots, \gamma_k)$. By substituting (4.23) and (4.24) into (4.22) with $\xi_0' = \dot\eta_0$ by (4.5) and (4.6), we obtain

$$J''(0) = (\nu_0, \int_{t_0}^{t_1} [\dot\eta_0, \eta_0]\, dt) + \int_{t_0}^{t_1} \mathbb{I}_t(\dot\eta_0, \dot\eta_0)\, dt.$$

In order for $\gamma$ to be optimal, we must have $J''(0) \geq 0$ for all feasible $\eta_0$. Therefore,

**Theorem 5** *Suppose that $\langle\gamma_i\rangle_{i=1}^k$ is an optimal solution to the OCA (or OFS) problem. Let $\nu_0 \in \mathfrak{g}^*$ be defined as in Theorem 4. Then for any $C^\infty$ curve $\eta_0 : [t_0, t_1] \to \mathfrak{g}$ such that $\eta_0(t_0) = \eta_0(t_1) = 0$,*

$$(\nu_0, \int_{t_0}^{t_1} [\dot\eta_0, \eta_0]\, dt) + \int_{t_0}^{t_1} \mathbb{I}_t(\dot\eta_0, \dot\eta_0)\, dt \geq 0. \tag{4.26}$$

**Remark 11** *Consider the OCA problem with $L = \frac{1}{2}\|\cdot\|^2$. If $k = 1$, then solutions $\gamma$ to this problem are geodesics of $M$. If the action $\Phi$ is transitive, then any local proper variation of $\gamma$ in $M$ can be generated as $h\gamma$ by some proper variation $h$ of $c_e$ in $G$. So in this case Theorem 5 characterizes the first* conjugate point *along $\gamma$. If $k > 1$, then solutions $\gamma$ are geodesics in $M^{(k)} \setminus W$, a manifold with boundary whose dimension is usually much larger than that of $G$. The variations of $\gamma$ in the form of $h\gamma$ can only perturb the $k$ components of $\gamma$ uniformly by multiplying all of them from the left by the* same *elements of $G$. Hence the condition in Theorem 5 is in general only necessary for the local optimality of $\gamma$ when $k > 1$.*

It is often difficult to apply Theorem 5 directly. In the following we shall derive some of its implications that are easier to check. Note that if $\dim(\mathfrak{g}) = 1$ (or if $\mathfrak{g}$ is abelian), condition (4.26) holds trivially, since the first term is zero and the integrand of the second term is nonnegative. So we shall assume that $\dim(\mathfrak{g}) > 1$.

Choose an arbitrary inner product $\langle\cdot,\cdot\rangle_{\mathfrak{g}}$ on $\mathfrak{g}$, whose corresponding norm is denoted by $\|\cdot\|_{\mathfrak{g}}$. In many cases there is a natural choice for $\langle\cdot,\cdot\rangle_{\mathfrak{g}}$. At each time $t$, define the *spectral radius* of $\mathbb{I}_t$ as

$$\rho(\mathbb{I}_t) = \inf\{\lambda \in \mathbb{R} : \lambda\langle\cdot,\cdot\rangle_{\mathfrak{g}} - \mathbb{I}_t(\cdot,\cdot) \text{ is nonnegative definite on } \mathfrak{g}\}.$$

Then $\rho(\mathbb{I}_t) \geq 0$ is the largest eigenvalue of the symmetric matrix representing $\mathbb{I}_t$ in any orthonormal basis of $\mathfrak{g}$. For any subspace $\mathfrak{h}$ of $\mathfrak{g}$, the restriction $\mathbb{I}_t|_{\mathfrak{h}}$ is still nonnegative definite. Define

$$\rho(\mathbb{I}_t;\mathfrak{h}) = \rho(\mathbb{I}_t|_{\mathfrak{h}}) = \inf\{\lambda \in \mathbb{R} : \lambda\langle\cdot,\cdot\rangle_{\mathfrak{g}} - \mathbb{I}_t(\cdot,\cdot) \text{ is nonnegative definite on } \mathfrak{h}\}. \quad (4.27)$$

An immediate result of definition (4.27) is

$$\mathbb{I}_t(\zeta_1,\zeta_2) \leq \rho(\mathbb{I}_t;\mathfrak{h})\ \langle\zeta_1,\zeta_2\rangle_{\mathfrak{g}}, \quad \forall\zeta_1,\zeta_2 \in \mathfrak{h}.$$

Pick a two dimensional subspace $\mathfrak{h}$ of $\mathfrak{g}$, and let $\{\zeta_1,\zeta_2\}$ be an orthonormal basis of $\mathfrak{h}$. Denote

$$\zeta_0 = [\zeta_1,\zeta_2]. \quad (4.28)$$

Now consider condition (4.26) in the special case when $\eta_0$ as a curve in $\mathfrak{g}$ is contained entirely in $\mathfrak{h}$. Then there exist $C^\infty$ functions $x_1, x_2 : [t_0,t_1] \to \mathbb{R}$ such that $\eta_0 = x_1\zeta_1 + x_2\zeta_2$. The constraints that $\eta_0(t_0) = \eta_0(t_1) = 0$ imply that $x_1(t_0) = x_1(t_1) = 0$ and $x_2(t_0) = x_2(t_1) = 0$. Moreover,

$$[\dot\eta_0,\eta_0] = [\dot x_1\zeta_1 + \dot x_2\zeta_2, x_1\zeta_1 + x_2\zeta_2] = (\dot x_1 x_2 - x_1\dot x_2)\zeta_0.$$

Therefore, on the left hand side of inequality (4.26), the first term becomes

$$(\nu_0, \int_{t_0}^{t_1} [\dot{\eta}_0, \eta_0]\, dt) = \nu_0(\zeta_0) \int_{t_0}^{t_1} (\dot{x}_1 x_2 - x_1 \dot{x}_2)\, dt = -2\nu_0(\zeta_0) S_{\eta_0},$$

where $S_{\eta_0}$ is the (oriented) planar area encircled by $\eta_0$ in $\mathfrak{h}$. The second term is dominated by

$$\begin{aligned}\int_{t_0}^{t_1} \mathbb{I}_t(\dot{\eta}_0, \dot{\eta}_0)\, dt &\le \int_{t_0}^{t_1} \rho(\mathbb{I}_t; \mathfrak{h}) \|\dot{\eta}_0\|_{\mathfrak{g}}^2\, dt \\ &\le \sup_{t_0 \le t \le t_1} \rho(\mathbb{I}_t; \mathfrak{h}) \int_{t_0}^{t_1} \|\dot{\eta}_0\|_{\mathfrak{g}}^2\, dt \\ &= 2E_{\eta_0} \sup_{t_0 \le t \le t_1} \rho(\mathbb{I}_t; \mathfrak{h}),\end{aligned}$$

where $E_{\eta_0} = \frac{1}{2} \int_{t_0}^{t_1} \|\dot{\eta}_0\|_{\mathfrak{g}}^2\, dt$ is the energy of the curve $\eta_0$. As a result, (4.26) implies

$$\nu_0(\zeta_0) S_{\eta_0} \le E_{\eta_0} \sup_{t_0 \le t \le t_1} \rho(\mathbb{I}_t; \mathfrak{h}). \tag{4.29}$$

By reversing the parameterization of $\eta_0$ in (4.29), the sign of the left hand side is flipped, while the right hand side remains unchanged. Therefore,

$$|\nu_0(\zeta_0)|\, |S_{\eta_0}| \le E_{\eta_0} \sup_{t_0 \le t \le t_1} \rho(\mathbb{I}_t; \mathfrak{h}). \tag{4.30}$$

Since (4.30) holds for all $\eta_0$ with $\eta_0(t_0) = \eta_0(t_1) = 0$, and $\sup_{t_0 \le t \le t_1} \rho(\mathbb{I}_t; \mathfrak{h})$ is independent of the choice of $\eta_0$, we have

$$|\nu_0(\zeta_0)| \le \sup_{t_0 \le t \le t_1} \rho(\mathbb{I}_t; \mathfrak{h}) \inf_{\eta_0} \frac{E_{\eta_0}}{|S_{\eta_0}|}, \tag{4.31}$$

where the infimum is taken over all closed curves $\eta_0$ in $\mathfrak{h}$ with $\eta_0(t_0) = \eta_0(t_1) = 0$ and $S_{\eta_0} \ne 0$.

Denote by $l_{\eta_0} = \int_{t_0}^{t_1} \|\dot{\eta}_0\|_{\mathfrak{g}}\, dt$ the arc length of $\eta_0$. By [50] we have

$$E_{\eta_0} \ge \frac{l_{\eta_0}^2}{2(t_1 - t_0)},$$

with equality if and only if $\eta_0$ has constant speed. Since $|S_{\eta_0}|$ is independent of the parameterizations of $\eta_0$, we can always choose $\eta_0$ with constant speed, which implies that (4.31) is equivalent to

$$|\nu_0(\zeta_0)| \leq \frac{1}{2(t_1 - t_0)} \sup_{t_0 \leq t \leq t_1} \rho(\mathbb{I}_t; \mathfrak{h}) \inf_{\eta_0} \frac{l_{\eta_0}^2}{|S_{\eta_0}|}. \tag{4.32}$$

From an ancient theorem stated below without proof (Theorem 6), $l_{\eta_0}^2/|S_{\eta_0}|$ achieves its infimum when $\eta_0$ draws a circle in $\mathfrak{h}$ of arbitrary radius through the origin, and the infimum is $4\pi$. So (4.32) can be written as

$$|\nu_0(\zeta_0)| \leq \frac{2\pi}{t_1 - t_0} \sup_{t_0 \leq t \leq t_1} \rho(\mathbb{I}_t; \mathfrak{h}).$$

**Theorem 6 (Isoperimetric Problem, [21])** *Using a string of fixed length, one can encircle the maximal area by arranging the string into a circle. Or equivalently, among all the closed curves that enclose a fixed area, the one with the shortest length is a circle.*

Recalling the expression for $\zeta_0$ in (4.28), we have

**Corollary 2** *Suppose that $\gamma = \langle \gamma_i \rangle_{i=1}^k$ is an optimal solution to the OCA (or OFS) problem, and $\nu_0$ is defined as in Theorem 4. Let $\langle \cdot, \cdot \rangle_{\mathfrak{g}}$ be an arbitrary inner product on $\mathfrak{g}$. Then*

$$|\nu_0([\zeta_1, \zeta_2])| \leq \frac{2\pi}{t_1 - t_0} \sup_{t_0 \leq t \leq t_1} \rho(\mathbb{I}_t; \mathfrak{h}), \tag{4.33}$$

*for any orthonormal pair $\zeta_1, \zeta_2 \in \mathfrak{g}$. Here $\mathfrak{h} = span\{\zeta_1, \zeta_2\}$, and $\rho(\mathbb{I}_t; \mathfrak{h})$ is defined in (4.27).*

**Remark 12** *The choice of the inner product $\langle \cdot, \cdot \rangle_{\mathfrak{g}}$ affects both the choices of $\zeta_1, \zeta_2$ and the values of $\rho(\mathbb{I}_t, \mathfrak{h})$, so in this sense the conclusion of Corollary 2 is not intrinsic.*

In certain cases, Corollary 2 takes an especially simple form. Suppose for instance that $L = \frac{1}{2}\|\cdot\|^2$ and that the inner product $\langle\cdot,\cdot\rangle_{\mathfrak{g}}$ on $\mathfrak{g}$ is chosen such that

$$\langle \zeta_1 q, \zeta_2 q\rangle = \langle \zeta_1, \zeta_2\rangle_{\mathfrak{g}}, \quad \forall \zeta_1, \zeta_2 \in \mathfrak{g}, q \in M. \tag{4.34}$$

Then at each $t$, $\mathbb{I}_t(\zeta_1,\zeta_2) = \sum_{i=1}^{k} \lambda_i \langle \zeta_1\gamma_i, \zeta_2\gamma_i\rangle = (\sum_{i=1}^{k}\lambda_i)\langle\zeta_1,\zeta_2\rangle_{\mathfrak{g}}$, $\forall \zeta_1,\zeta_2 \in \mathfrak{g}$, which implies that

$$\rho(\mathbb{I}_t;\mathfrak{h}) = \rho(\mathbb{I}_t) = \sum_{i=1}^{k}\lambda_i$$

for any $t$ and any two dimensional subspace $\mathfrak{h}$ of $\mathfrak{g}$. Therefore,

**Corollary 3** *If in addition to the hypotheses of Corollary 2, we have $L = \frac{1}{2}\|\cdot\|^2$, and $\langle\cdot,\cdot\rangle_{\mathfrak{g}}$ satisfying condition (4.34), then for any orthonormal pair $\zeta_1, \zeta_2 \in \mathfrak{g}$,*

$$|\nu_0([\zeta_1,\zeta_2])| \leq \frac{2\pi\sum_{i=1}^{k}\lambda_i}{t_1 - t_0}. \tag{4.35}$$

**Example 10 (Lie Group with a Bi-Invariant Metric)** *Consider a Lie group $G$ with a bi-invariant metric $\langle\cdot,\cdot\rangle$, and $L = \frac{1}{2}\|\cdot\|^2$. Choose the metric $\langle\cdot,\cdot\rangle_{\mathfrak{g}}$ to be the restriction of $\langle\cdot,\cdot\rangle$ on $\mathfrak{g}$. This metric obviously satisfies condition (4.34). Hence Corollary 3 holds, where $\nu_0 \in \mathfrak{g}$ is given by (4.18). In particular, let $G = \mathbf{SO}_3$ be equipped with the bi-invariant metric described in Example 7. Due to the well known fact that $\mathfrak{so}_3$ is isomorphic to $(\mathbb{R}^3, \times)$ as a Lie algebra ([20]), the set of $[\zeta_1,\zeta_2]$ for orthonormal pairs $\zeta_1,\zeta_2 \in \mathfrak{so}_3$ is the unit sphere in $\mathfrak{so}_3$, hence (4.35) implies*

$$\|\nu_0\|_{\mathfrak{so}_3} \leq \frac{2\pi\sum_{i=1}^{k}\lambda_i}{t_1 - t_0}. \tag{4.36}$$

*If $k = 1$, $\lambda_1 = 1$, then solutions $\gamma$ to the OCA problem are geodesics in $\mathbf{SO}_3$. Consider the example $\gamma(t) = \begin{bmatrix} \cos t & -\sin t & 0 \\ \sin t & \cos t & 0 \\ 0 & 0 & 1 \end{bmatrix}$, $\forall t \in [t_0, t_1]$. Then $\nu_0 = \dot\gamma\gamma^{-1} =$*

$\begin{bmatrix} 0 & -1 & 0 \\ 1 & 0 & 0 \\ 0 & 0 & 0 \end{bmatrix}$. *Thus (4.36) becomes* $t_1 - t_0 \leq 2\pi$*, which indeed characterizes the first conjugate point along the geodesic* $\gamma$ *in* $\mathbf{SO}_3$*, as is pointed out in Remark 11.*

**Example 11 (Grassmann Manifold)** *We continue the discussion in Example 8, where* $G = \mathbf{SO}_n$, $M = G_{n,p}$*, and* $L = \frac{1}{2}\|\cdot\|^2$*. Suppose that* $\gamma = \langle \gamma_i \rangle_{i=1}^k$ *is an optimal solution to the OCA (or OFS) problem defined on* $[t_0, t_1]$*, and that* $\langle A_i \rangle_{i=1}^k$ *is a lifting of* $\gamma$ *in* $\mathbf{SO}_n$*. At each time* $t$*, we have*

$$\begin{aligned} \mathbb{I}_t(X, X) &= \sum_{i=1}^k \lambda_i \langle d\Phi^{\gamma_i}(X), d\Phi^{\gamma_i}(X) \rangle_{T_{\gamma_i} G_{n,p}} && (4.37) \\ &= \sum_{i=1}^k \lambda_i \langle P_{A_i}(XA_i), P_{A_i}(XA_i) \rangle_{T_{A_i}\mathbf{SO}_n} \\ &\leq \sum_{i=1}^k \lambda_i \langle XA_i, XA_i \rangle_{T_{A_i}\mathbf{SO}_n} = \sum_{i=1}^k \lambda_i \|X\|^2_{\mathfrak{so}_n}, \quad \forall X \in \mathfrak{so}_n. && (4.38) \end{aligned}$$

*where equality holds if and only if* $XA_i \in hor_{A_i}\mathbf{SO}_n$ *for each* $i$*. Hence* $\rho(\mathbb{I}_t) \leq \sum_{i=1}^k \lambda_i$*, and Corollary 2 implies that*

$$|\nu_0([X_1, X_2])| \leq \frac{2\pi \sum_{i=1}^k \lambda_i}{t_1 - t_0} \tag{4.39}$$

*for all orthonormal pairs* $X_1, X_2 \in \mathfrak{so}_n$*, where* $\nu_0$ *is defined in (4.20). In particular, if* $n = 3$*, then the set of possible* $[X_1, X_2]$ *is the unit sphere in* $\mathfrak{so}_3$*. Hence (4.39) reduces to*

$$\|\nu_0\|_{\mathfrak{so}_3} \leq \frac{2\pi \sum_{i=1}^k \lambda_i}{t_1 - t_0}.$$

**Example 12 (Stiefel Manifold)** *For the Stiefel manifold* $V_{n,p}$ *studied in Example 9, a similar argument shows that (4.39) still holds, with* $\nu_0$ *now defined in (4.21).*

### 4.3.5 A topological optimality condition

In this section we focus on OCA and OFS problems on a Riemannian manifold $M$ satisfying Assumption 1, with the Lagrangian function given by $L = \frac{1}{2}\|\cdot\|^2$. Let $\gamma = \langle\gamma_i\rangle_{i=1}^k$ be an optimal solution to the OCA (or OFS) problem defined on $[t_0, t_1]$. Based on the first variational analysis, we have proved in Theorem 4 that the quantity $\nu_0$ is conserved along $\gamma$. In this section, we derive additional optimality conditions based on topological properties of $M$. Roughly speaking, we shall prove in Theorem 7 below that for every possible way of embedding a circle in $G$, $\nu_0$ is bounded when evaluated along the corresponding direction in $\mathfrak{g}$, for otherwise one can get a better solution generated by "going the other way" around the circle. The results in this section generalize the result in Proposition 4 in Chapter 2.

#### Two lemmas

First we shall prove two lemmas useful later in this section.

Assume that $\mathfrak{so}_n$ $(n \geq 2)$ is equipped with the inner product $\langle\cdot,\cdot\rangle_{\mathfrak{so}_n} = \frac{1}{2}\langle\cdot,\cdot\rangle_F$.

**Lemma 3** *Suppose that $Y \in \mathfrak{so}_n$ and $\lambda > 0$ are constants. Then the following are equivalent:*

1. $|\langle Y, X\rangle_{\mathfrak{so}_n}| \leq \lambda\|X\|^2_{\mathfrak{so}_n}$ *for all $X \in \mathfrak{so}_n$ such that $e^{2\pi X} = I_n$;*
2. *The $L^2$-norm of $Y$, $\|Y\|_2$, is bounded by $\lambda$.*

**Proof:** $1 \to 2$: For any unit vector $v_1 \in \mathbb{R}^n$ such that $Yv_1 \neq 0$, define $v_2 = Yv_1/\|Yv_1\|$, which is a unit vector orthogonal to $v_1$ by the skew symmetry of $Y$. Let $v_1, v_2, \ldots, v_n$ be an orthonormal basis of $\mathbb{R}^n$, hence $A = [v_1|v_2|\ldots|v_n] \in \mathbf{O}_n$.

Define $X = AZA^t$, where $Z = (z_{ij}) \in \mathfrak{so}_n$ is such that $z_{21} = -z_{12} = 1$, and $z_{ij} = 0$ otherwise. Then $X \in \mathfrak{so}_n$, and $e^{2\pi X} = I_n$. Hence $|\langle Y, X\rangle_{\mathfrak{so}_n}| \leq \lambda \|X\|^2_{\mathfrak{so}_n} = \lambda$. But $\langle Y, X\rangle_{\mathfrak{so}_n} = \langle Y, AZA^t\rangle_{\mathfrak{so}_n} = \langle A^tYA, Z\rangle_{\mathfrak{so}_n} = v_2^t Y v_1 = \|Yv_1\|$. Therefore, $\|Yv_1\| \leq \lambda$. That this holds for every unit vector $v_1 \in \mathbb{R}^n$ implies that $\|Y\|_2 \leq \lambda$. $2 \to 1$: For each $X \in \mathfrak{so}_n$ with $e^{2\pi X} = I_n$, there exist $A \in \mathbf{O}_n$ and $Z \in \mathfrak{so}_n$ such that $X = AZA^t$, where $Z = \mathrm{diag}(\begin{bmatrix} 0 & -m_1 \\ m_1 & 0 \end{bmatrix}, \ldots, \begin{bmatrix} 0 & -m_l \\ m_l & 0 \end{bmatrix}, 0, \ldots, 0)$ for some $m_1, \ldots, m_l \in \mathbb{Z}$ $(2l \leq n)$. Write $A = [u_1|v_1|\ldots|u_l|v_l|w_1|\ldots|w_{n-2l}]$ in column vectors. Then

$$\begin{aligned} |\langle Y, X\rangle_{\mathfrak{so}_n}| &= |\langle A^tYA, Z\rangle_{\mathfrak{so}_n}| = |\sum_{j=1}^{l} m_j v_j^t Y u_j| \\ &\leq \sum_{j=1}^{l} |m_j| \cdot |v_j^t Y u_j| \leq \|Y\|_2 \sum_{j=1}^{l} m_j^2 \leq \lambda \|X\|^2_{\mathfrak{so}_n}, \end{aligned}$$

since $|v_j^t Y u_j| \leq \|v_j\| \|Y\|_2 \|u_j\| = \|Y\|_2$, and $\|X\|^2_{\mathfrak{so}_n} = \|Z\|^2_{\mathfrak{so}_n} = \sum_{j=1}^{l} m_j^2$. ∎

**Lemma 4** *Suppose that $n = 2l$ is even, and that $Y \in \mathfrak{so}_n$ and $\lambda > 0$ are constants such that $|\langle Y, X\rangle_{\mathfrak{so}_n}| \leq \lambda \|X\|^2_{\mathfrak{so}_n}$ for all $X \in \mathfrak{so}_n$ satisfying $e^{\pi X} = -I_n$. Then*

$$\frac{1}{n} \sum_{j=1}^{n} \mu_j \leq \lambda,$$

*where $\mu_1, \ldots, \mu_n$ are the singular values of $Y$.*

**Proof:** Since $Y \in \mathfrak{so}_n$, there exist $A \in \mathbf{O}_n$ and $\omega_1, \ldots, \omega_l \geq 0$ such that $Y = AZA^t$, where $Z = \mathrm{diag}(\begin{bmatrix} 0 & -\omega_1 \\ \omega_1 & 0 \end{bmatrix}, \ldots, \begin{bmatrix} 0 & -\omega_l \\ \omega_l & 0 \end{bmatrix}) \in \mathfrak{so}_n$. Hence the singular values of $Y$ are simply $\omega_1, \omega_1, \ldots, \omega_l, \omega_l$. Define

$$X = A \cdot \mathrm{diag}(\begin{bmatrix} 0 & -1 \\ 1 & 0 \end{bmatrix}, \ldots, \begin{bmatrix} 0 & -1 \\ 1 & 0 \end{bmatrix}) \cdot A^t.$$

Then $X \in \mathfrak{so}_n$ and $e^{\pi X} = -I_n$. So by hypothesis, $|\langle Y, X\rangle_{\mathfrak{so}_n}| = \sum_{j=1}^{l} \omega_j \leq \lambda \|X\|^2_{\mathfrak{so}_n} = \lambda l$, which is the desired conclusion. ■

Now consider $\mathbf{T}^1 = \mathbb{R}/2\pi\mathbb{Z} = \{\theta \mod 2\pi : \theta \in \mathbb{R}\}$ with the quotient metric of $\mathbb{R}$. $\mathbf{T}^1$ is a Lie group under addition modulo $2\pi$, and its Lie algebra is isomorphic to $\mathbb{R}$ under the correspondence $\lambda \frac{\partial}{\partial \theta} \in T_0\mathbf{T}^1 \mapsto \lambda \in \mathbb{R}$. Hence we shall denote it by $\mathbb{R}$. Suppose that there exists a Lie group homomorphism $\varphi : \mathbf{T}^1 \to G$. Then $d\varphi : \mathbb{R} \to \mathfrak{g}$ is a Lie algebra homomorphism.

Let $h_0 : [t_0, t_1] \to \mathbf{T}^1$ be a continuous and piecewise $C^\infty$ curve in $\mathbf{T}^1$ starting from and ending at 0. Then $\varphi(h_0)$ is a curve in $G$ that starts from and ends at $e$, and hence the $k$-tuple of curves in $M$ define by $\varphi(h_0)\gamma = \langle \varphi(h_0)\gamma_i \rangle_{i=1}^k$ has the same starting and destination positions as $\gamma$. Since $\varphi$ is a homomorphism, the following diagram commutes at each $t \in [t_0, t_1]$:

$$\begin{array}{ccc} T_0\mathbf{T}^1 & \xrightarrow{d\varphi} & T_eG \\ {\scriptstyle dm_{h_0^{-1}}}\big\uparrow & & \big\uparrow{\scriptstyle dm_{\varphi(h_0^{-1})}} \\ T_{h_0}\mathbf{T}^1 & \xrightarrow{d\varphi} & T_{\varphi(h_0)}G \end{array}$$

where we recall that $m_g$ stands for left group multiplication by $g \in G$. We then have

$$\begin{aligned} \frac{d}{dt}[\varphi(h_0)\gamma_i] &= d\varphi(\dot{h}_0)\gamma_i + \varphi(h_0)\dot{\gamma}_i = \varphi(h_0)[\varphi(h_0^{-1})d\varphi(\dot{h}_0)\gamma_i + \dot{\gamma}_i] \\ &= \varphi(h_0)[d\varphi(h_0^{-1}\dot{h}_0)\gamma_i + \dot{\gamma}_i]. \end{aligned}$$

Therefore, the energy of $\varphi(h_0)\gamma$ is

$$J[\varphi(h_0)\gamma] = \sum_{i=1}^{k} \lambda_i \int_{t_0}^{t_1} \frac{1}{2} \|\varphi(h_0)[d\varphi(\xi_0)\gamma_i + \dot{\gamma}_i]\|^2 \, dt, \tag{4.40}$$

where we set

$$\xi_0(t) = h_0(t)^{-1}\dot{h}_0(t), \quad \forall t \in [t_0, t_1].$$

Note that $\xi_0$ is a piecewise $C^\infty$ curve in the Lie algebra $\mathbb{R}$ such that $\int_{t_0}^{t_1} \xi_0(t)dt = 2m\pi$ for some $m \in \mathbb{Z}$. Conversely, every curve $\xi_0$ in $\mathbb{R}$ satisfying $\frac{1}{2\pi}\int_{t_0}^{t_1} \xi_0(t)dt \in \mathbb{Z}$ can be realized as $h_0^{-1}\dot{h}_0$ for some curve $h_0$ in $\mathbf{T}^1$ that starts from and ends at 0.

Since $\varphi(h_0)$ is an isometry on $M$, equation (4.40) can be further simplified to

$$\begin{aligned}
J[\varphi(h_0)\gamma] &= \sum_{i=1}^{k} \lambda_i \int_{t_0}^{t_1} \frac{1}{2}\|d\varphi(\xi_0)\gamma_i + \dot{\gamma}_i\|^2 \, dt \\
&= \int_{t_0}^{t_1} \left[\frac{1}{2}\sum_{i=1}^{k} \lambda_i \|\dot{\gamma}_i\|^2 + \frac{1}{2}\sum_{i=1}^{k} \lambda_i \|d\varphi(\xi_0)\gamma_i\|^2 \right.\\
&\qquad \left. + \sum_{i=1}^{k} \lambda_i ((d\Phi^{\gamma_i})^*\dot{\gamma}_i, d\varphi(\xi_0))\right] dt \\
&= J(\gamma) + \int_{t_0}^{t_1} \frac{1}{2}\{\mathbb{I}_t[d\varphi(\xi_0), d\varphi(\xi_0)] + (\nu_0, d\varphi(\xi_0))\}\, dt,
\end{aligned}$$

where in the last step we have used Theorem 4, and the definition (4.25) of $\mathbb{I}_t$. Denote by $\varphi^*\mathbb{I}_t$ the pull back of $\mathbb{I}_t$ via $\varphi$ defined by $\varphi^*\mathbb{I}_t(x_1, x_2) \triangleq \mathbb{I}_t[d\varphi(x_1), d\varphi(x_2)]$, $\forall x_1, x_2 \in \mathbb{R}$. Then $\varphi^*\mathbb{I}_t : \mathbb{R} \times \mathbb{R} \to \mathbb{R}$ is a quadratic function, and is obviously of the form

$$\varphi^*\mathbb{I}_t(x_1, x_2) = \|\varphi^*\mathbb{I}_t\| x_1 x_2, \quad \forall x_1, x_2 \in \mathbb{R},$$

where $\|\varphi^*\mathbb{I}_t\| \geq 0$ is the spectral radius of $\varphi^*\mathbb{I}_t$ given by

$$\|\varphi^*\mathbb{I}_t\| \triangleq \varphi^*\mathbb{I}_t(1,1) = \mathbb{I}_t[d\varphi(1), d\varphi(1)]. \tag{4.41}$$

Similarly, denote by $\varphi^*\nu_0 \in \mathbb{R}^* \simeq \mathbb{R}$ the pull back of $\nu_0$ via $\varphi$ such that $(\nu_0, d\varphi(x)) = (\varphi^*\nu_0)x$, $\forall x \in \mathbb{R}$. From the above equations, the difference between the energy of $\varphi(h_0)\gamma$ and $\gamma$ is given by

$$\Delta J(\xi_0) \triangleq J[\varphi(h_0)\gamma] - J(\gamma) = \int_{t_0}^{t_1} \left[\frac{1}{2}\|\varphi^*\mathbb{I}_t\|\xi_0^2 + (\varphi^*\nu_0)\xi_0\right] dt. \tag{4.42}$$

A necessary condition for $\gamma$ to be optimal is that $\Delta J(\xi_0) \geq 0$ for all possible $\xi_0$. By (4.42), this implies

$$\int_{t_0}^{t_1} \left[ \frac{1}{2} \|\varphi^* \mathbb{I}_t\| \xi_0^2 + (\varphi^* \nu_0) \xi_0 \right] dt \geq 0, \tag{4.43}$$

for all curves $\xi_0$ in $\mathbb{R}$ such that $\frac{1}{2\pi} \int_{t_0}^{t_1} \xi_0(t) dt \in \mathbb{Z}$.

Fix an $m \in \mathbb{Z}$. To find the $\xi_0$ that minimizes $\Delta J(\xi_0)$ subject to the constraint that $\int_{t_0}^{t_1} \xi_0(t) dt = 2m\pi$, we use the Lagrangian multiplier approach. Assume that $\|\varphi^* \mathbb{I}_t\| > 0$ for almost all $t \in [t_0, t_1]$. Define

$$\mathcal{L}(\xi_0, \mu) \triangleq \Delta J(\xi_0) + \mu\left(\int_{t_0}^{t_1} \xi_0 dt - 2m\pi\right) = \int_{t_0}^{t_1} \left[ \frac{1}{2} \|\varphi^* \mathbb{I}_t\| \xi_0^2 + (\mu + \varphi^* \nu_0) \xi_0 \right] dt - 2\mu m\pi$$

for $\mu \in \mathbb{R}$. Note that $\mathcal{L}(\xi_0, \mu)$ is minimized when $\xi_0 = -(\mu + \varphi^* \nu_0)/\|\varphi^* \mathbb{I}_t\|$. The constraint that $\int_{t_0}^{t_1} \xi_0(t) dt = 2m\pi$ implies that $\mu + \varphi^* \nu_0 = -2m\pi/[\int_{t_0}^{t_1} \frac{1}{\|\varphi^* \mathbb{I}_t\|} dt]^{-1}$. Hence

$$\xi_0 = \frac{2m\pi}{\|\varphi^* \mathbb{I}_t\| \int_{t_0}^{t_1} \frac{1}{\|\varphi^* \mathbb{I}_t\|} dt} \tag{4.44}$$

minimizes $\Delta J(\xi_0)$ among $\xi_0$ such that $\int_{t_0}^{t_1} \xi_0(t) dt = 2m\pi$. Substituting (4.44) into (4.43), we have

$$m^2 \pi + m(\varphi^* \nu_0) \int_{t_0}^{t_1} \frac{1}{\|\varphi^* \mathbb{I}_t\|} dt \geq 0.$$

Note that the above inequality must hold for all $m \in \mathbb{Z}$, which implies

$$|\varphi^* \nu_0| \leq \pi \left[ \int_{t_0}^{t_1} \frac{1}{\|\varphi^* \mathbb{I}_t\|} dt \right]^{-1}.$$

Therefore, we have

**Theorem 7** *Suppose that $\gamma = \langle \gamma_i \rangle_{i=1}^k$ is a solution to the OCA (or OFS) problem with $L = \frac{1}{2} \| \cdot \|^2$. Let $\nu_0$ and $\mathbb{I}_t$ be defined in (4.14) and (4.25) respectively. Then,* *for any Lie group homomorphism $\varphi : \mathbf{T}^1 \to G$ such that $\|\varphi^* \mathbb{I}_t\| > 0$ for almost all $t \in [t_0, t_1]$,*

$$|\varphi^* \nu_0| \le \pi \left[ \int_{t_0}^{t_1} \frac{1}{\|\varphi^* \mathbb{I}_t\|} \, dt \right]^{-1}. \tag{4.45}$$

**Example 13** **($G = M = \mathbf{T}^n$)** *Let $G = \mathbf{T}^n = \mathbb{R}^n/\mathbb{Z}^n$ be the flat $n$-torus with the metric inherited from $\mathbb{R}^n$. $\mathbf{T}^n$ is a Lie group under componentwise modulo $\mathbb{Z}$ addition, and its metric is bi-invariant. Its Lie algebra is $\mathbb{R}^n$ with trivial Lie bracket, and is equipped with the standard metric. Let $\gamma = \langle \gamma_i \rangle_{i=1}^k$ be a solution to the OCA (or OFS) problem. In Example 7 we have shown that*

$$\sum_{i=1}^k \lambda_i \dot{\gamma}_i \gamma_i^{-1} = \sum_{i=1}^k \lambda_i \dot{\gamma}_i \equiv \nu_0 \in \mathbb{R}^n.$$

*Pick any $z \in \mathbb{Z}^n$, $z \neq 0$. The map $\varphi(\theta \mod 2\pi) = \frac{\theta}{2\pi} z \mod \mathbb{Z}^n$, $\forall \theta \in \mathbb{R}$, is a homomorphism from $\mathbf{T}^1$ to $\mathbf{T}^n$ with $d\varphi(1) = z/2\pi$. So $\varphi^* \nu_0 = \langle \nu_0, d\varphi(1) \rangle = \langle \nu_0, z \rangle / 2\pi$, and $\|\varphi^* \mathbb{I}_t\| = \mathbb{I}_t[d\varphi(1), d\varphi(1)] = \sum_{i=1}^k \lambda_i \|z/2\pi\|^2$. As a result, Theorem 7 implies that*

$$|\langle \nu_0, \frac{z}{\|z\|^2} \rangle| \le \frac{\sum_{i=1}^k \lambda_i}{2(t_1 - t_0)}, \quad \textit{for all } z \in \mathbb{Z}^n,\ z \neq 0. \tag{4.46}$$

*In particular, if $\nu_0 = (\nu_{0,1}, \ldots, \nu_{0,n})$ in coordinates, and $z = e_j$ is the element in $\mathbb{R}^n$ with the $j$-th coordinate 1 and the rest 0, then a necessary condition of (4.46) is*

$$|\nu_{0,j}| \le \frac{\sum_{i=1}^k \lambda_i}{2(t_1 - t_0)}, \quad j = 1, \ldots, n. \tag{4.47}$$

*It can be verified that (4.47) is also sufficient for (4.46).*

**Example 14** **($G = \mathbf{SO}_2$, $M = \mathbb{R}^2$)** *Suppose $G = \mathbf{SO}_2$, $M = \mathbb{R}^2$ with the standard metric, and $G$ acts on $M$ by matrix multiplication. As before, choose the metric on*

*$\mathfrak{so}_2$ to be $\frac{1}{2}\langle\cdot,\cdot\rangle_F$. By following the same arguments as in Example 5, we conclude that for any solution $\gamma = \langle\gamma_i\rangle_{i=1}^k$ to the OCA (or OFS) problem,*

$$\sum_{i=1}^k \lambda_i(\dot\gamma_i\gamma_i^t - \gamma_i\dot\gamma_i^t) \equiv \nu_0 \in \mathfrak{so}_2.$$

*Note that $\mathbf{SO}_2 \simeq \mathbf{T}^1$ under the isomorphism $\varphi(\theta \mod 2\pi) = \begin{bmatrix}\cos\theta & -\sin\theta \\ \sin\theta & \cos\theta\end{bmatrix}$, $\forall\theta \in \mathbb{R}$, and $d\varphi(1) = \begin{bmatrix}0 & -1 \\ 1 & 0\end{bmatrix}$. Hence $\varphi^*\nu_0 = \langle\nu_0, d\varphi(1)\rangle_{\mathfrak{so}_2} = \sum_{i=1}^k \lambda_i(\gamma_{i,1}\dot\gamma_{i,2} - \gamma_{i,2}\dot\gamma_{i,1})$ if we write each $\gamma_i$ in coordinates, and $\|\varphi^*\mathbb{I}_t\| = \sum_{i=1}^k \lambda_i\|d\varphi(1)\gamma_i\|^2 = \sum_{i=1}^k \lambda_i\|\gamma_i\|^2$. Therefore, by Theorem 7,*

$$\left|\sum_{i=1}^k \lambda_i(\gamma_{i,1}\dot\gamma_{i,2} - \gamma_{i,2}\dot\gamma_{i,1})\right| \le \pi\left[\int_{t_0}^{t_1} \frac{dt}{\sum_{i=1}^k \lambda_i\|\gamma_i\|^2}\right]^{-1}. \tag{4.48}$$

*In Chapter 2, equation (4.48) is derived through an elementary approach.*

**Example 15** **($G = M = \mathbf{SO}_n$)** *Let $G = \mathbf{SO}_n$ be equipped with the bi-invariant metric defined in Example 7. So the conserved quantity is $\nu_0 = \sum_{i=1}^k \lambda_i\dot\gamma_i\gamma_i^{-1} \in \mathfrak{so}_n$ along a solution $\gamma = \langle\gamma_i\rangle_{i=1}^k$ to the OCA (or OFS) problem. Let $X \in \mathfrak{so}_n$ be such that $e^{2\pi X} = I_n$, $X \ne 0$. Define a Lie group homomorphism $\varphi_X : \mathbf{T}^1 \to \mathbf{SO}_n$ by $\varphi_X(\theta \mod 2\pi) = e^{\theta X}$, $\forall\theta \in \mathbb{R}$. Then $d\varphi_X(1) = X$, $\varphi_X^*\nu_0 = \langle\nu_0, X\rangle_{\mathfrak{so}_n}$, and $\|\varphi_X^*\mathbb{I}_t\| = \sum_{i=1}^k \lambda_i\|X\|_{\mathfrak{so}_n}^2$. Theorem 7 thus implies that*

$$|\langle\nu_0, X\rangle_{\mathfrak{so}_n}| \le \pi\sum_{i=1}^k \lambda_i\|X\|_{\mathfrak{so}_n}^2/(t_1 - t_0)$$

*for all $X \in \mathfrak{so}_n$ such that $e^{2\pi X} = I_n$. By Lemma 3, this is equivalent to*

$$\|\nu_0\|_2 \le \frac{\pi}{t_1 - t_0}\sum_{i=1}^k \lambda_i, \tag{4.49}$$

*where* $\|\nu_0\|_2$ *is the* $L^2$ *norm of the matrix* $\nu_0$*. Or equivalently,*

$$\text{the maximum of the singular values of } \nu_0 \leq \frac{\pi}{t_1 - t_0} \sum_{i=1}^{k} \lambda_i.$$

**Example 16 (Grassmann Manifold)** *Let* $G = \mathbf{SO}_n$*,* $M = G_{n,p}$ *be as in Example 8. So for any solution* $\gamma = \langle \gamma_i \rangle_{i=1}^k$ *to the OCA (or OFS) problem in* $G_{n,p}$ *and its lifting* $\langle A_i \rangle_{i=1}^k$ *in* $\mathbf{SO}_n$*,* $\sum_{i=1}^k \lambda_i P_{A_i}(\dot{A}_i) A_i^t \equiv \nu_0 \in \mathfrak{so}_n$*. Let* $X \in \mathfrak{so}_n$ *be such that* $e^{2\pi X} = I_n$*,* $X \neq 0$*. Define the homomorphism* $\varphi_X : \mathbf{T}^1 \to \mathbf{SO}_n$ *as in Example 15. Then* $\varphi_X^* \nu_0 = \langle \nu_0, X \rangle_{\mathfrak{so}_n}$*, and by (4.38),* $\|\varphi_X^* \mathbb{I}_t\| = \mathbb{I}_t(X, X) \leq \sum_{i=1}^k \lambda_i \|X\|_{\mathfrak{so}_n}^2$*. Theorem 7 then implies that*

$$|\langle \nu_0, X \rangle_{\mathfrak{so}_n}| \leq \pi \sum_{i=1}^{k} \lambda_i \|X\|_{\mathfrak{so}_n}^2 / (t_1 - t_0), \tag{4.50}$$

*for all* $X \in \mathfrak{so}_n$ *such that* $e^{2\pi X} = I_n$*. Therefore, by Lemma 3, bound (4.49) still holds. However, it is possible to improve this bound by considering an additional symmetry of* $G_{n,p}$*. Suppose* $X \in \mathfrak{so}_n$ *is chosen such that* $e^{\pi X} = -I_n$ *(such* $X$ *exists only if* $n$ *is even). Consider* $\{\pm I_n\}$*, a discrete subgroup of* $\mathbf{SO}_n$*. The action of each of* $\{\pm I_n\}$ *on* $G_{n,p}$ *is the identity map, so* $\Phi$ *induces naturally an action of the quotient group* $\mathbf{SO}_n/\{\pm I_n\}$ *on* $G_{n,p}$*, which also satisfies Assumption 1 in Section 4.2. Since* $\{\pm I_n\}$ *is discrete, the Lie algebra of* $\mathbf{SO}_n/\{\pm I_n\}$ *is* $\mathfrak{so}_n$*, and the conserved quantity* $\nu_0$ *and the map* $\mathbb{I}_t$ *remain the same for this induced action. Now the map* $\varphi(\theta \mod 2\pi) = e^{\theta X/2}$*,* $\forall \theta \in \mathbb{R}$*, is a homomorphism from* $T^1$ *to* $\mathbf{SO}_n/\{\pm I_n\}$ *with* $d\varphi(1) = X/2$*. So* $\varphi^* \nu_0 = \langle \nu_0, X/2 \rangle_{\mathfrak{so}_n}$*, and* $\|\varphi^* \mathbb{I}_t\| \leq \sum_{i=1}^k \lambda_i \|X/2\|_{\mathfrak{so}_n}^2$*. Applying Theorem 7, we have*

$$|\langle \nu_0, X \rangle_{\mathfrak{so}_n}| \leq \frac{\pi}{2} \sum_{i=1}^{k} \lambda_i \|X\|_{\mathfrak{so}_n}^2 / (t_1 - t_0)$$

*for all $X \in \mathfrak{so}_n$ such that $e^{\pi X} = -I_n$. By Lemma 4, this implies that*

$$\text{the average of the singular values of } \nu_0 \leq \frac{\pi}{2(t_1 - t_0)} \sum_{i=1}^{k} \lambda_i.$$

**Example 17 (Stiefel Manifold)** *Consider $G = \mathbf{SO}_n$ and $M = V_{n,p}$ defined in Example 9. Let $\gamma = \langle \gamma_i \rangle_{i=1}^k$ be a solution to the OCA (or OFS) problem on $V_{n,p}$. Then, in Example 9 it is shown that $\sum_{i=1}^k \lambda_i \hat{P}_{A_i}(\dot{A}_i) A_i^t \equiv \nu_0 \in \mathfrak{so}_n$, where $\langle A_i \rangle_{i=1}^k$ is a lifting of $\gamma_i$ in $\mathbf{SO}_n$. By following the same steps as in the previous example, we conclude that (4.50), hence (4.49), holds.*

## 4.4 Collision avoidance of bodies

The OCA and OFS problems studied in Section 4.3 can be thought of as optimal motion planning problems for $k$ agents moving on a Riemannian manifold, with each agent represented by a disk of radius $r/2$. The arguments in Section 4.3 can be generalized to the situation where agents have shape other than disks. To be precise, let $M$ be a Riemannian manifold.

**Definition 11 (Shape of Body)** *The shape of a body on $M$ is specified by a map $\mathcal{S} : M \to 2^M$ that assigns to each $q \in M$ a subset $\mathcal{S}(q) \subset M$ corresponding to the subset of $M$ the body occupies if it is at $q$. $\mathcal{S}$ is called the* shape (map) *of the body.*

Consider $k$ bodies on $M$ whose shapes are given by the maps $\mathcal{S}_i$, $i = 1, \ldots, k$, respectively. Suppose that during the time interval $[t_0, t_1]$ their trajectories are given by a $k$-tuple of curves $\gamma = \langle \gamma_i \rangle_{i=1}^k$ in $M$. $\gamma$ is called *collision-free* if $\mathcal{S}_i(\gamma_i(t))$, $i = 1, \ldots, k$, are disjoint at any time $t \in [t_0, t_1]$. Fix the starting position $\langle a_i \rangle_{i=1}^k$ and the destination position $\langle b_i \rangle_{i=1}^k$ of the $k$ bodies such that $\mathcal{S}_i(a_i)$, $i = 1, \ldots, k$, and $\mathcal{S}_i(b_i)$,

$i = 1, \ldots, k$, are disjoint, respectively. Let $L : TM \to \mathbb{R}$ be a Lagrangian function and let the energy of $\gamma$, $J(\gamma)$, be defined by (4.2). Then the OCA problem for bodies is

**Problem 3 (OCA of Bodies)** *Among all collision-free $\gamma$ that start from $\langle a_i \rangle_{i=1}^k$ at time $t_0$ and end at $\langle b_i \rangle_{i=1}^k$ at time $t_1$, find the one (or ones) minimizing $J(\gamma)$.*

The OFS problem of bodies can be similarly formulated. However, it is omitted here for brevity. In analogy to Assumption 1 in Section 4.3, we consider the following special case.

**Assumption 2** *There is a $C^\infty$ action $\Phi : G \times M \to M$ of a Lie group $G$ on $M$ such that*

1. *the shapes of the bodies are $G$-invariant. Namely, $\Phi_g \circ \mathcal{S}_i = \mathcal{S}_i \circ \Phi_g$, $\forall g \in G$, $i = 1, \ldots, k$;*
2. *the Lagrangian function $L$ is $G$-invariant.*

Under Assumption 2, if $G$ acts on $M$ transitively, then each $\mathcal{S}_i$ is completely determined by $\mathcal{S}_i(q)$ at an arbitrary point $q \in M$. In general, one needs to specify $\mathcal{S}_i(q)$ for one $q$ in each $G$-orbit of $M$ to fully determine $\mathcal{S}_i$.

A key implication of Assumption 2 is that, if $\gamma = \langle \gamma_i \rangle_{i=1}^k$ is collision-free, so is $h_0\gamma = \langle h_0\gamma_i \rangle_{i=1}^k$ for any continuous and piecewise $C^\infty$ curve $h_0 : [t_0, t_1] \to G$, since at any time $t$, $1 \le i < j \le k$,

$$\mathcal{S}_i(h_0\gamma_i) \cap \mathcal{S}_j(h_0\gamma_j) = \Phi_{h_0}[\mathcal{S}_i(\gamma_i)] \cap \Phi_{h_0}[\mathcal{S}_j(\gamma_j)] = \Phi_{h_0}[\mathcal{S}_i(\gamma_i) \cap \mathcal{S}_j(\gamma_j)],$$

hence $\mathcal{S}_i(h_0\gamma_i) \cap \mathcal{S}_j(h_0\gamma_j) = \emptyset$ if and only if $\mathcal{S}_i(\gamma_i) \cap \mathcal{S}_j(\gamma_j) = \emptyset$. This property enables one to apply the variational approach in Section 4.3 without modification. Therefore,

**Theorem 8** *For the OCA and the OFS problems of bodies, all the necessary conditions derived in Section 4.3 remain true, including Theorem 4, 5, 7, and all their corollaries.*

As an example, consider $\mathbf{SE}_2$, the group of orientation-preserving isometries of $\mathbb{R}^2$. Elements of $\mathbf{SE}_2$ are of the form

$$A(x,y,\theta) \triangleq \begin{bmatrix} \cos\theta & -\sin\theta & x \\ \sin\theta & \cos\theta & y \\ 0 & 0 & 1 \end{bmatrix}, \quad \forall x, y, \theta \in \mathbb{R}.$$

$\mathbf{SE}_2$ acts on $\mathbb{R}^2 \simeq \mathbb{R}^2 \times \{1\} \subset \mathbb{R}^3$ by left matrix multiplication. Then $A(x,y,\theta)$ corresponds to the rigid body motion in $\mathbb{R}^2$ of a rotation by $\theta$ counterclockwise followed by a translation by $(x,y)$. The Lie algebra of $\mathbf{SE}_2$, $\mathfrak{se}_2$, is the set of all matrices of the form

$$\zeta(u,v,w) \triangleq \begin{bmatrix} 0 & -w & u \\ w & 0 & v \\ 0 & 0 & 0 \end{bmatrix}, \quad \forall u, v, w \in \mathbb{R}.$$

Define an inner product on $\mathfrak{se}_2$ by

$$\langle \zeta(u_1,v_1,w_1), \zeta(u_2,v_2,w_2) \rangle \triangleq u_1u_2 + v_1v_2 + \kappa w_1w_2,$$

where $\kappa > 0$ is a constant, and extend it to a left invariant Riemannian metric $\langle \cdot, \cdot \rangle$ on $\mathbf{SE}_2$ through left translation. Consider Problem 3 with $M = \mathbf{SE}_2$ and the Lagrangian function $L = \frac{1}{2}\|\cdot\|^2$. Let $G = \mathbf{SE}_2$ and the action $\Phi$ be the group multiplication. Suppose that the shapes of the bodies are given by

$$\mathcal{S}_i[A(x,y,\theta)] = \{A(\hat{x},\hat{y},\hat{\theta}) \in \mathbf{SE}_2 : (\hat{x},\hat{y}) \in A(x,y,\theta)D_i\}, \quad \forall A(x,y,\theta) \in \mathbf{SE}_2, \tag{4.51}$$

where $D_i$ is a subset of $\mathbb{R}^2$ containing the origin, for $i = 1, \ldots, k$. It is easy to verify that all $\mathcal{S}_i$ are $G$-invariant, hence Assumption 2 is satisfied.

**Remark 13** *To justify the choice of $\mathcal{S}_i$ in (4.51), note that $\mathbf{SE}_2$ is the configuration space of a rigid body moving on $\mathbb{R}^2$, in the sense that each element $A(x, y, \theta) \in \mathbf{SE}_2$ can be thought of as a configuration of the rigid body whose pivot point is at $(x, y) \in \mathbb{R}^2$ and whose orientation is in the direction that makes an angle $\theta$ with the positive $x$-axis. The shape of the rigid body can be specified by the region $D \subset \mathbb{R}^2$ it occupies when it is in configuration $A(0, 0, 0)$, i.e., when it has its pivotal point at the origin and points at the positive $x$-axis. The region it occupies in any other configuration $A(x, y, \theta)$ is obtained by applying on $D$ the rigid body motion that transforms configuration $A(0, 0, 0)$ to $A(x, y, \theta)$, hence the definition in (4.51). In this perspective, the problem can be alternatively formulated as the optimal motion planning problem for $k$ rigid bodies in $\mathbb{R}^2$, such that no two of them can overlap at any time, and that the energy $\sum_{i=1}^{2} \frac{1}{2}\lambda_i \int_{t_0}^{t_1} (\dot{x}_i^2 + \dot{y}_i^2 + \kappa\dot{\theta}_i^2)\, dt$ is minimized.*

Let $\gamma = \langle\gamma_i\rangle_{i=1}^k = \langle A(x_i, y_i, \theta_i)\rangle_{i=1}^k$ be an optimal solution to Problem 3, where $x_i, y_i, \theta_i$ are continuous and piecewise $C^\infty$ curves in $\mathbb{R}$ defined on $[t_0, t_1]$. Then it is easy to show that $\sum_{i=1}^k \lambda_i (d\Phi^{\gamma_i})^* \dot{\gamma}_i = \zeta(\sum_{i=1}^k \lambda_i \dot{x}_i, \sum_{i=1}^k \lambda_i \dot{y}_i, \sum_{i=1}^k \lambda_i [\dot{\theta}_i + (x_i \dot{y}_i - \dot{x}_i y_i)/\kappa]) \in \mathfrak{se}_2$, which by Theorem 4 should be constant for all $t$. In other words, the following quantities are conserved:

$$\sum_{i=1}^k \lambda_i \dot{x}_i, \quad \sum_{i=1}^k \lambda_i \dot{y}_i, \quad \sum_{i=1}^k \lambda_i [\dot{\theta}_i + (x_i \dot{y}_i - \dot{x}_i y_i)/\kappa].$$

In some simple cases, it is possible to construct the optimal solutions from these necessary conditions. We next discuss one of these cases. Consider $k = 2$, and denote by $\langle A(x_i^0, y_i^0, \theta_i^0)\rangle_{i=1}^2$ and $\langle A(x_i^1, y_i^1, \theta_i^1)\rangle_{i=1}^2$ the starting and the destination positions respectively. Integrating the first two conserved quantities, we get

$$\sum_{i=1}^{2} \lambda_i \begin{bmatrix} x_i(t) \\ y_i(t) \end{bmatrix} = \frac{t_1 - t}{t_1 - t_0} \sum_{i=1}^{2} \lambda_i \begin{bmatrix} x_i^0 \\ y_i^0 \end{bmatrix} + \frac{t - t_0}{t_1 - t_0} \sum_{i=1}^{2} \lambda_i \begin{bmatrix} x_i^1 \\ y_i^1 \end{bmatrix}, \quad \forall t \in [t_0, t_1]. \tag{4.52}$$

Hence the weighted center of the two-body system moves at constant speed from the weighted center of their starting position to the weighted center of their destination position. Another fact we need is summarized in the following lemma.

**Lemma 5** *Suppose that* $\gamma = \langle A(x_i, y_i, \theta_i) \rangle_{i=1}^k$ *is an optimal solution to the OCA problem of* $k$ *bodies on* $\mathbf{SE}_2$ *with starting position* $\langle A(x_i^0, y_i^0, \theta_i^0) \rangle_{i=1}^k$ *and destination position* $\langle A(x_i^1, y_i^1, \theta_i^1) \rangle_{i=1}^k$*. Then for any* $(x, y) \in \mathbb{R}^2$, $\tilde{\gamma} = \langle A(x_i + \frac{t-t_0}{t_1-t_0} x, y_i + \frac{t-t_0}{t_1-t_0} y, \theta_i) \rangle_{i=1}^k$ *is an optimal solution of the OCA problem of the same* $k$ *bodies on* $\mathbf{SE}_2$ *with starting position* $\langle A(x_i^0, y_i^0, \theta_i^0) \rangle_{i=1}^k$ *and destination position* $\langle A(x_i^1 + x, y_i^1 + y, \theta_i^1) \rangle_{i=1}^k$*.*

**Proof:** Note that $\tilde{\gamma}$ is collision-free if and only if $\gamma$ is, and that the energies of $\gamma$ and $\tilde{\gamma}$ are related by $J(\tilde{\gamma}) = J(\gamma) +$ some constant independent of $\gamma$. Hence the conclusion. ■

By Lemma 5, we may assume without loss of generality that

$$\sum_{i=1}^{2} \lambda_i \begin{bmatrix} x_i^0 \\ y_i^0 \end{bmatrix} = \sum_{i=1}^{2} \lambda_i \begin{bmatrix} x_i^1 \\ y_i^1 \end{bmatrix} = \begin{bmatrix} 0 \\ 0 \end{bmatrix}. \tag{4.53}$$

So by (4.52), for all $t \in [t_0, t_1]$,

$$\sum_{i=1}^{2} \lambda_i \begin{bmatrix} x_i(t) \\ y_i(t) \end{bmatrix} \equiv \begin{bmatrix} 0 \\ 0 \end{bmatrix}, \quad \text{i.e.,} \quad \begin{bmatrix} x_2(t) \\ y_2(t) \end{bmatrix} = -\frac{\lambda_1}{\lambda_2} \begin{bmatrix} x_1(t) \\ y_1(t) \end{bmatrix}. \tag{4.54}$$

Assume in addition that $D_2$ is an open disk of radius $r_2$ centered at the origin. Then $\dot{\theta}_2$ must be constant since $\gamma$ is collision-free under any reparameterization of $\theta_2$ and the one with constant velocity minimizes the term $\int_{t_0}^{t_1} \dot{\theta}_2^2 \, dt$, which is the contribution of $\theta_2$ to the energy of $\gamma_1$ (see Remark 13). Hence $\theta_2$ moves at constant speed from $\theta_2^0$ to the nearest point in $\theta_2^1 + 2\pi\mathbb{Z}$ in $\mathbb{R}$.

Since $x_2, y_2$ are related to $x_1, y_1$ as in (4.54), it remains only to specify $x_1, y_1, \theta_1$. The set of feasible $(x_1, y_1, \theta_1)$ is

$$\begin{aligned}
F =& \{(x,y,\theta) : A(x,y,\theta)D_1 \cap (-\frac{\lambda_1}{\lambda_2}\begin{bmatrix} x \\ y \end{bmatrix} + D_2) = \emptyset\} \\
=& \{(x,y,\theta) : (A(0,0,\theta)D_1 + \begin{bmatrix} x \\ y \end{bmatrix}) \cap (-\frac{\lambda_1}{\lambda_2}\begin{bmatrix} x \\ y \end{bmatrix} + D_2) = \emptyset\} \\
=& \{(x,y,\theta) : A(0,0,\theta)D_1 \cap (-\frac{\lambda_1+\lambda_2}{\lambda_2}\begin{bmatrix} x \\ y \end{bmatrix} + D_2) = \emptyset\} \\
=& \{(x,y,\theta) : \text{distance of } \begin{bmatrix} x \\ y \end{bmatrix} \text{ to } -\frac{\lambda_2}{\lambda_1+\lambda_2}A(0,0,\theta)D_1 \text{ is at least } \frac{\lambda_2 r_2}{\lambda_1+\lambda_2}\},
\end{aligned}$$

which defines a *static* obstacle in $\mathbb{R}^3$. Denote by $F_\theta = \{(x,y) : (x,y,\theta) \in F\}$ a section of $F$. Then it is easy to check that $F_\theta = A(0,0,\theta)F_0$, where $F_0$ can be obtained by first "outgrowing" $-D_1$ by $r_2$, and then scaling the resultant set by a factor of $\frac{\lambda_2}{\lambda_1+\lambda_2}$. See Figure 4.2 for two examples of how to outgrow a set $D_1$, and see Figure 4.3 for two examples of $F$.

The optimal solution corresponds to a curve $(x_1, y_1, \theta_1)$ in $\mathbb{R}^3 \backslash F$ that starts from $(x_1^0, y_1^0, \theta_1^0)$ at time $t_0$ and ends in $(x_1^1, y_1^1, \theta_1^1 + 2m\pi)$ for some integer $m$ at time

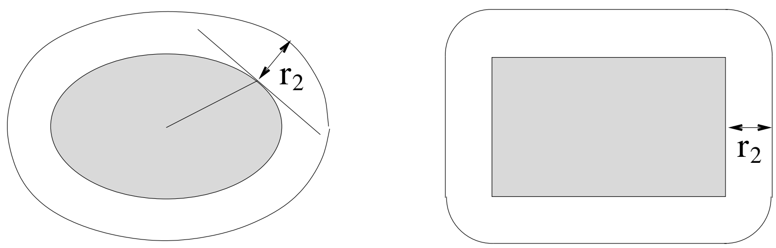


Figure 4.2: Two examples of outgrowing a set (shown by shaded areas) by $r_2$. Left: an ellipse; Right: a rectangle

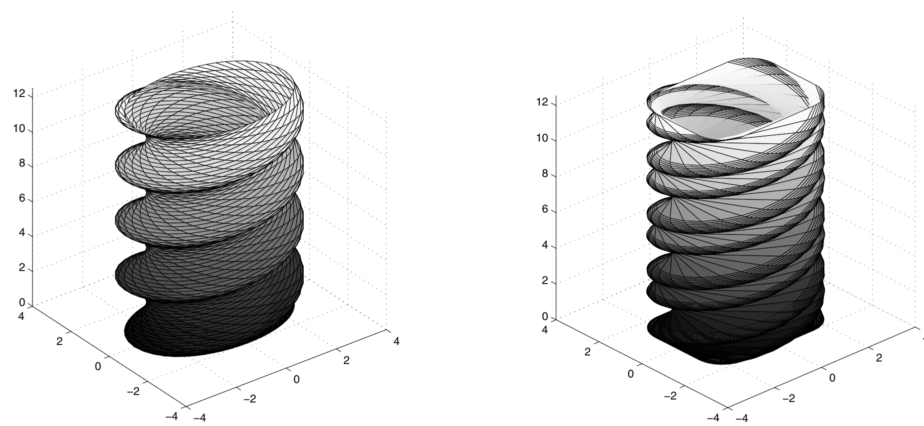

Figure 4.3: Plots of $F$ when $D_1$ is an ellipse (left) and a rectangle (right).

$t_1$, while minimizing the energy

$$J(\gamma) = \frac{1}{2}\sum_{i=1}^{2}\lambda_i \int_{t_0}^{t_1} (\dot{x}_i^2 + \dot{y}_i^2 + \kappa\dot{\theta}_i^2)\,dt = \frac{\lambda_1(\lambda_1+\lambda_2)}{2\lambda_2}\int_{t_0}^{t_1}\left[\dot{x}_1^2 + \dot{y}_1^2 + \kappa_1\dot{\theta}_1^2\right]dt + C,$$

where $\kappa_1 = \frac{\lambda_2}{\lambda_1+\lambda_2}\kappa$, and $C$ is a constant. By scaling the $\theta_1$-axis by a factor of $\sqrt{\kappa_1}$, the integral above coincides with the usual definition of curve energy, and the problem is then reduced to finding the shortest curve between two points in the scaled feasible set. Except for very simple cases (for example, when $D_1$ is a disk of radius $r_1$ centered at the origin, then the problem is reduced to Problem 1 on $\mathbb{R}^2$ with $r = r_1 + r_2$, and solutions can be constructed geometrically), analytic solutions are not available. However, given the geometrical interpretation, there are various numerical algorithms to solve it approximately such as, for example, the fast marching algorithm proposed in [65].

## 4.5 Summary of contributions

The problems of optimal collision avoidance and optimal formation control are studied for multiple agents moving on a Riemannian manifold. Under the assumption that there is a group of symmetries for the underlying manifold, we derive various necessary conditions for the optimal solutions. These include a generalization of the classical Noether theorem to the nonsmooth solutions to the OCA and OFS problems, and the bounds on the conserved quantities obtained through second variation and topological considerations. We also propose a generalization of the results to the OCA problem for bodies with arbitrary shape moving on a Riemannian manifold. As a future direction of research, it will be interesting to see how the derived necessary conditions can help to find a numerical solution of these problems.

# Chapter 5

# Conclusions

We study the problem of optimal coordinated motion planning for multiple agents moving in two dimensional Euclidean space, three dimensional Euclidean space, and general Riemannian manifolds. Necessary conditions for optimal solutions are derived through variational analysis. In certain cases, these conditions characterize the solutions completely. Numerical algorithms are devised to obtain approximated solutions to the problem, and their effectiveness is illustrated by extensive simulation results.

Based on these results, there are many possible future directions. For example, for Chapter 2 and Chapter 3, an analysis of the proposed numerical algorithms in terms of their performance and robustness with respect to uncertainty on the agents' positions and velocities is highly preferable; and one needs to study more realistic (and more complicated) models for the agent dynamics than the simple one adopted in this dissertation. Some contributions in this direction can be found in [26], which focuses exclusively on air traffic management systems. For Chapter 4, it will be an interesting problem to see how the obtained necessary conditions can help in designing efficient numerical algorithm to find optimal solutions on Riemannian manifolds.

# Bibliography

[1] A. Abrams. *Configuration Spaces and Braid Groups of Graphs.* PhD thesis, University of California, Berkeley, 2000.

[2] F. Albrecht and I.D. Berg. Geodesics in Euclidean space with analytic obstacle. *Proceedings of Amer. Math. Soc.*, 113(1):201–207, 1991.

[3] V. I. Arnold, K. Vogtmann, and A. Weinstein. *Mathematical Methods of Classical Mechanics*. Springer-Verlag, New York, 2nd edition, 1989.

[4] B. Aronov, M. de Berg, A.F. van der Stappen, P. Svestka, and J. Vleugels. Motion planning for multiple robots. *Discrete & Computational Geometry*, 22(4):502–525, 1999.

[5] A. Bicchi and L. Pallottino. On optimal cooperative conflict resolution for air traffic management systems. *IEEE Trans. on Intelligent Transport. Systems*, 1(4):221–231, 2000.

[6] J. Birman. *Braids, Links, and Mapping Class Groups.* Princeton University Press, Princeton, NJ, 1974.

[7] A. M. Bloch, P. S. Krishnaprasad, J. E. Marsden, and T. S. Ratiu. The

Euler-Poincare equations and double bracket dissipation. *Comm. Math. Phys.*, 175(1):1–42, 1996.

[8] J. C. P. Bus. The lagrange multiplier rule on manifolds and optimal control of nonlinear systems. *SIAM J. Control and Optimization*, 22(5):740–757, 1984.

[9] Y.-B. Chen, M. Hsieh, A. Inselberg, and H. Q. Lee. Planar conflict resolution for air traffic control. In *Proc. Second Canadian Conference on Computational Geometry*, pages 160–163, Ottawa, Ontario, Canada, 1990. University of Ottawa.

[10] Y.-J. Chiang, J. T. Klosowski, C. Lee, and J. S. B. Mitchell. Geometric algorithms for conflict detection/resolution in air traffic management. In *Proc. 36th IEEE Int. Conf. on Decision and Control*, volume 2, pages 1835–1840, 1997.

[11] J. P. Desai and V. Kumar. Nonholonomic motion planning for multiple mobile manipulators. In *Proc. IEEE Int. Conf. on Robotics and Automation*, volume 4, pages 3409–3414. IEEE, 1997.

[12] M. P. do Carmo. *Riemannian Geometry.* Birkhäuser Boston Inc., Boston, MA, 1992.

[13] J. J. Duistermaat and J. A. C. Kolk. *Lie Groups.* Springer-Verlag, Berlin, 2000.

[14] A. Edelman, T. A. Arias, and S. T. Smith. The geometry of algorithms with orthogonality constraints. *SIAM J. Matrix Anal. Appl.*, 20(2):303–353, 1998.

[15] M. Erdmann and T. Lozano-Perez. On multiple moving objects (motion planning). *Algorithmica*, 2(4):477–521, 1987.

[16] H. Erzberger, R.A. Paielli, D.R. Isaacson, and M.M. Eshow. Conflict detection and resolution in the presence of prediction error. In *1st USA/Europe Air Traffic Management R & D Seminar*, 1997.

[17] J. A. Fax. *Optimal and Cooperative Control of Vehicle Formations*. PhD thesis, California Institute of Technology, 2002.

[18] E. Frazzoli, Z.-H. Mao, J.-H. Oh, and E. Feron. Resolution of conflicts involving many aircraft via semidefinite programming. *J. of Guidance, Control, and Dynamics*, 24(1):79–86, 2001.

[19] K. Fujimura. *Motion Planning in Dynamic Environments*. Springer-Verlag, Tokyo, 1991.

[20] W. Fulton and J. Harris. *Representation Theory*. Springer-Verlag, 1991.

[21] H. Howards, M. Hutchings, and F. Morgan. The isoperimetric problem on surfaces. *Amer. Math. Monthly*, 106(5):430–439, 1999.

[22] J. Hu. A study of conflict detection and resolution in free flight. Master's thesis, University of California, Berkeley, 1999.

[23] J. Hu, J. Lygeros, M. Prandini, and S. Sastry. Aircraft conflict prediction and resolution using brownian motion. In *Proc. 38th IEEE Int. Conf. on Decision and Control*, volume 3, pages 2438–2443, 1999.

[24] J. Hu, M. Prandini, K. H. Johansson, and S. Sastry. Hybrid geodesics as optimal solutions to the collision-free motion planning problem. In M. Domenica, D. Benedetto, and A. Sangiovanni-Vincentelli, editors, *Hybrid Systems: Computation and Control. 4th International Workshop (HSCC01)*, volume 2034 of

*Lecture Notes in Computer Science*, pages 305–318, Rome, Italy, March 2001. Springer-Verlag, Berlin.

[25] J. Hu, M. Prandini, and S. Sastry. Optimal maneuver for multiple aircraft conflict resolution: a braid point of view. In *Proc. 39th IEEE Int. Conf. on Decision and Control*, volume 4, pages 4164–4169, 2000.

[26] J. Hu, M. Prandini, and S. Sastry. Optimal coordinated maneuvers for three dimensional aircraft conflict resolution. *J. of Guidance, Control, and Dynamics*, 25(5):888–990, 2002.

[27] J. Hu, M. Prandini, and S. Sastry. Optimal collision avoidance and formation switching on Riemannian manifolds. submitted to SIAM J. on Control and Optimization, 2003.

[28] J. Hu, M. Prandini, and S. Sastry. Optimal coordinated maneuvers for multiple agents moving on a plane. *SIAM Journal on Control and Optimization*, 42(2):637–668, 2003.

[29] J. Hu, M. Prandini, and S. Sastry. Probabilistic safety analysis in three dimensional aircraft flight. In *Proc. 42nd IEEE Int. Conf. on Decision and Control,*. IEEE, Dec. 2003.

[30] J. Hu and S. Sastry. Hybrid geodesic flows on manifolds with boundary. Technical report, University of California, Berkeley, in preparation, 2003.

[31] Yong K. Hwang and Narendra Ahuja. Gross motion planning. *ACM Computing Surveys*, 24(3):219–291, 1992.

[32] A. Inselberg. Conflict resolution, one-shot problem, and air traffic control. In *Abstracts of the First Canadian Conference on Computional Geometry*, page 26, Montreal, Quebec, Canada, 1989. McGill University.

[33] J. Jost. *Riemannian Geometry and Geometric Analysis*. Springer-Verlag, Berlin, 2nd edition, 1998.

[34] W.-S. Koon and J. E. Marsden. Optimal control for holonomic and nonholonomic mechanical systems with symmetry and Lagrangian reduction. *SIAM J. on Control and Optimization*, 35(3):901–929, 1997.

[35] J. Kosecka, C. Tomlin, G. J. Pappas, and S. Sastry. Generation of conflict resolution maneuvers for air traffic management. In *Proc. 1997 IEEE Int. Conf. on Intelligent Robot and Systems. Innovative Robotics for Real-World Applications, IROS '97, Grenoble, France*, volume 3, pages 1598–1603, 1997.

[36] P. S. Krishnaprasad. Eulerian many-body problems. In *Dynamics and Control of Multibody Systems (Brunswick, ME, 1988)*, pages 187–208, Providence, RI, 1989. Amer. Math. Soc.

[37] J. Krozel and M. Peters. Conflict detection and resolution for free flight. *Air Traffic Control Quarterly*, 5(3):181–212, 1997.

[38] J. Krozel and M. Peters. Strategic conflict detection and resolution for free flight. In *Proc. 36th IEEE Conference on Decision and Control*, volume 2, pages 1822–1828, 1997.

[39] J. Kuchar and L. C. Yang. Survey of conflict detection and resolution modeling methods. *IEEE Trans. on Intelligent Transport. Systems*, 1(4):179–189, 2000.

[40] J.C. Latombe. *Robot Motion Planning.* Kluwer Academic, Boston, MA, 1991.

[41] S.M. LaValle and S.A. Hutchinson. Optimal motion planning for multiple robots having independent goals. *IEEE Trans. on Robotics and Automation*, 14(6):912–925, 1998.

[42] N. E. Leonard and E. Fiorelli. Virtual leaders, artificial potentials and coordinated control of groups. In *Proc. 40th IEEE Int. Conference on Decision and Control*, volume 3, pages 2968–2973, 2001.

[43] M. Lobo, L. Vandenberghe, S. Boyd, and H. Lebret. Applications of second-order cone programming. *Linear Algebra and Its Applications*, 284(1-3):193–228, 1998.

[44] J. E. Marsden. Park City lectures on mechanics, dynamics, and symmetry. In *Symplectic Geometry and Topology (Park City, UT, 1997)*, pages 335–430. Amer. Math. Soc., Providence, RI, 1999.

[45] J. E. Marsden and T. S. Ratiu. *Introduction to Mechanics and Symmetry.* Springer-Verlag, New York, 2nd edition, 1999.

[46] C. De Medio and G. Oriolo. Robot obstacle avoidance using vortex fields. In S. Stifter and J. Lenarcic, editors, *Advances in Robot Kinematics*, pages 227–235. Springer-Verlag, Wien, 1991.

[47] F. Medioni, N. Durand, and J. M. Alliot. Air traffic conflict resolution by genetic algorithms. In *Artificial Evolution, European Conference (AE 95), Brest, France*, pages 370–383, Berlin, Germany, 1995. Springer-Verlag.

[48] P. K. Menon, G. D. Sweriduk, and B. Sridhar. Optimal strategies for free-flight air traffic conflict resolution. *Journal of Guidance, Control, and Dynamics*, 22(2):202–211, 1999.

[49] A. Miele, T. Wang, C.S. Chao, and J.B. Dabney. Optimal control of a ship for collision avoidance maneuvers. *J. of Optimization Theory and App.*, 103(3):495–519, 1999.

[50] J. W. Milnor. *Morse Theory*. Princeton University Press, Princeton, NJ, 1963.

[51] J. S. B. Mitchell. Shortest paths and networks. In J. E. Goodman and J. O'Rourke, editors, *CRC Handbook of Discrete and Computational Geometry*, pages 445–466. CRC Press LLC, Boca Raton, FL, 1997.

[52] J. S. B. Mitchell. Geometric shortest paths and network optimization. In J.-R. Sack and J. Urrutia, editors, *Handbook of Computational Geometry*, pages 633–701. North-Holland, Amsterdam, 2000.

[53] R. Montgomery. *A Tour of Subriemannian Geometries, Their Geodesics and Applications*. Amer. Math. Society, Providence, RI, 2002.

[54] S. Morgan. *The Mathematical Theory of Knots and Braids: an Introduction*. North-Holland, Amsterdam, 1991.

[55] K. Murasugi and Bohdan I. Kurpita. *A Study of Braids*. Kluwer Academic, Boston, MA, 1999.

[56] W. P. Niedringhaus. Stream option manager (som): Automated integration of aircraft separation, merging, stream management, and other air traffic control

functions. *IEEE Trans. on Systems, Man, and Cybernetics*, 25(9):1269–1280, 1995.

[57] R. A. Paielli and H. Erzberger. Conflict probability estimation for free flight. *Journal of Guidance, Control, and Dynamics*, 20(3):588–596, 1997.

[58] G. J. Pappas, C. Tomlin, J. Lygeros, D. Godbole, and S. Sastry. A next generation architecture for air traffic management systems. In *Proc. 36th IEEE Int. Conf. on Decision and Control*, volume 3, pages 2405–2410, 1997.

[59] M. Prandini, J. Hu, J. Lygeros, and S. Sastry. A probabilistic approach to aircraft conflict detection. *IEEE Trans. on Intelligent Transport. Systems*, 1(4):199–220, 2000.

[60] M. Prandini, J. Hu, J. Lygeros, and S. Sastry. A probabilistic approach to aircraft conflict detection. *IEEE Trans. on Intelligent Transportation Systems, Special Issue on Air Traffic Control - Part I*, 1(4):199–220, 2000.

[61] Radio Technical Commission for Aeronautics (RTCA). Minimum operational performance standards for traffic alert and collision avoidance system ii (TCAS ii) airborne equipment. In *Technical Report #RTCA/DO-185A*, Washington, DC, December 1997. RTCA, Inc.

[62] E. Rimon and D.E. Koditschek. Exact robot navigation using artificial potential functions. *IEEE Trans. on Robotics and Automation*, 8(5):501–519, 1993.

[63] K. H. Rosen. *Discrete Mathematics and its Applications*. McGraw-Hill, 1998.

[64] M. Rude. Collision avoidance by using space-time representations of motion processes. *Autonomous Robots*, 4(1):101–119, 1997.

[65] J. A. Sethian. *Level Set Methods: Evolving Interfaces in Geometry, Fluid Mechanics, Computer Vision and Materials Sciences*. Cambridge University Press, 1996.

[66] M. Sharir and S. Sifrony. Coordinated motion planning for two independent robots. *Ann. Math. Artificial Intelligence*, 3(1):107–130, 1991.

[67] M. Spivak. *A Comprehensive Introduction to Differential Geometry. Vol. I.* Publish or Perish Inc., Wilmington, Del., second edition, 1979.

[68] P. Tabuada, G. J. Pappas, and P. Lima. Feasible formations of multi-agent systems. In *Proc. American Control Conference*, volume 1, pages 56–61, Arlington, VA, June 2001.

[69] R. Teo and C. Tomlin. Computing provably safe aircraft to aircraft spacing for closely spaced parallel approaches. In *Proc. 19th Digital Avionics Systems Conference (DASC00), Philadelphia, PA*, volume 1, pages 2D2/1–9, 2000.

[70] C. Tomlin, J. Lygeros, and S. Sastry. A game theoretic approach to controller design for hybrid systems. *Proceedings of the IEEE*, 88(7):949–970, 2000.

[71] C. Tomlin, G. J. Pappas, and S. Sastry. Conflict resolution for air traffic management: A study in multi-agent hybrid systems. *IEEE Trans. on Automatic Control*, 43(4):509–521, 1998.

[72] G. C. Walsh, R. Montgomery, and S. Sastry. Optimal path planning on matrix Lie groups. In *Proc. 33rd IEEE Conference on Decision and Control*, volume 2, pages 1258–1263, 1994.

[73] L.C. Yang and J. Kuchar. Prototype conflict alerting logic for free flight. In *Proc. 35th AIAA Airspace Science Meeting & Exhibit, AIAA 97-0220*, January 1997.

[74] Y. Zhao and R. Schultz. Deterministic resolution of two aircraft conflict in free flight. In *Proc. AIAA Guidance, Navigation, and Control Conference, AIAA-97-3547*, New Orleans, LA, August 1997.

[75] L. Zheng and D. Tse. Communicating on the Grassmann manifold: a geometric approach to the non-coherent multiple antenna channel. *IEEE Trans. on Information Theory*, 48(2):359–383, 2002.